Titre: Title:	Measurement of Load-Induced Electrical Potentials at the Surface of the Knee
Auteur: Author:	Lin Zhu
Date:	2016
Type:	Mémoire ou thèse / Dissertation or Thesis
Référence: Citation:	Zhu, L. (2016). Measurement of Load-Induced Electrical Potentials at the Surface of the Knee [Thèse de doctorat, École Polytechnique de Montréal]. PolyPublie. https://publications.polymtl.ca/2145/

UNIVERSITÉ DE MONTRÉAL

MEASUREMENT OF LOAD-INDUCED ELECTRICAL POTENTIALS AT THE SURFACE OF THE KNEE

LIN ZHU

INSTITUT DE GÉNIE BIOMÉDICAL

ÉCOLE POLYTECHNIQUE DE MONTRÉAL

THÈSE PRÉSENTÉE EN VUE DE L'OBTENTION

DU DIPLÔME DE PHILOSOPHIÆ DOCTOR

(GÉNIE BIOMÉDICAL)

AVRIL 2016

UNIVERSITÉ DE MONTRÉAL

ÉCOLE POLYTECHNIQUE DE MONTRÉAL

Cette thèse intitulée:

MEASUREMENT OF LOAD-INDUCED ELECTRICAL POTENTIALS AT THE SURFACE OF THE KNEE

présentée par : ZHU Lin

en vue de l'obtention du diplôme de : Philosophiæ Doctor

a été dûment acceptée par le jury d'examen constitué de :

M. SHIRAZI-ADL Aboulfazl, Ph. D., président

M. SAVARD Pierre, Ph. D., membre et directeur de recherche

M. BUSCHMANN Michael, Ph. D., membre et codirecteur de recherche

M. PRINCE François, Ph. D., membre

Mme NUÑO Natalia, Ph. D., membre externe

To my beloved family

ACKNOWLEDGEMENTS

This thesis completes my life as a PhD student in Montreal, Canada. The experience was stimulating and challenging. And this thesis embraces efforts from many people and their invaluable contributions, both directly and indirectly to my research.

First, I would like to express my deepest gratitude toward Prof. Pierre Savard, my supervisor, for providing me such a wonderful opportunity to deepen my scientific knowledge and for his consistent encouragement and guidance during my PhD. He has walked me through all the stages of my project. His patient and enthusiastic coaching let me get into my research project and gain problem solving ability. Moreover, his direction and effective discussion helped me gradually built confidence and develop deep interest in this research field. Without his illuminating instruction, this thesis could not have reached its present form.

Besides, I would also like to thank Prof. Michael Buschmann for his insightful guidance and constructive suggestions. His helpful advice really inspired me and broadened my perspectives.

Many thanks to the members from Biomomentum Inc., Martin Garon and Eric Quenneville. They designed the whole acquisition system for the EAG measurement and guided me to design the experimental protocol. Without their help, all the experimental investigations could not have been done.

I sincerely appreciate all the members who I had worked with and all the volunteers who were willing to join the experiments.

I am deeply indebted to my beloved family, parents -Guiwen Shang and Luchuan Zhu-, and husband -Baoqiang Li-, who have always been helping me out of difficulties and supporting without a word of complaint. Also, this dissertation is dedicated to my son, Julian, who continues to show me new ways to enjoy life.

I also owe my sincere gratitude all my kind friends living in Montreal, with whom I spent many holidays to explore the city, finding new and interesting aspects to enrich my live.

The funding for this research was provided by the China Scholarship Council (CSC), the Canadian Institutes of Health Research and the Canadian Natural Sciences and Engineering Research Council.

RÉSUMÉ

L'arthrose (OA), la maladie chronique la plus répandue chez les personnes âgées, est l'une des principales causes d'invalidité dans notre société avec une incidence qui s'accroit dans le monde entier. L'arthrose résulte de la détérioration ou de la perte du cartilage articulaire qui agit comme un coussin de protection entre les os. Comme l'incidence de l'arthrose est en progression constante, il y a un besoin urgent de techniques d'évaluation non invasives pouvant être efficaces avant le début de la dégradation irréversible du cartilage. Les techniques actuelles d'évaluation comprennent l'évaluation clinique, l'arthroscopie et les modalités d'imagerie telles que les rayons X, l'imagerie par résonance magnétique (IRM) et la tomographie par ordinateur (CT). Bien que ces techniques soient couramment utilisées pour le diagnostic de l'arthrose en évaluant la formation d'ostéophytes, le pincement articulaire et les lésions osseuses, aucune d'elles ne peut détecter les changements précoces dus à l'arthrose du genou.

La nécessité d'une évaluation précoce et précise de l'intégrité du cartilage a incité de nombreux chercheurs à explorer une variété de techniques. Par exemple, la transduction électromécanique du cartilage, connu sous le nom de « potentiels d'écoulement », est un indice sensible de l'intégrité du cartilage articulaire qui a été validé par de nombreuses expériences *in vitro*. Le mécanisme sous-jacent est associé à la séparation des charges négatives fixes et des contre-ions mobiles dans la phase liquide du cartilage durant sa compression. Un instrument arthroscopique (Arthro-BST) a ainsi été conçu pour mesurer les potentiels d'écoulement directement sur la surface du cartilage articulaire comprimé pour en évaluer la qualité lors d'une intervention chirurgicale. Une approche similaire, mais non invasive, a ensuite été développée pour mesurer les potentiels apparaissant à la surface du genou pendant son chargement et reflétant les potentiels d'écoulement sous-jacents. Cette technique est appelée électroarthrographie (EAG). La mise en charge du cartilage consiste simplement, pour un sujet debout, à déplacer son poids sur la jambe instrumentée. Même si les premières mesures de l'EAG étaient reproductibles, une certaine variabilité des signaux EAG enregistrés chez le même sujet a été observée, ce qui peut entraver son application comme outil de diagnostic de l'arthrose. Le but de notre étude était donc d'étudier la nature de la variabilité des signaux EAG afin de contribuer à l'élaboration de meilleures techniques de mesure.

Notre premier objectif était d'étudier comment la contraction de certains muscles de la jambe peut modifier la force de contact de l'articulation du genou et, à son tour, l'amplitude des signaux EAG. Six sujets en décubitus dorsal ont volontairement produit des contractions musculaires isométriques activant sélectivement quatre groupes de muscles de la jambe. Les signaux suivants furent enregistrés lors de cycles de chargement répétés : deux signaux EAG mesurés sur les deux côtés du genou, quatre électromyogrammes (EMG) des muscles gastrocnémiens, ischio-jambier, quadriceps et tensor fascia latae, ainsi que la force produite par la contraction musculaire et mesurée par une plaque de force placée contre le pied. Nous avons observé que les signaux de force et EAG augmentaient et diminuaient en même temps que les signaux EMG. Les signaux de force et EAG étaient très bien corrélés: 86% des coefficients de corrélation calculés en utilisant tous les échantillons au cours de chaque cycle de chargement étaient statistiquement significatifs ($p < 0,05$). Des contractions musculaires isolées étaient possibles pour les gastrocnémiens et ischio-jambiers, mais pas toujours pour les quadriceps et tensor fascia latae. Les résultats obtenus soutiennent l'hypothèse selon laquelle la contraction musculaire peut modifier la force de contact du genou et les signaux EAG. Pour approfondir la contribution des contractions musculaires aux signaux EAG enregistrées avec le protocole de chargement utilisé en clinique, nous avons comparé les signaux EMG avec les signaux EAG générés par transfert du poids corporel. Nous avons constaté que les signaux EAG étaient plus élevés lorsque l'activité EMG était plus élevée. Plus précisément, les quadriceps et ischio-jambiers ont toujours montré une activité EMG minimale tandis que les cycles de chargement avec une amplitude EAG accrue furent observés lorsque l'activité EMG des gastrocnémiens était supérieure. Ces muscles sont impliqués dans le maintien de l'équilibre.

Le deuxième objectif était d'étudier la source des variations EAG observées lorsqu'un sujet se maintient en équilibre sur une jambe, en association avec la force de réaction du sol (GRF) et les déplacements du centre de pression (COP) qui reflètent l'activité des muscles impliqués dans le maintien de l'équilibre. Les signaux EAG ont été enregistrés à quatre sites sur le genou chez 20 sujets alors qu'ils déplaçaient leur poids corporel sur la jambe instrumentée en se tenant sur une plaque permettant de mesurer les signaux GRF et COP. Deux modèles de régression linéaire ont été construits de manière à estimer le *rapport électromécanique* (EMR) qui indique la capacité du cartilage à générer un certain potentiel électrique pour une force de réaction du sol donnée. Les erreurs relatives entre les signaux EAG mesurés et modélisés ont été significativement réduites

pour trois sites d'électrodes ($p < 0,05$) en utilisant le modèle GRF+COP qui prend en compte les signaux GRF et COP, par rapport au modèle qui ne tient compte que du signal GRF. Les expériences de test-retest ont confirmé que la reproductibilité des mesures de l'EMR a été améliorée avec le modèle de GRF+COP en comparaison avec le modèle GRF. Nous concluons que les signaux EAG sont très bien corrélés avec la force de réaction du sol et les déplacements du centre de pression, et que la modélisation électromécanique permet de tenir compte de ces effets et d'accroître la reproductibilité des mesures.

Le troisième et dernier objectif était d'étudier l'évolution des signaux EAG pendant les cycles de chargement successifs en utilisant le protocole de transfert de poids précédent, ainsi qu'un nouveau protocole d'hyperextension passive. Le protocole de transfert de poids a été appliqué chez 20 sujets qui se tenaient debout sur une plaque de mesure de la force de réaction du sol. Vingt cycles de chargement ont été enregistrés au cours de deux séquences: la séquence initiale comprenait 10 cycles de chargement successifs; la séquence suivante comprenait 10 cycles enregistrés après une période d'exercice de 15 minutes au cours de laquelle les sujets ont continuellement déplacé leur poids d'une jambe à l'autre. Les valeurs de l'EMR pour quatre sites d'électrode ont été calculées pour chaque cycle de chargement en utilisant le modèle GRF+COP. Les résultats ont montré que les valeurs de l'EMR ont lentement diminué au fil du temps: pour la séquence initiale, les coefficients de corrélation entre les valeurs de l'EMR et les numéros de séquence étaient significatifs pour trois sites d'électrodes ($p < 0,05$); pour la séquence suivante, les valeurs du EMR ont encore diminué, mais les coefficients de corrélation n'étaient plus significatifs, indiquant un possible effet de nivellement. Pour éliminer l'implication possible de la contraction des muscles dans cette diminution de l'EMR, un nouveau protocole de chargement passif a été développé. Ainsi, une force externe a été appliquée manuellement sur le tibia des sujets en décubitus dorsal tandis que la force sous le talon de la jambe instrumentée était mesurée. Ces expériences de chargement par hyperextension passive ont été effectuées chez six sujets avec cinq cycles de chargement successifs. Deux signaux EAG ont été enregistrés sur les deux côtés du genou, ainsi que la force sous le talon et quatre EMG des gastrocnémiens, ischio-jambiers, quadriceps et tensor fascia latae. Les signaux EMG provenant des quatre groupes musculaires sont restés silencieux pendant tous les cycles de chargement supportant l'hypothèse que le chargement par hyperextension passive peut induire des signaux EAG avec une activité musculaire minime. Les résultats ont également montré que les valeurs de l'EMR ont diminué au

cours du temps durant les cycles de chargement successifs. La réduction des valeurs de l'EMR n'impliquerait donc pas l'activité musculaire et une possible accoutumance du réflexe d'étirement, mais plutôt les propriétés électromécaniques du cartilage articulaire.

En conclusion, cette thèse permet de mieux comprendre les techniques de chargement pour générer les signaux EAG et confirme le rôle de l'EAG en tant que "capteur" naturel des changements de force de contact du genou. L'importance de la contraction des muscles de la jambe en tant que source de variabilité EAG a été démontrée. De plus, cette variabilité a pu être compensée par un modèle électromécanique pouvant prédire l'EAG en fonction de la force de réaction du sol et des déplacements du centre de pression, ce qui a amélioré la répétabilité des mesures obtenues par transfert de poids. Un nouveau protocole de chargement d'hyperextension passif minimisant l'activité musculaire pendant les mesures EAG et produisant des potentiels proportionnels à la force appliquée a également été mis au point.

ABSTRACT

Osteoarthritis (OA), the most prevalent chronic progressive disease of the elderly, is one of the leading causes of disability in our society with increasing incidence throughout the world. OA results from the deterioration or loss of articular cartilage acting as protective cushion between the bones. As the incidence of OA is on a continuous increase, there is an urgent need for non-invasive assessment techniques that can be effective before the onset of irreversible degradation. Current technologies to assess the joint function include clinical evaluation, arthroscopy and imaging techniques such as X-ray, magnetic resonance imaging (MRI) and computed tomography (CT). Although these techniques are widely used to assist the diagnosis of OA by evaluating osteophyte formation, joint space narrowing and bone damage, none of them can show osteoarthritic changes of the knee until the later OA stages.

The need for an early and accurate evaluation of the integrity of cartilage has prompted many investigators to explore a variety of techniques. For example, the electromechanical transduction of cartilage, known as streaming potentials, is a sensitive index of the integrity of articular cartilage that has been validated by many *in-vitro* experiments. The underlying mechanism is associated with the separation of fixed negative charges and mobile counterions in the liquid phase of the cartilage under compression. A hand-held arthroscopic instrument (Arthro-BST) has thus been designed to measure the electrical potentials directly over compressed articular cartilage to assess its quality. A non-invasive approach, electroarthrography (EAG) was later developed to measure the electrical potentials appearing on the surface of knee during loading and reflecting the underlying streaming potentials. Mechanical loading simply consisted of shifting the body weight of the erect subject to the instrumented leg. Even though the first EAG measurements were repeatable, variability in the EAG signals recorded in the same subject was observed, which can hamper its application as a diagnostic tool for OA. The aim of our study was thus to investigate the nature of the variability of the EAG signals and to contribute to the development of better measurement techniques.

The first objective of this study was to investigate how the contraction of certain leg muscles in supine subjects affects the contact force of the knee joint and, in turn, the EAG values. Voluntary isometric muscle contractions were repeatedly conducted to selectively activate four leg muscle groups while six subjects were lying on their back. Two EAG signals were recorded on both

sides of the knee, as well as electromyograms (EMG) from the gastrocnemius, hamstring, quadriceps and tensor fascia latae muscles. Meanwhile, the signal from a force plate fixed against the foot according to the direction of the force was monitored. We found that the EAG and force signals increased and decreased simultaneously with the EMG signals. The EAG and force signals were very well correlated: 86% of the correlation coefficients computed using all the samples during each loading cycle were statistically significant ($p<0.05$). Isolated muscle contraction was possible for the gastrocnemius and hamstring, but not always for the quadriceps and tensor fascia latae. The results obtained from these experiments supported the hypothesis that muscle contraction can modify the knee contact force and the EAG values measured in the supine position. To further investigate the contribution of muscle contractions on the EAG signals recorded with the clinical loading protocol in erect subjects, we monitored the EMG signals in parallel with the EAG signals during body weight shifting. We found that higher EAG values were observed during higher EMG activity. Specifically, the quadriceps and hamstring EMGs showed minimal activity whereas loading cycles with increased EAG amplitude were associated with higher EMG activity from the gastrocnemius, which is involved in maintaining balance.

The second objective was to investigate the source of EAG variations observed during a one-legged stance in association with the ground reaction force (GRF) and the displacements of the centre of pressure (COP) which reflect muscle activity involved in maintaining balance. The EAG signals were recorded at four electrode sites in 20 erect subjects while they repeatedly shifted their body weight to the instrumented leg and stood on a force plate measuring the GRF and COP displacements. Two linear regression models were constructed to estimate the *electro-mechanical ratio* (EMR) interpreting the ability of cartilage to generate a certain electrical potential for a given ground reaction force. Using the GRF+COP model that took into account the GRF and COP displacements, the relative errors between the reconstructed and measured EAG signals were significantly reduced at three electrode sites when compared to the model that only considered the GRF. The test-retest experiments confirmed that the reproducibility of the EMR measurements obtained with the GRF+COP model was improved by eliminating the impact of muscle activation during weight shifting. It also pointed out that the COP displacements during a one-legged stance reflect the knee joint contact force due to body weight and muscle forces associated with postural balance.

The third and last objective was to investigate the evolution of the EAG signals during successive loading cycles using the weight shifting protocol, and a novel passive hyperextension loading protocol. The weight shifting protocol was conducted on 20 subjects who stood on a force plate measuring the GRF. A total of 20 loading cycles were recorded during two sequences: the initial sequence comprised 10 successive loading cycles; the subsequent sequence comprised 10 cycles recorded after a 15 min exercise period during which the subjects repeatedly shifted their weight from one leg to the other. The EMR values were computed at four electrode sites for each cycle using the GRF+COP model. The results showed that the EMR values slowly decreased over time: for the initial sequence, the correlation coefficients between EMR values and sequence numbers were significant at three electrode sites ($p < 0,05$); for the subsequent sequence, the EMR values still decreased, but the correlation coefficients were no longer significant, indicating a possible levelling off effect. To eliminate the possible involvement of muscle contraction in this EMR decrease, a novel passive loading protocol was developed. Thus, an external force was manually applied over the tibia of the supine subjects while the force under the heel of the measured leg was monitored. These passive hyperextension loading experiments were conducted on six subjects with five successive loading cycles. Two EAG signals were recorded on both sides of the knee, as well as the heel force and four EMG signals from the gastrocnemius, hamstring, quadriceps and tensor fascia latae. The EMG signals from the four muscle groups remained silent during all the loading cycles, supporting the hypothesis that passive hyperextension loading can induce EAG signals with minimal muscle activity. The results also showed that the EMR values decreased with time during the successive loading cycles. We concluded that the reduction of EMR values does not arise from muscle activity and possible habituation of the stretch reflex, but from the electromechanical properties of articular cartilage.

In conclusion, this thesis provides a basic understanding of EAG loading techniques and confirms the role of EAG as a natural “sensor” of the knee contact force. The importance of leg muscle contraction as a source of EAG variability was demonstrated. Moreover, this variability was accounted with an electromechanical model predicting the EAG as a function of the GRF and COP displacements, which improved the repeatability of the measurements obtained during a one-legged stance. A novel passive hyperextension loading protocol was finally developed that minimizes muscle activity during the EAG measurements.

TABLE OF CONTENTS

DEDICATION III

ACKNOWLEDGEMENTS IV

RÉSUMÉ V

ABSTRACT IX

LIST OF TABLES XVI

LIST OF FIGURES XVII

LIST OF SYMBOLS AND ABBREVIATIONS XIX

CHAPTER 1 INTRODUCTION 1

1.1 General context 1

1.2 Hypotheses and objectives 4

1.3 Organization of the thesis 5

CHAPTER 2 CRITICAL REVIEW OF THE LITERATURE 6

2.1 Knee joint 6

2.1.1 Knee anatomy 6

2.1.2 Knee biomechanics 8

2.2 Articular cartilage 10

2.2.1 Composition 10

2.2.2 Structure 12

2.3 Biomechanics of articular cartilage 14

2.3.1 Nonlinear elasticity 16

2.3.2 Viscoelasticity 17

2.4 Cartilage degeneration 19

2.4.1 Epidemiology 19

2.4.2 Pathophysiology 20
2.5 Assessing cartilage quality 22
2.5.1 Clinical evaluation 22
2.5.2 Imaging techniques 22
2.5.3 Arthroscopy 25
2.6 Electroarthrography 27
2.6.1 Streaming potentials 27
2.6.2 Arthro-BST 30
2.6.3 First electroarthrography studies 31
2.6.4 Postural control 34
CHAPTER 3 ARTICLE 1: MECHANICAL LOADING OF KNEE ARTICULAR CARTILAGE INDUCED BY MUSCLE CONTRACTION CAN BE ASSESSED BY MEASURING ELECTRICAL POTENTIALS AT THE SURFACE OF THE KNEE 35
3.1 Abstract 37
3.2 INTRODUCTION 37
3.3 Methods 39
3.4 RESULTS 42
3.5 Discussion 49
3.6 Conflict of interest 51
3.7 Acknowledgements 52
3.8 References 52
CHAPTER 4 ARTICLE 2: ELECTRICAL POTENTIALS MEASURED ON THE SURFACE OF THE KNEE REFLECT THE CHANGES OF THE CONTACT FORCE IN THE KNEE JOINT PRODUCED BY POSTURAL SWAY 56
4.1 Abstract 58

4.2 Introduction 58
4.3 Methodology 60
4.3.1 Experiments 60
4.3.2 Modeling 62
4.4 Results 65
4.5 Discussion 68
4.6 Acknowledgements 70
4.7 References 70
CHAPTER 5 ARTICLE 3: DECREASE OF THE ELECTRICAL POTENTIALS MEASURED ON THE SURFACE OF THE KNEE AND PRODUCED BY CARTILAGE COMPRESSION DURING SUCCESSIVE LOADING CYCLES 74
5.1 Abstract 76
5.2 Introduction 76
5.3 Methodology 78
5.3.1 Weight shifting protocol 78
5.3.2 Passive hyperextension loading protocol 79
5.3.3 Data acquisition and processing 79
5.3.4 WSP modeling 80
5.4 Results 83
5.5 Discussion 89
5.6 Acknowledgements 91
5.7 References 91
CHAPTER 6 GENERAL DISCUSSION 97
6.1 Effects of muscle activity on the EAG measurements 97
6.2 Development of electromechanical models 100

6.3 Evolution of the EAG signals....103

CHAPTER 7 CONCLUSION AND RECOMMENDATIONS....106

7.1 Conclusion....106

7.2 Recommendations....106

BIBLIOGRAPHY....109

LIST OF TABLES

Table 3.1: Characteristics of the subjects.....39

Table 4.1 : Intraclass correlation coefficient (ICC) between the EMRs obtained on the first and second days for the two models 68

Table 5.1: The electromechanical ratios obtained with the weight shifting protocol during the initial and post-exercise sequences at the four electrode sites. 86

LIST OF FIGURES

Figure 2.1: Structure of the knee 6

Figure 2.2: Structure of Proteoglycans aggregate 11

Figure 2.3: Schematic structure of healthy articular cartilage. 13

Figure 2.4: Unconfined, confined and indentation loading geometries for testing the mechanical properties of articular cartilage. 15

Figure 2.5: Typical stress-strain curve for articular cartilage. 16

Figure 2.6: Temporal profiles of displacement and loading during compression tests.....18

Figure 2.7: Representation of articular cartilage degeneration in two phases. 21

Figure 2.8: Sample arthroscopic images demonstrating different grades of the modified Outerbridge grading system 26

Figure 2.9: The Arthro-BST device. 30

Figure 2.10: Mean values of EAG signals at eight electrode sites.....32

Figure 2.11: Simulated electric potential distribution over the knee surface.....33

Figure 3.1: Schematic representation of some forces acting on the knee joint.....40

Figure 3.2: Representative data for gastrocnemius contraction 42

Figure 3.3: Representative data for hamstring contraction 43

Figure 3.4 : Representative data for quadriceps contraction. 44

Figure 3.5 : Representative data for contraction of the tensor fasciae latae.....45

Figure 3.6 : Statistics for the EAG, EMG and force signals. 46

Figure 3.7 : The EAG, EMG and ground reaction force signals recorded on an erect subject. 48

Figure 4.1 : Position of electrodes and coordinate system of force transducers 61

Figure 4.2 : Conceptual 2D models of WSP 64

Figure 4.3 : Representative EAG signals and the signals predicted by the two models. 66

Figure 4.4 : The mean and SE of the EMR estimated with the GRF and GRF+COP models. 67

Figure 4.5 : The mean and SE of the RE computed between the measured EAG and the modeled signals using the GRF and GRF+COP models. 68

Figure 5.1: Knee loading during hyperextension (top) and unipedal stance (bottom).....82

Figure 5.2 : Measured and modeled EAG signals during a loading cycle with the WSP.....83

Figure. 5.3: Evolution of the EMR observed during successive loading cycles with the WSP.....85

Figure 5.4: Representative data obtained during one loading cycle with the PHLP.....87

Figure 5.5: Evolution of the EMR observed during successive loading cycles with the PHLP 88

Figure 6.1: Representative data obtained during a loading cycle with WSP. 100

LIST OF SYMBOLS AND ABBREVIATIONS

ACL	Anterior cruciate ligament
ACR	American College of Rheumatology
BF	Biceps femoris
BW	Body weight
CKC	Closed kinetic chain
COM	Centre of mass
COP	Centre of pressure
CT	Computed tomography.
CV	Coefficient variation
EAG	Electroarthrography
ECM	Extracellular matrix
EMG	Electromyography
EMR	Electro-mechanical ratio
GAG	Glycosaminoglycan
GRF	Ground reaction force
ICC	Intraclass correlation coefficient
ICRS	International Cartilage Repair Society
LCL	Lateral collateral ligament
LG	Lateral gastrocnemius
MCL	Medial collateral ligament
MG	Medial gastrocnemius
MRI	Magnetic resonance imaging
OA	Osteoarthritis

OCT	Optical coherence tomography
OKC	Open kinetic chain
PCL	Posterior cruciate ligament
PG	Proteoglycan
PHLP	Passive hyperextension loading protocol
QP	Quantitative parameter
RA	Rheumatoid arthritis
RE	Relative error
RF	Rectus femoris
STZ	Superficial tangential zone
SD	Standard deviation
SE	Standard error
SM	Semimembranous
ST	Semitendinosus
TKR	Total knee replacement
VL	Vastus lateralis
VM	Vastus medialis
WSP	Weight shifting protocol

CHAPTER 1 INTRODUCTION

1.1 General context

Articular cartilage is a hydrated soft tissue covering the subchondral bone and providing a frictionless joint surface. The primary function of articular cartilage is to transmit and distribute the forces acting across the knee joint (Netti & Ambrosio, 2002). Osteoarthritis (OA), which is characterized by the degradation of cartilage, is the most common joint disorder across the world as identified in a number of international reports. According to the World Health Organization, 9.6 percent of men and 18 percent of women over the age of 60 years worldwide have symptomatic OA, making OA one of the most prevalent chronic diseases (Woolf & Pfleger, 2003). As reported by the Arthritis Alliance of Canada, more than 4.6 million Canadians currently live with OA, which will rise to more than 10 million in the next 30 years (Bombardier, Hawker, & Mosher, 2011). OA can lead to pain, stiffness or even joint dysfunction, which severely impacts the quality of life.

No specific laboratory diagnostic is associated with OA and evaluation of articular cartilage is usually based on clinical and diagnostic imaging findings. Plain radiography has been widely used to detect secondary gross changes of cartilage, manifested by joint space narrowing, as well as subchondral bony sclerosis and cyst formation (Choi & Gold, 2011). However, these changes can only be detected at a late stage of OA when degeneration is already irreversible. Magnetic resonance imaging (MRI) is an extensively used imaging modality for the assessment of articular cartilage because of its excellent soft tissue contrast and its sensitivity to bone marrow and soft tissue edema (Ma, 1999). Conventional MRI has the ability to directly visualize articular cartilage depicting mostly morphological changes such as partial or full thinning of cartilage (Eckstein et al., 2006). However it is limited by cost, spatial resolution and complex data processing (Delakis, Xanthis, & Kitney, 2009). Conventional or computed tomography (CT) arthrography, which allows direct visualization of the cartilage, has also been used to evaluate surface irregularities of the cartilage; but it is limited by its invasiveness (Coumas & Palmer, 1998).

Clinical OA is frequently in an advanced condition for which joint surgery is needed to relieve chronic pain. The recommended treatments of OA can be non-pharmacological treatments, followed by pharmacological treatments, as there are several medicines on the market that

alleviate pain and improve joint function of OA patients. Currently, there are no clinically available therapies that can reverse or stop the progression of OA as cartilage has very limited capacity to heal itself. Early diagnosis of OA may lead to treatments that can slow the progression of the disease or reverse it altogether since OA typically develops over decades (Stolz et al., 2009). In the early stage of OA, treatments like physical exercise, weight control or medicines can reduce the risk factors of OA.

The extracellular matrix (ECM) of the cartilage is mainly composed of proteoglycan (PG) macromolecules, collagen and water (Nissi et al., 2004). The main PGs in cartilage, aggrecan, consist of numerous glycosaminoglycan (GAG) chains covalently bonding to a core protein (Légaré et al., 2002a). The stiffness of cartilage is primarily provided by the repulsive force between the negatively charged GAG chains which are trapped inside the cross-linked collagen network. These negative ions attract positive counter-ions such as sodium in the electrolyte to maintain electrical neutrality (Bartel, Davy, & Keaveny, 2006a). In equilibrium conditions, these positive ions are symmetrically distributed. When the cartilage is compressed, mobile cations are displaced away from the collagen network with synovial fluid and a mechanically derived streaming potential arises along the flow direction. During the onset of OA, degeneration of cartilage includes decrease in PGs content, disruption of the collagen network and increase in water content, therefore this electromechanical characteristic is associated with the integrity of the cartilage (Nissi et al., 2004; Frank et al., 1987). The loss of GAG from the ECM of hyaline cartilage is the hallmark of early OA and is observed before any radiographic changes are evident (Tiderius et al., 2003).

Streaming potentials have been studied on isolated samples of cartilage in a laboratory setting during mechanical compression. The results suggest that the measurement of streaming potentials from articular cartilage might reflect the structure and composition of cartilage and provide a sensitive index of cartilage degradation (Frank et al., 1987; Bonassar et al., 1995; Garon et al., 2002). Also, an ex-vivo experiment with electrodes embedded in explanted joints revealed that the magnitude of electrical potentials is almost linearly related with the applied force (Schmidt-Rohlfing et al., 2002). Arthro-BST, an arthroscopic device that measures streaming potentials, could be used to assess cartilage quality by manually compressing the indenter against the cartilage surface. The electromechanical quantitative parameter obtained on human tibial plateau

samples by Arthro-BST correlated strongly with both histological and biochemical properties of the cartilage (Sim et al., 2014).

Recently, a novel non-invasive technique called electroarthrography (EAG), based on the non-invasive measurement of streaming potentials, was proposed to assess articular cartilage and diagnose OA by measuring load-induced electrical potentials at the knee surface. The knee is mechanically loaded as the upright subjects shift their weight from one leg to the other during measurements. A clinical study showed that patients with OA had significantly lower EAG values than normal subjects and that patients with total knee replacement (TKR) had almost zero EAG values when the knee was loaded (Préville et al., 2013). Previous modelling work indicated that EAG signals resulting from streaming potentials can be assessed at the surface of the knee, and that the simulated potential distributions are well correlated with the *in vivo* potential distributions (Han, Buschmann, & Savard, 2014). These studies demonstrated that EAG signals originate from the streaming potentials which are sensitive indicator of joint cartilage quality. Therefore, EAG measurements could be used as a promising non-invasive method to characterize cartilage degeneration at an early stage.

However, owing to the structural and mechanical complexity of the knee, the EAG signals depend on many factors. Inter-individual differences can be attributed to characteristics such as the cartilage geometry, thickness, collagen density, gender and alignment of the lower extremities (Fukubayashi & Kurosawa, 1980; Otterness & Eckstein, 2007; Maquet, 1976). This can be investigated with population studies. On the other hand, the mechanisms determining the EAG signals within an individual are not entirely elucidated, which needs further investigation.

The amplitude of streaming potentials depends not only on cartilage integrity, but also on the loading conditions (Garon et al., 2002). In the first EAG experiments, the subjects initially stood on both legs with the foot shoulder-width apart, and then swung slowly to transfer all their body weight to the instrumented leg, which loaded the articular cartilage. Normally, each loading period lasted for 2-3 seconds. After that, the subjects returned to the initial position, with the body weight equally distributed on both legs. In short, the subjects changed from a two-legged stance to one-legged stance to load the measured cartilage. We initially assumed that the change of force acting on the cartilage equals to half of the body weight. However, the leg muscles and soft tissues are programmed to maintain equilibrium, even under static conditions. Overlooking

the muscles' co-contraction would grossly underestimate the load of the knee joint. Indeed, it has been demonstrated that the contact force of the knee joint measured *in vivo* with instrumented knee prostheses is about 2 to 3 times the body weight during a one-legged weight bearing stance, which is similar to the loading technique used during the EAG measurements (Kutzner et al., 2010). Knowledge of the muscle forces that are applied on the tibial plateau during weight shifting is therefore important for explaining the EAG amplitude and to further optimize the measurement protocol.

Being aware of the possible role of muscle forces, the study will focus on the effects of these forces during EAG measurements. The general objective of this study is to validate the hypothesis that muscle contractions impact the EAG signals, and also contribute to the development of new optimized EAG measurement protocols with improved repeatability. Three specific objectives are elaborated in this thesis, each being associated with different hypotheses and developed in a specific paper, as follows.

1.2 Hypotheses and objectives

Objective & hypothesis for paper I

Objective: The objective of the first paper is to investigate how the contraction of specific leg muscles in supine subjects affects the contact force of the knee joint and, in turn, the EAG values.

Hypothesis 1: Muscle contraction can modify the knee contact force and the EAG values measured in the supine position.

Objective & hypotheses for paper II

Objective: The objective of the second paper is to investigate the source of EAG variations observed during a one-legged stance by building two electromechanical models predicting the EAG signal as a function of the ground reaction force (GRF) and the displacement of the centre of pressure (COP).

Hypothesis 1: The COP displacement during a one-legged stance reflects the knee joint contact force due to body weight and muscle forces associated with postural balance.

Hypothesis 2: The combination of GRF and COP displacements can accurately predict EAG potentials.

Objective & hypotheses for paper III

Objective: The objectives of the last paper are to validate the feasibility of a new passive hyperextension loading protocol (PHLP) in the supine position, and to investigate the evolution the electrical potentials measured on the surface of the knee during successive loading cycles of both PHLP and the usual weight shifting protocol (WSP).

Hypothesis 1: PHLP can induce EAG signals with minimal muscle activity.

Hypothesis 2: EAG amplitude decreases with time due to the electromechanical properties of articular cartilage.

1.3 Organization of the thesis

This thesis comprises seven chapters. Chapter 1 describes the general context, the objectives and hypotheses of our study. Chapter 2 presents a critical review of the literature on the knee joint, articular cartilage, cartilage degeneration, OA diagnostic techniques and the EAG technique. Chapters 3, 4 and 5 consist of the three papers whose objectives and hypotheses are respectively described above. Chapter 6 presents a general discussion on our achievements while chapter 7 suggests future work and concludes this thesis.

CHAPTER 2 CRITICAL REVIEW OF THE LITERATURE

2.1 Knee joint

2.1.1 Knee anatomy

A joint is defined as a location in the body where two or more bones meet (Coulson, 2014). The knee joint is one of the largest and most complex joint in the body that connects the bones of the upper and lower leg (Whittle, 2014). It is made up of four main parts: bone, cartilage, ligament and tendon (Figure 2.1) (Kulowski, 1932).

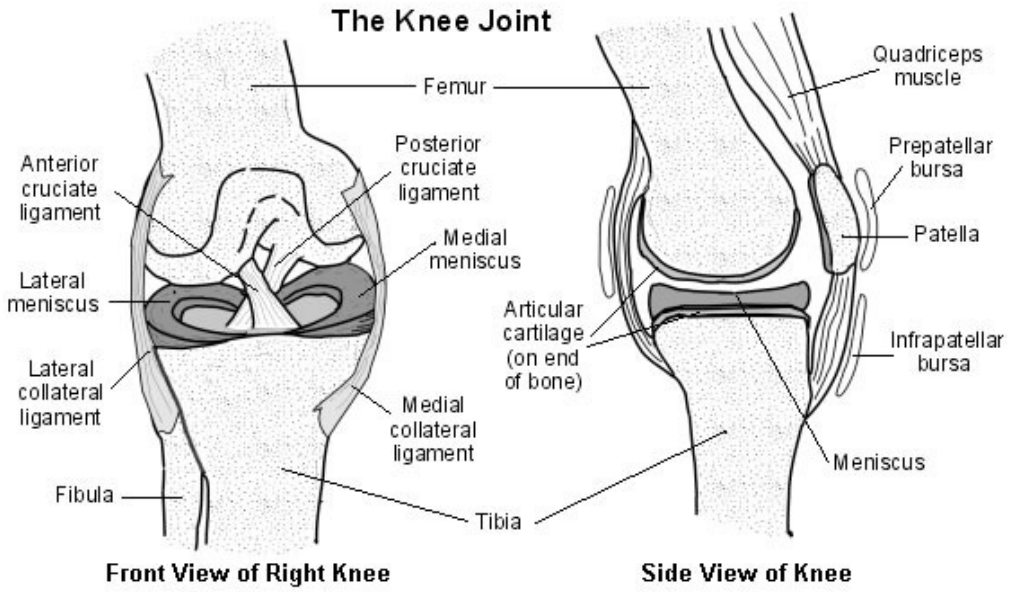

Figure 2.1: Front view (left) and side view (right) of the structure of the knee (Macmull et al., 2010).

The knee joint is formed by the femur (thigh bone), the tibia (shin bone) and the patella (kneecap). The fibula (calf bone), the other bone in the lower leg connecting to the joint, is not directly affected by the hinge action. The distal part of the femur consists of two condyles, which are continuous anteriorly but separated posteriorly by the intercondylar fossa (O'Rahilly & Müller, 1983). The proximal tibia is expanded for articulation with the distal end of the femur

consisting of two condyles separated by an intercondylar area (Drake, Vogl, & Mitchell, 2010). The medial plateau is about 50 percent larger than that of the lateral tibial plateau and the articular cartilage of the medial plateau is thicker than the lateral one (Préville, 2011). This is relevant because of the larger loads in the medial compartment (Laubenthal, Smidt, & Kettelkamp, 1972). The patella is a triangular sesamoid bone embedded in the quadriceps tendon that increases the leverage to lift the leg. In full extension, the lowermost portion of the patella is in contact with the femur. During full flexion, the patella rests entirely in the intercondylar notch, with approximately 7 cm of translation from full extension to flexion (Phillip, 1952).

The ends of the femur and tibia, and the back of the patella are covered with a layer of white shiny substance called hyaline cartilage that protects the knee and makes the joint surfaces slide easily over each other. Moreover, there are two wedge-shaped pieces of fibrous cartilage, called menisci, resting on the medial and lateral tibial plateau. The menisci help to stabilize the knee joint during activities and minimize the amount of stress acting on the articucar cartilage. The combination of the menisci and surface cartilage produces a nearly frictionless surface as the joint flexes, extends or twists.

Ligaments are elastic fibrous bands of tissue that connect a bone to another bone. Two ligaments on either side of the knee, called the medial collateral ligament (MCL) and the lateral collateral ligament (LCL), provide varus-valgus constraint in the frontal plane. The anterior cruciate ligament (ACL) and posterior cruciate ligament (PCL) cross each other to form an “X” inside the knee joint connecting the femur with the tibia. The cruciate ligaments provide anterior-posterior constraint preventing the femur from sliding backward and forward on the tibia respectively. The ligaments surrounding the knee make sure that the weight transmitted through the knee joint is centered within the joint, thus minimizing the amount of wear and tear on the articular cartilage (“Anatomy of knee joint | Aash Arthroscopy Center,” 2011).

Tendons are tough cords of tissue that connect the muscles to the bones. Muscles are responsible for the movement of the knee joint by pulling the bones in different directions (Schmidler, 2015). The muscle shortens when contracting. The bone attached to the muscle is pulled in the direction of the shortening. The main muscles that move the knee joint are the quadriceps and hamstring muscles. The quadriceps attaches to the patella via the quadriceps tendon; the patella is attached

to the tibia via the patellar ligament. The quadriceps muscle, located on the front of the thigh, extend the leg, and the hamstring muscles, located on the back of the thigh, flex the leg.

Besides, numerous bursae surround the knee joint assisting the knee move smoothly. Taken together, these structures work cooperatively to achieve a normal movement of knee joint.

2.1.2 Knee biomechanics

The knee can be conceptualized as two joints: tibiofemoral joint and patellofemoral joint (Flandry & Hommel, 2011).

The two important biomechanical functions of the patellofemoral articulation are to increase the lever arm of the extensor mechanism and to transmit the tensile forces generated by the quadriceps to the patellar ligament. The patellofemoral joint is subjected to complex loading. In full extension, the joint transmits almost all the force of the quadriceps contraction and is thus primarily loaded in tension. When the knee flexes, the patellofemoral joint is subjected to a compressive force, also known as the patellofemoral joint reaction force. At 25 degree of flexion, the force acting on the patellofemoral joint equals that passing through the tibiofemoral joint. The patellofemoral reaction force varies during open kinetic chain (OKC) exercises and closed kinetic chain (CKC) exercises. During OKC activities, which means the feet are free to move, the patellofemoral reaction force increases with increased extension. Conversely, in CKC activities, typically weight bearing exercises, patellofemoral reaction force increases with increased flexion (Scifers, 2008). The patellofemoral joint reaction force can be up to seven times the body weight (BW) during squatting and jogging.

Transmission of the BW from the femur to the tibia is the primary biomechanical function of the tibiofemoral articulation. The knee is the largest weight-bearing joint of the body. In a normal knee, 52 percent of load transmission is absorbed by the knee joint (Hoshino & Wallace, 1987). The tibiofemoral joint reaction force can reach up to three times the BW during walking and five times the BW during stairs climbing (Taylor et al., 2004). The tibiofemoral joint is capable of three translations and rotations (Oatis, 2009).

- *Flexion-extension rotation*. The primary motion of the knee occurs in the sagittal plane. Normal knee flexion ranges from zero degree to 160 degree of deep flexion (Nagura et al., 2002). A small amount of hyperextension, 3 to 5 degree or so, is also possible.

- *Varus-valgus rotation*. The motion in the frontal place is affected by the amount of knee flexion. In full extension, the motion in the frontal plane is the least. The range increases as the knee moves to 30 degree of flexion. Beyond 30 degree of flexion, the motion range decreases due to the soft tissues. The varus-valgus rotation is mainly restrained by the collateral ligaments (Tobias & Johnston, 2013). Varus-valgus rotation of the femur with respect to the tibia can provide unequal loading on the tibial plateau, meaning compression on one plateau and relaxation on the other.
- *Internal-external rotation*. The range of motion in the transverse plane is also influenced by the knee position in the sagittal plane. In full extension, movement is almost completely limited by the interlocking of the femoral and tibial condyles (Nordin & Frankel, 2001). The range of rotation increases as the knee is flexed, reaching its maximum at 90 degree of flexion. In this position, external rotation ranges from zero to approximately 45 degree and internal rotation ranges from zero to around 30 degree (Thambyah, 2005).
- *Medial-lateral translation*. In the normal knee, pure medial-lateral translation is relatively small, ranging from 1 to 2 mm. The collateral ligaments, MCL and LCL, constrain this translation.
- *Anterior-posterior translation*. The allowable anterior-posterior translation ranges from 5 to 10 mm typically, which provides enough laxity in this direction to facilitate optimum tibiofemoral contact (Dennis et al., 1996). The translation is constrained by the cruciate ligaments and the geometry of the condyles, plateau and menisci (Bartel, Davy, & Keaveny, 2006b).
- *Compression-distraction translation*. Another important degree of freedom in the knee joint is the translation along the proximal-distal axis. The translation in this direction includes the available space between the tibia and femur bone and allowable deformation of the cartilage. In compression-distraction testing, displacement can range from 2 to 5 mm (Wiegant et al., 2013).

Despite these multiple degrees of freedom, the primary motion of the knee is flexion and extension, with the other motions coupling together to complete a variety of complex activities. The knee is a vulnerable joint that undergoes a wide range of motion and stress such as lifting and kneeling, and high-impact activities such as jogging and aerobics. In the healthy knee, the

articulation between the bones is lined with articular cartilage to reduce joint friction. The next sections in this chapter will describe the structure, composition and biomechanics of articular cartilage.

2.2 Articular cartilage

Articular cartilage is a highly specialized tissue that covers the bone extremities in diarthrodial joints (Sophia Fox, Bedi, & Rodeo, 2009a). The physiological functions of the articular cartilage are, first, to provide a frictionless joint surface, and second, to sustain and distribute loads between the bones, allowing the joint to have relative motion along multiple directions (Légaré et al., 2002b). The knee joint is highly loaded during daily life. The average peak load on the tibiofemoral joint is around 3 to 4.4 times the BW during walking cycles in healthy subjects (Kumar, Manal, & Rudolph, 2013). Generally, cartilage acts as a shock absorber, enabling joint mobility and movement over a lifetime. In order to accomplish these functions, articular cartilage has unique mechanical properties determined by the composition and structure of this tissue.

2.2.1 Composition

Articular cartilage is composed of a dense ECM with a sparse distribution of chondrocyte cells. In principle, the ECM of cartilage consists of water (65 to 80 percent of wet weight), collagen (15 to 20 percent of wet weight), PGs (10 to 15 percent of wet weight) and other noncollagenous proteins present in smaller amounts (Nap & Szleifer, 2008; Hayes, Brower, & John, 2001).

The main component of articular cartilage is water that accounts for 80% of the wet weight at the superficial zone and decreases to 65% in the deep zone (Bhosale & Richardson, 2008; Comper, 1996). Approximately 30% of the water is saved in the intra-fibrillar space, while the remainder is contained in the pore space of the ECM. The presence of water permits the deformation of the cartilage during loading. In addition, the water flowing through the ECM helps transport nutrients to the chondrocytes (Sophia Fox et al., 2009a). The water content increases with degenerative changes, resulting in a degradation of the compressive properties of the cartilage (Mankin & Thrasher, 1975).

Collagen is the most abundant macromolecule in the ECM which takes up to 60% of the dry weight of the cartilage. It is defined as a structural protein that interacts to form a cartilaginous framework. Type II collagen represents 90% to 95% of the collagen in ECM, while a small

amount of types V, VI, IX, X, and XI collagen are also present (Blitterswijk & Boer, 2014). The collagen fibril acts as a "biological rope" and is mainly responsible for the tensile strength of the cartilage during compression. It has been reported that the tensile stiffness of cartilage is strongly influenced by the natural variation of collagen content (Sokoloff, 2014). Collagen cannot sustain compression by itself. The collagen plays a role in compressive behaviour by constraining the separation and free expansion of the PG molecules (Anila Namboodiripad, 2014; Bartel et al., 2006b).

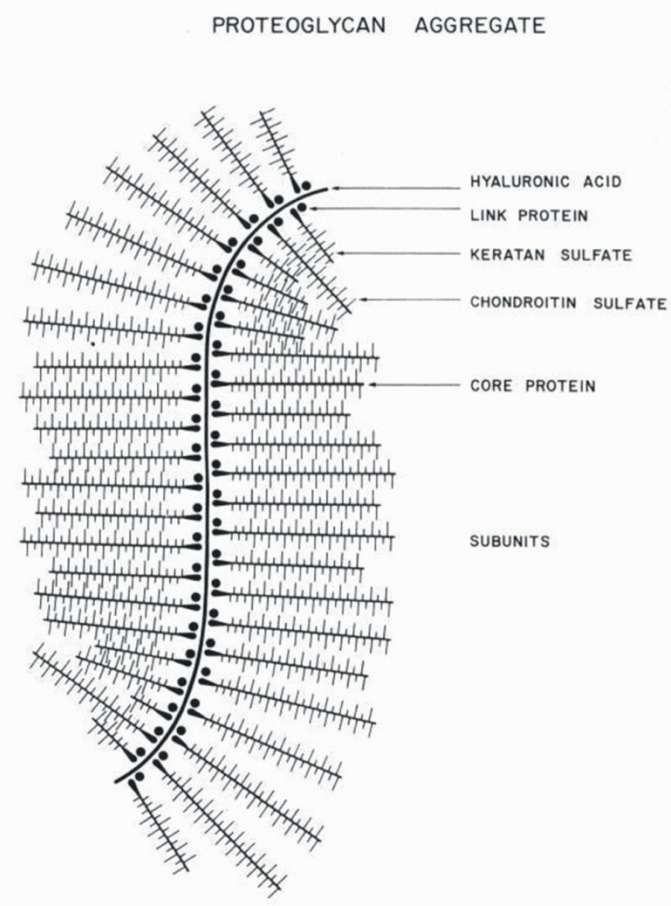

Figure 2.2: Structure of Proteoglycans aggregate (Mow & Lai, 1979).

PG is a glycosylated protein monomer that consists of a central long protein core which is covalently bounded by chondroitin sulfate and keratan sulfate GAG chains (Bartel et al., 2006b). The main PG macromolecule (Figure 2.2) in cartilage is the large aggregating type, called

aggrecans. Many aggrecans molecules link together on a long hyaluronic acid backbone forming a large proteoglycan complex that is immobilized in the collagen network. The GAG chains contain ample negatively charged carboxyl and sulphate groups, which in turn attract positive counter-ions such as calcium and sodium to maintain electroneutrality (Ronald E. Hileman, 1998). The negatively charged groups are very close to each other (1.0 to 1.5 nm); therefore, the charge-to-charge repulsive force acting between charged groups contributes significantly to the rigidity of the tissue in compression (Barbucci, 2007).

The cells in the cartilage are chondrocytes, which account for around 1% to 5% of the wet weight; they are sparsely distributed within the ECM. Chondrocytes derive from chondroblasts that are trapped in small spaces called lacunae (Miller, Thompson, & Hart, 2012). They are responsible for synthesizing all the matrix components and regulating the metabolism. Hence, the existence and maintenance of the matrix depend on the chondrocytes (James & Uhl, 2001).

2.2.2 Structure

Typical thickness of healthy cartilage varies from 2 to 4 mm (Sophia Fox, Bedi, & Rodeo, 2009b). The structure of articular cartilage exhibits depth-dependent anisotropic properties (Xia, Ramakrishnan, & Bidthanapally, 2007). Cartilage also displays zonal heterogeneity in concentrations of collagen fibre, PG, and water (Boskey & Camacho, 2007). Cartilage can be divided into four major zones: superficial tangential zone (STZ), middle zone, deep zone and calcified zone, based on the shape of the chondrocytes and the orientation of collagen fibres (Figure 2.3).

In the STZ, which accounts for 10% to 20% of the total thickness of articular cartilage, the collagen fibres are organized firmly and aligned tangential to the surface. The collagen and water content is highest, while the sparsely distributed PG has the lowest concentration in this region. This is the layer where the tissue is exposed to the highest tensile and compressive stresses. The orientation of collagen fibres in this zone helps to resist the shear force created during joint use (Joseph A et al., 2005). In fact, this zone is responsible for withstanding most of the tensile forces in the cartilage. The superficial zone includes flattened chondrocytes.

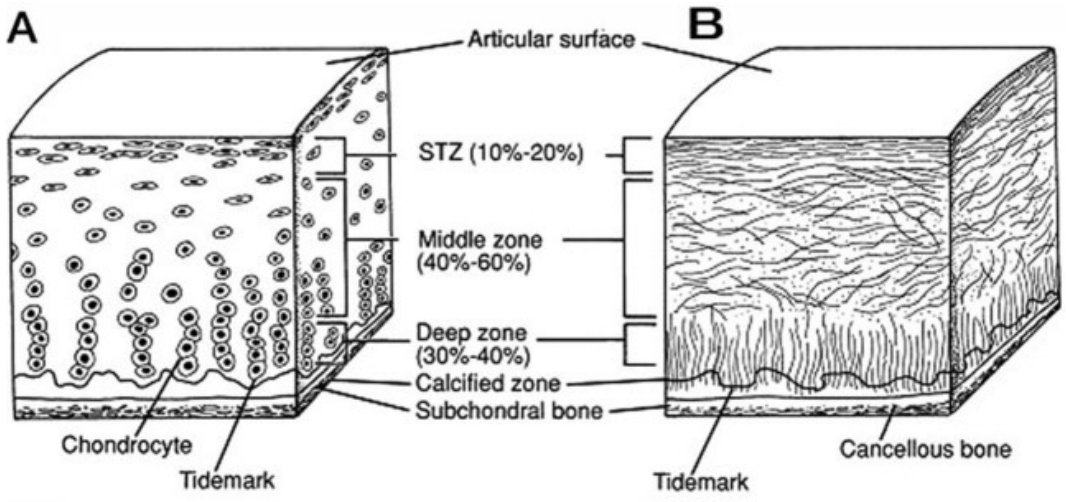

Figure 2.3: Schematic structure of healthy articular cartilage: A: cellular organization in the zones of cartilage; B: collagen fiber orientation (Buckwalter, Mow, & Ratcliffe, 1994).

The middle zone is located immediately below the STZ, and it occupies about 40 to 60 percent of the total layer volume. This region tends to be isotropic with abundant PG content. The collagen fibres have a larger diameter and are arranged randomly in this layer (Mow & Huiskes, 2005). The round chondrocytes are distributed sparsely in this region.

The next zone, which comprises 30 to 40 percent of the total thickness, is the deep zone. In this zone, the collagen fibres, which increase to their largest diameter, are woven together to form large bundles perpendicular to the surface and that cross the tidemark. The collagen content decreases by 15 percent from the STZ to the middle and deep zones. Conversely, the PG content increases by 15 percent from the surface layer to the deep zone (Jackson & Gu, 2009). Therefore, the deep zone provides the greatest resistance to the compression due to the highest PG content. Water content generally decreases with depth also, herein the deep zone contains the lowest water concentration. The round chondrocytes are aligned in a columnar fashion, parallel to the collagen fibres in this layer.

Finally, a visible border called the tidemark distinguishes the deep zone from the calcified zone which is next to the underlying subchondral bone. Of note, the calcified zone contains a combination of cartilage and mineral; so this mineralized zone exhibits a very low metabolic activity due to the small volume of cells embedded in the calcified matrix. The chondrocytes in

this zone express an hypertrophic phenotype (Bronner & Farach-Carson, 2007). The calcified zone plays an importance role in separating the cartilage and the bone, by anchoring the collagen fibres from the deep zone to the subchondral bone (Hwang, 2010).

2.3 Biomechanics of articular cartilage

The unique mechanical behaviour of cartilage is attributed to its complex structure, specifically, the interactions among the various components of the ECM. From a biomechanical perspective, articular cartilage can be considered as a biphasic medium: a liquid phase, composed of fluids and electrolytes, and a solid phase, composed of collagen in a fibrillar form, PGs and chondrocytes (Hasler et al., 1999). The interstitial space of the permeable matrix which is constituted by collagen fibres and PG is filled with water and dissolved electrolytes. Under compressive loading, the interstitial fluid is redistributed as it flows out of the deformed solid matrix generating a large frictional drag on the matrix (Mow, Holmes, & Lai, 1984). When the compressive load is removed, interstitial fluid flows back into the tissue which returns to its original shape. The low permeability of articular cartilage prevents the fluid from being quickly squeezed out of the matrix to reach its final equilibrium state (Mow, Kuei, Lai, & Armstrong, 1980).

Compressive testing has been widely used for the determination of the mechanical properties of soft tissues. Experimentally, three different measurement configurations can be used: unconfined compression, confined compression and indentation (Figure 2.4). In unconfined compression, an articular cartilage sample is compressed between two smooth non-porous plates by a predefined stress. The lateral edges of the cartilage disk remain free allowing interstitial fluid flow out of the tissue only in the lateral direction (Langelier & Buschmann, 2003). In confined compression, the sample disk is placed in a sealed chamber and the disk surface is compressed by a permeable filter. In this geometry, the interstitial fluid can only flow uniaxially through the sample surface into the filter. The compression tests are carried out, either in confined or unconfined geometries, on full thickness cartilage disks which are extracted from the joint surface (Soulhat, Buschmann, & Shirazi-Adl, 1999). For indentation testing, the load is applied through a cylindrical indenter, impermeable or permeable, while the sample remains on the subchondral bone. In this condition, fluid is able to flow outside the indenter-tissue contact point in both the lateral and axial directions. Since indentation testing does not require a preparation of separate tissue samples, it is

not limited to the laboratory and it can be performed also *in vivo* (Korhonen & Saarakkal, 2011). Unconfined compression and indentation may provide better representations of physiological loading compared to confined compression because interstitial fluid is permitted to flow laterally in these geometries (Changoor, 2011; Vasara et al., 2005). The advantage of confined compression is that the stress, strain, and flow of water are wholly axial which makes the results easier to interpret (Lanza, Langer, & Vacanti, 2011).

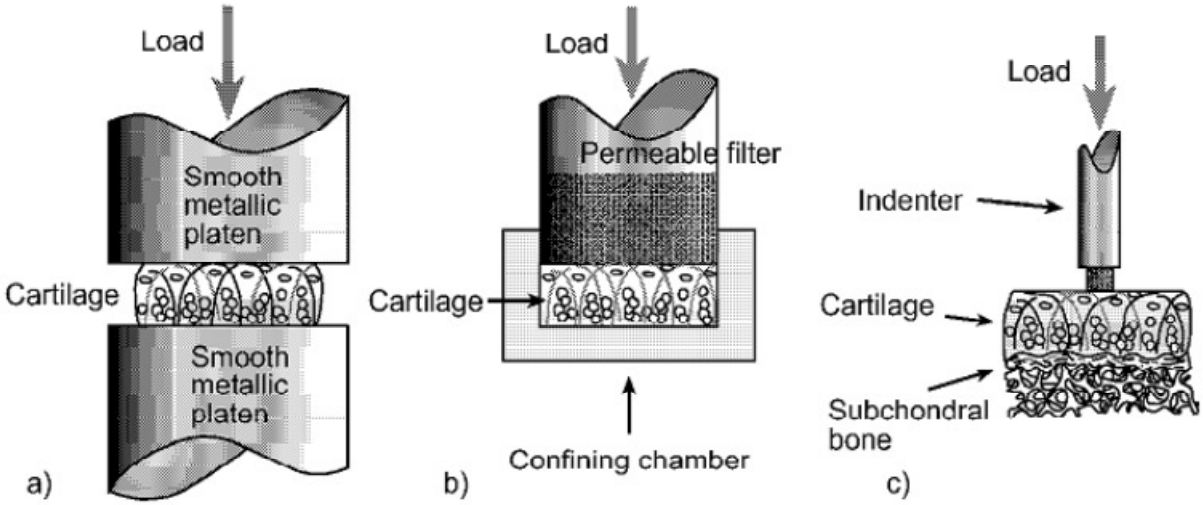

Figure 2.4: Unconfined, confined and indentation loading geometries for testing the mechanical properties of articular cartilage (Korhonen, 2003).

Articular cartilage displays anisotropy, heterogeneity, nonlinear elasticity and viscoelasticity properties under compression. As discussed previously, articular cartilage as well as other soft tissues is an anisotropic and heterogeneous material (Netti & Ambrosio, 2002). Cartilage shows an anisotropic behaviour in tension, exhibiting a higher tensile stiffness along a direction parallel to the surface (Huang et al. 2005). Also, it has been well established that cartilage is inhomogeneous, thus the measured properties in tension or compression may vary from the superficial to the deep zones (Krishnan et al., 2003).

2.3.1 Nonlinear elasticity

It is important to investigate the stress-strain behaviour of the tissue to predict its load carrying capacity. A typical static stress-strain curve is represented in Figure 2.5 when no fluid flow is assumed.

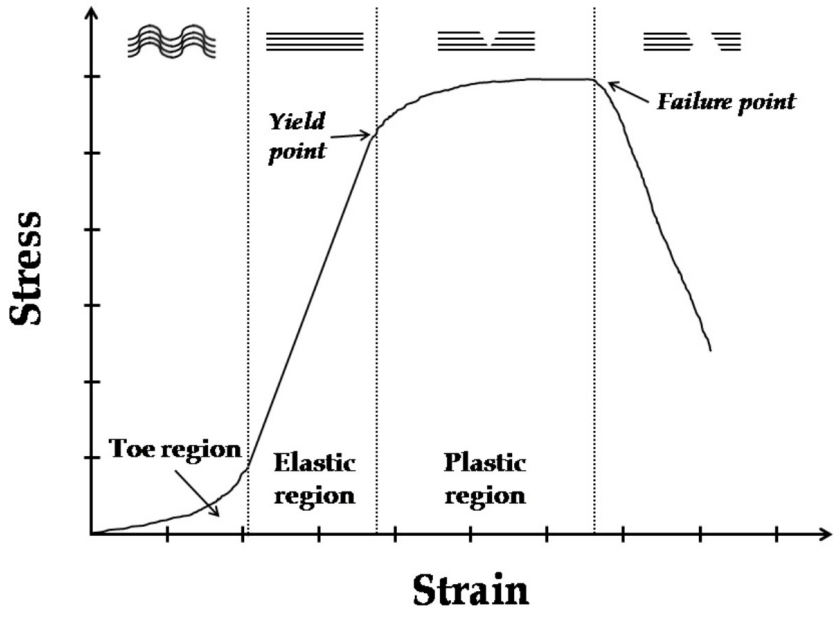

Figure 2.5: Typical stress-strain curve for articular cartilage subjected to tensile loading at low constant rate. The diagrams at the top of the figure indicate collagen fibres straightening and failure, related to the different regions of the stress-strain curve (Korhonen & Saarakkal, 2011).

At the initial phase of the tension test, the relation between stress and strain is nonlinear, presenting an initial upward curvature (toe region). The reason for the increasing slope is the straightening of the randomly arranged collagen fibrils in the middle zone. When the collagen fibres are completely straightened, the stress-strain curve reaches its elastic region. In this region, the stress and strain are linearly related and the slope of this region is called the Young's modulus, it represents the resistance ability of the tissue (Barber, 2011). The linear relationship arises from the alignment of the collagen fibrils in the stretched direction and all changes in the tissue are still reversible. When the stress is further increased after the elastic region, the slope of the curve changes and the plastic region begins. The yield point is the transition point between

the elastic and plastic deformations (Screen, 2008). After the yield point, microstructural damage in the collagen fibres network occurs and the material will not return to its original shape (Tanaka & Eijden, 2003). After the plastic region, further stretching causes progressive fibre disruption and ultimately, complete rupture. The location of the breakdown is called the failure point, which is a typical parameter reported for soft tissues under destructive tensile testing.

This type of static tensile test can induce a flow of fluid from the cartilage sample. Therefore, to better assess the tensile property of the solid matrix, the test should be performed at a very low rate. In faster testing, the Young's modulus increases with the increasing strain rate, which can be interpreted as strain rate sensitivity (Bartel et al., 2006b). Also, the Young's modulus depends on the depth and orientation of the sample due to the anisotropy and heterogeneity of the cartilage.

2.3.2 Viscoelasticity

Articular cartilage is a viscoelastic material exhibiting time-dependent mechanical behaviour (Poitout, 2013). Specifically, the relationship between stress and strain is not constant but depends on the time of displacement or load (Desrochers, Amrein, & Matyas, 2012). There are three major characteristics of viscoelastic materials: stress-relaxation, creep and hysteresis (Robi et al., 2013).

In a stress-relaxation test (Figure 2.6, top), a predefined compressive displacement is applied as a ramp followed by a constant displacement. Meanwhile, the loading rises to a peak value at timet_0, which is followed by a progressive stress-relaxation process until an equilibrium value is reached. Creep is another feature of articular cartilage indicating an increasing deformation under a constant load (Figure 2.6, bottom). When a constant loading is suddenly applied to the cartilage, the deformation of cartilage increases with time until an equilibrium condition is reached. All biphasic and viscoelastic soft tissues show an initial relaxation phase in both testing protocols, and finally when no fluid flow or pressure gradients persist, the tissue reaches its equilibrium state. Consequently, a constant level of strain (in a creep test) or stress (in a stress-relaxation test) follows a relaxation phase, and then the entire load is carried by the solid matrix of tissue (Korhonen & Saarakkal, 2011). Hysteresis indicates that the loading curve and the unloading curve are different from each other. When articular cartilage is loaded and unloaded, the unloading curve will not follow the loading curve due to the energy dissipation which is lost

as heat. If compressive tests are repeated several times, different curves are obtained expressing the reduction of hysteresis under cyclic loading (Kelm, 2002).

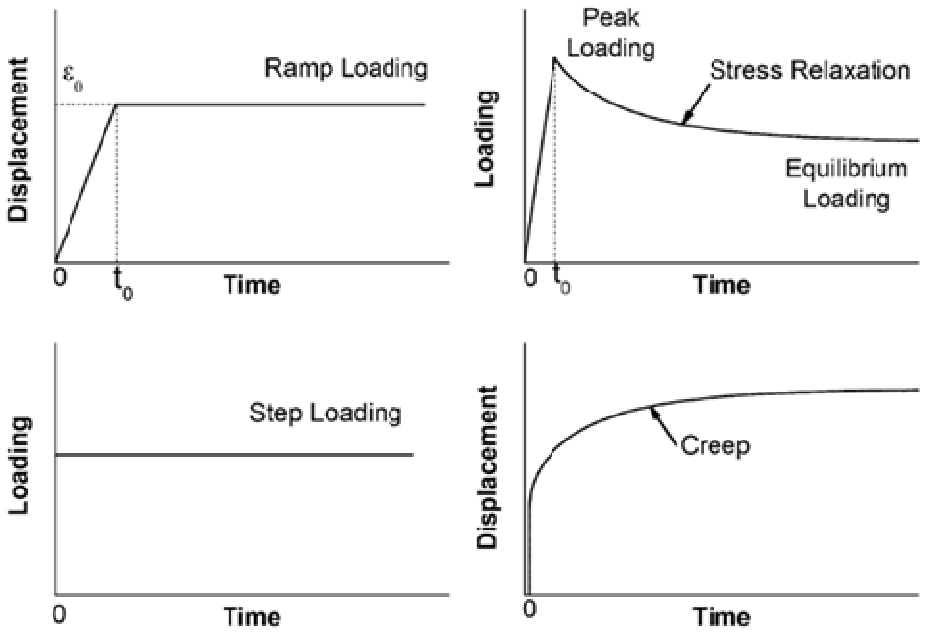

Figure 2.6: Temporal profiles of displacement and loading during compression tests showing stress relaxation (top) and creep (bottom) (Lu & Mow, 2008).

To date, the most successful theory explaining cartilage compressive viscoelastic behaviour is the biphasic theory developed by Mow et al. (1980). Using the biphasic theory, creep and stress relaxation behaviour in compression of articular cartilage can be well understood. The viscoelastic response of articular cartilage mainly arises from two sources: a) the fluid-dependent mechanism caused by the frictional drag force of interstitial fluid flow through the porous solid matrix; b) the fluid-independent mechanism that depends on the intrinsic viscoelastic properties of the macromolecules that form the solid matrix (Huang, 2001; June et al., 2011).

Physically, when cartilage is compressed, the fluid phase flows and is extruded from the matrix under the influence of the pressure gradient produced by mechanical deformation. The fluid passing through the porous solid matrix generates very high frictional drag which is the primary mechanism responsible for the viscoelastic behaviour of articular cartilage under compression

(Lu & Mow, 2008). More importantly, since the permeability of normal cartilage is extremely small, when cartilage is compressed and fluid is forced out, its permeability decreases further to prevent loss of fluid (Mansour, 2003). As a result, the pressurized fluid component provides a significant component of total load support, thereby reducing the stress acting upon the solid matrix (Netti & Ambrosio, 2002). The stiffness of the solid matrix mainly depends on the rigidity of the network resulting from the repulsive force acting between the charged groups of PG (Soltz & Ateshian, 1998).

In conclusion, the fluid and solid phases of the cartilage play a significant role in the mechanical behaviour of cartilage. Subsequent sections will describe cartilage degeneration and summarize current assessment techniques.

2.4 Cartilage degeneration

There are two major forms of arthritis, OA and rheumatoid arthritis (RA). The former is known as a joint disease resulting from the degeneration of joint cartilage and underlying bone, while the latter one is related to the inflammation of the tissue (Arden et al., 2015). OA is a chronic degenerative disease known to damage the composition, structure and functional properties of cartilage tissue leading to pain, loss of ability or joint deformity.

2.4.1 Epidemiology

OA is the most prevalent joint disorder globally (Felson et al., 2000). According to a report from the Dutch Institute for Public Health, the prevalence of knee OA is 15.6 percent in men and 30.5 percent in women for those aged 55 and above (Bijlsma & Knahr, 2007). In participants aged from 55 to 64 y.o. of the Johnston County Osteoarthritis Project, the prevalence of radiographic knee OA is 28 percent and symptomatic knee OA is 16 percent (Jordan et al., 2007). Prevalence rates for knee OA, based on population studies in the US, are comparable to those in Europe (Litwic et al., 2013). Eighty percent of subjects with symptomatic OA have limitations in movement, and a quarter of them even cannot complete their daily activities of life. Due to the aging of the population and the obesity epidemic, the number of people affected with symptomatic OA is likely to increase. It is estimated that by 2050, 130 million people will suffer from OA worldwide, of whom 40 million will have severe disability. In the United States, OA

carries an annual cost of nearly $65 billion surveyed by Centers for Disease Control and Prevention (DeFrances & Podgornik, 2006).

OA has multifactorial etiologies, which can be categorized as modifiable and non-modifiable factors (Inoue et al., 2011). The modifiable factors include obesity, knee injury, occupation, muscle weakness and metabolic syndrome, while the non-modifiable factors are associated with gender showing higher prevalence in female than male, age, genetics and race. The modifiable factors are more related with the excessive knee stress and their modification may reduce the risk and development of joint OA (Zhang & Jordan, 2010). There are strong evidences indicating that genetic inheritance is a factor, as approximately 60 percent of all OA cases are associated to genetic factors (Wittenauer, Smith, & Aden, 2013). The most significant risk factor of OA is advancing age (Chaganti & Lane, 2011).

2.4.2 Pathophysiology

Damage from mechanical loading with insufficient self-repair ability is believed to be the primary cause of initiation and progression of OA (Brandt, Dieppe, & Radin, 2008; Felson, 2013). The chondrocytes in the matrix produce collagen, PGs and enzymes to maintain the mechanical function of cartilage. Because cartilage is avascular, the chondrocytes rely on diffusion from the articular surface and subchondral bone for exchange of nutrients and oxygen (Sharma & Berenbaum, 2007). Consequently, the biological repair mechanisms are inhibited and the synthesis of matrix components is very slow (Bijlsma, Berenbaum, & Lafeber, 2011a). The turnover of collagen is estimated to occur with a half-life between 100 and 400 years (Verzijl et al., 2000). On one hand, the mechanical loading of articular cartilage can stimulate the metabolism of chondrocytes and matrix synthesis. On the other hand, excess stress suppresses matrix synthesis and promotes chondrolysis. Furthermore, with loss of tissue integrity, the injured cartilage is more vulnerable to damage during subsequent joint loading. Animal studies have shown that when excessive knee loading is induced, OA progression is accelerated (Appleton et al., 2007). On the contrary, when cartilage is unloaded, progression of OA may be slowed or even reversed (Lafeber et al., 2006). Normally, the threshold for harmful loading is quantified as 5 MPa (Beecher et al., 2007).

Besides, the cartilage is also aneural. Patients often experience little pain until substantial cartilage damage has occurred. At this point, cartilage degeneration is usually in an advanced

phase, for which joint surgeries are needed. Therefore, OA is the most common reason for total knee replacement (TKR) (DeFrances & Podgornik, 2006).

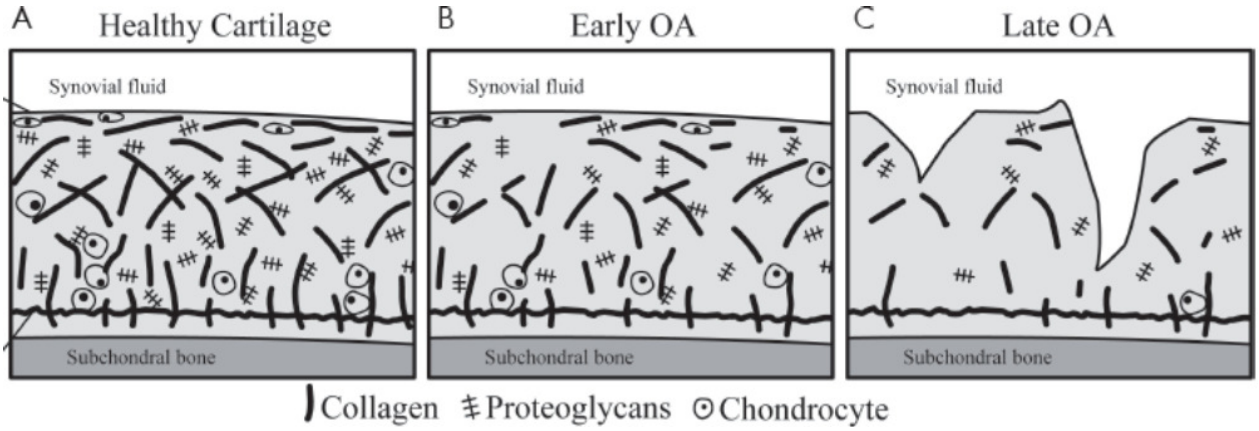

Figure 2.7: Representation of articular cartilage degeneration in two phases (adjusted from (Matzat et al., 2013)).

In OA, the degeneration of cartilage can be divided into the following two phases. In healthy cartilage (Figure 2.7A), articular cartilage provides a frictionless and shock-absorbing layer between the bones. The collagen matrix is well organized and PGs are abundant (Matzat et al., 2013). In early stage of OA (Figure 2.7B), the collagen matrix begins to break down and PGs are initially depleted. The tensile properties of the cartilage are widely maintained by the collagen network, its disruption is known to be irreversible (Buckwalter & Mankin, 1997). The breakdown of collagen fibres results in a net increase in water content and decrease of PGs content. In OA, water content becomes more than 90 percent due to increased permeability and disruption of the collagen framework (Bhosale & Richardson, 2008). This may decrease the elasticity of tissue and thus reduces the load bearing capability of the articular cartilage. This reduction in stiffness gives rise to further cartilage degradation. In this stage, little morphological structure change can be observed and the joint functions without any impairment or pain. In the late stage of OA (Figure 2.7C), PGs become severely depleted and the thickness of cartilage decreases leading to significant narrowing of joint space. The cartilage loss might take place progressively until the subchondral bone is exposed. Pain and loss of joint function are common manifestations in this stage.

Clinically, the International Cartilage Repair Society (ICRS) classifies the tissue status into five grades, from Grade 0 indicating healthy cartilage to Grade 4 showing absence of cartilage with exposed subchondral bone (Kleemann, 2005).

2.5 Assessing cartilage quality

Nowadays, there are a variety of techniques available to assess cartilage quality. The changes in symptoms, functional status, joint inflammation, physiology and structure of tissue are of particular interest (Jones et al., 1992). Methods currently employed for assessing cartilage quality can be divided into three categories.

2.5.1 Clinical evaluation

The first category is the clinical evaluation. It usually includes patient reported history and physical examination. Since the progression of OA is characteristically slow, lasting over several years or decades, a physician often discovers valuable information about possible causes of symptoms through the reported medical history. Pain and stiffness are the principle symptoms included in any clinical assessment of the patient with OA (Jones et al., 1992). It has been reported that 95 percent of patients suffer pain and 76 percent suffer stiffness (McGinty & Burkhart, 2003). During disease progression, the patient may suffer more and more pain and stiffness resulting in physical activity limitation. During the physical examination, the local temperature, joint tenderness, synovial swelling, range of motion and crepitus are usually evaluated. The American College of Rheumatology (ACR) has developed classification criteria for the clinical assessment of knee OA. However, these criteria cannot be used for a definitive diagnosis (Peat, Croft, & Hay, 2001). The advantages of clinical evaluation are non-invasiveness and potential long time follow-up.

2.5.2 Imaging techniques

The second class of techniques used in cartilage quality assessment is radiological imaging such as radiographs (X-rays), MRI and CT. OA is typically diagnosed on the basis of radiographic imaging findings. Since cartilage is not directly visualized through radiographic imaging, OA can eventually be definitively characterized through osteoarthritic related changes including joint

space narrowing, cartilage defect, subchondral sclerosis, osteophytosis and subchondral cysts (Chan et al., 1991).

Clinically, X-ray remains the most common and widely available diagnostic imaging technique despite the development of novel imaging techniques (Braun & Gold, 2012). Even if the patients need more sophisticated exam, they will probably get an initial X-ray due to its cost-efficiency and operating convenience. The knee joint being pictured is positioned between the X-ray source and photographic film or sensor array. The machine briefly sends X-rays through the joint, exposing the film or sensor array to reflect the internal structure of joint. X-ray is quite safe since the level of radiation exposure is low enough. Bones and other dense materials appear white because they absorb the radiation. On the other hand, less dense materials such as soft tissues and breaks of bone let radiation pass through, making these parts look darker on the X-ray image. This feature limits the use of X-ray to evaluate the bony characteristics like joint space narrowing, osteophytes and subchondral formation ("Primary Osteoarthritis Imaging," 2015). The standard X-ray assessment is performed as the patient is in a weight-bearing condition with both knees in full extension. In weight-bearing joints, the net loss of articular cartilage manifests itself as a reduction of joint space in those areas subjected to pressure; this effect is in contrast to that of inflammatory arthritis, in which uniform joint-space narrowing appears. Different abnormalities can be observed in the weight-bearing and non-weight-bearing areas of the affected joint. In the weight-bearing areas of the joint, X-ray can depicts joint space narrowing, as well as subchondral bony sclerosis and cyst formation. In the areas without pressure, osteophytes can be detected. More recently, X-ray may be performed from several angles because the flexed-knee X-ray can improve the intra-articular visualization (Braun & Gold, 2012). The disadvantages of X-rays are: 1) it may not show much detail of the soft tissues; 2) it is insensitive to early chondral damage (Gold et al., 2009).

MRI is a modern diagnostic imaging technique that produces cross-sectional images of the knee joint, which is considered to be the gold standard in medical imaging (Loeuille, 2012). It is a reliable technique that allows non-invasive evaluation of morphological changes in cartilage. Unlike X-ray, MRI can depict articular cartilage directly. The major advantage of MRI is that it manipulates image contrast to highlight the different tissue types in the cartilage (Crema et al., 2011). As a result, a variety of pulse sequences have been developed focusing on the morphologic assessment, quantification of tissue volume and evaluation of biochemical

composition over the past decades (Crema et al., 2011). MRI works without radiation. The MRI system creates a magnetic field and then pulses radio waves to the area around the knee joint as the patient lies motionless. The radio waves cause the nucleus to resonate. A computer records the rate at which various parts of knee (tendons, ligaments, nerves, etc.) give off these oscillations, and translates the data into a detailed, two-dimensional picture.

Nowadays, MRI enables both morphologic and physiologic imaging of cartilage tissue. Morphological assessments focus on imaging of tissue size and structural integrity. Fissuring, diffuse thinning and focal cartilage loss are signs of the abnormalities. The major techniques in morphologic imaging include spin echo (SE) and gradient-recalled echo (GRE) sequences, fast SE, three-dimension SE, GRE and three-dimension spoiled gradient recalled echo imaging with fat suppression (3D-SPGR) which is the current standard for morphological imaging of cartilage (Braun & Gold, 2012). In 3D-SPGR, excellent resolution images with high cartilage signal and low fluid signal can be obtained.

Quantitative MRI has demonstrated the ability to detect physiological changes associated with early OA degeneration prior to the morphological cartilage abnormalities that follows as OA progression (Matzat et al., 2013). Quantitative imaging techniques, such as T2 mapping, delayed gadolinium enhanced MR imaging of cartilage (dGEMRIC), T1rho mapping, sodium MRI and diffusion-weighted imaging (DWI), provide information about the molecular composition of cartilage (Matzat et al., 2014). In early OA, the collagen network breaks down and the PG content decreases which result in increased water content. These macromolecule changes are the hallmarks of early OA progression in quantitative MRI. For example, dGEMRIC, T1rho mapping and sodium MRI depend upon the estimation of GAG concentration. In dGEMRIC, contrast agent (Gd-DTPA2-) which distributes inversely with respect to the GAG molecules, is injected into the ECM. As such, relative concentration and spatial distribution of GAG can be mapped (Changoor, 2011). T2 mapping, performed without a contrast agent, is a commonly used tool for measuring water content in cartilage and allows indirect assessment of collagen content and organization (Choi & Gold, 2011). Physiological MRI shows promise to identify OA at an early stage. One major challenge of this technique is that there is no highly-sensitive reference standard with which to compare the results. The outcomes of physiological MRI have to be compared with morphological findings, operative examination or data from healthy subjects. So far, there is not

a well-established reference to quantify the molecular changes associated with histological grading (Matzat et al., 2013).

The sensitivity of MRI for cartilage quality assessments and bone marrow exceeds the X-ray; however, due to low resolution, it is still challenging for MRI to evaluate OA at an early stage. Moreover, MRI imaging is high-cost and requires long acquisition times and complex data processing (Chu et al., 2012).

CT is an imaging technique that combines X-rays with computer technology to produce cross-sectional images of the tissues. CT is superior to conventional X-ray because it provides tomographic assessment of soft tissue and a better evaluation of bone loss (Chan et al., 1991). In patients who cannot tolerate MRI, CT scanning after the intra-articular injection of contrast material can be useful for the depiction of articular cartilage disease and diagnosis of OA related to bony structure ("Primary Osteoarthritis Imaging," 2015). A CT scan costs more and takes more time than a regular X-ray.

2.5.3 Arthroscopy

The third class of diagnostic techniques is known as arthroscopy and is considered to be the clinical standard to assess the state of the articular cartilage. Arthroscopy is a minimally invasive surgical procedure permitting direct visualization and tactile feedback of intra-articular structures (Chu et al., 2012). It allows a more detailed description of the depth and extent of the lesions which are not visible through imaging, especially in early OA stage. These arthroscopic subtle changes include cartilage softening by palpation, superficial surface fibrillations, tangential flaking, when no bone marrow and cartilage loss are involved (Brismar et al., 2002; Chu et al., 2010). Several classifications of the pathology of articular cartilage have been proposed based on the depth and distribution of lesions. The most commonly cited classification describing chondral lesions is Outerbridge arthroscopic grading system determined by the gross appearance of the defects. Recently, a modified Outerbridge grading system is frequently used in literature and depends on the depth of fissuring or fibrillation (McGinty & Burkhart, 2003).

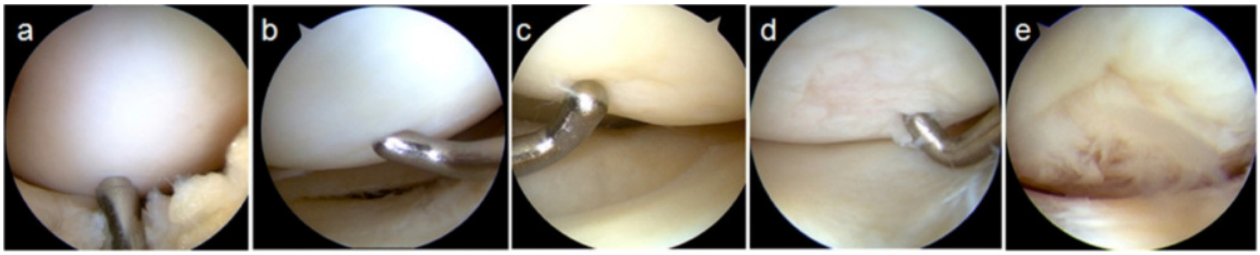

Figure 2.8: Sample arthroscopic images demonstrating different grades of the modified Outerbridge grading system. a) Grade 0: normal cartilage. b) Grade I: softening and swelling. c) Grade II: partial-thickness fissuring (<50% depth). d) Grade III: deep fissuring without exposed bone (>50% depth). e) Grade IV: full-thickness tissue disruption extending to the subchondral bone (Chu et al., 2012).

In this technique, a 3 to 4 mm incision is made on the knee to allow the insertion of a small optical fibre camera (arthroscope). The arthroscope is capable of sending pictures of the cartilage to a monitor (Figure 2.8). The surgeon can then assess the quality of cartilage, and at the same time perform some treatment through the incision including trimming, repairing torn cartilage, removing losses bodies or ligament reconstruction.

In addition, optical coherence tomography (OCT) incorporated into the arthroscope can provide cross-sectional images of articular cartilage in near real time. The resolution of this technique is around 10 to 20 μm, which is comparable to low-power histology (Chu et al., 2010). Arthroscopic OCT images of cartilage are obtained by placing a light source adjacent to the cartilage surface by a hand-held probe and capturing backscattered infrared light. OCT is sensitive to collagen structural changes and cartilage birefringence changes associated with early OA (Braun & Gold, 2012). Therefore, this technique has powerful potential for detection of early cartilage degeneration by providing quantifiable, microscopic resolution cross-sectional information of the cartilage surface.

Even though arthroscopy is the clinical standard of cartilage assessment by providing intra-tissue structure, the limitation of this technique is the invasiveness requiring direct contact with the articular surface. The potential complications of arthroscopy surgery are hemarthrosis, iatrogenic articular cartilage damage and neurovascular injury (Miller et al., 2012).

In conclusion, although there are many reliable techniques to diagnose knee OA as described, an economical method that can be used for early detection is not available. Pain and stiffness cannot be used as an early sign of knee degeneration since there is no sensation in cartilage area. Imaging technique permits non-invasive macroscopic resolution assessment of cartilage integrity; however the imaging findings may be normal in the early stage of OA. Arthroscopy is the most accurate approach, whereas the risks and cost coupled with surgical diagnosis are the largest. As discussed previously, the progression of OA is strongly associated with highly modifiable risk factors like overload, knee injury and obesity; thus characterization of early OA is critical to prevent, reverse or at least slow down the progression of the degeneration by appropriate interventions. Many attempts have been made to develop a simple technique to diagnosis OA at the very beginning. A novel technology exhibiting the potential ability to diagnosis OA in early stage will be introduced in the next section.

2.6 Electroarthrography

Electroarthrography (EAG) refers to a non-invasive measurement of loaded-induced electrical potentials produced by cartilage at the surface of the knee, based on the streaming potential theory. This recently proposed technology aims to assess articular cartilage quality and diagnose joint degeneration at the early stage. Previous studies have indicated that the amplitude of streaming potential could be sensitive to integrity of cartilage matrix, and EAG signals arising from the streaming potentials in cartilage could be detected at the surface of knee by electrodes. All of these make EAG a promising method for non-invasive assessment of cartilage degeneration (Légaré et al., 2002b; Préville et al., 2013).

2.6.1 Streaming potentials

We have discussed previously the mechanical response of articular cartilage in static compression. In a dynamic situation, the existence of fixed negative charges and the mobile counterions in the fluid gives rise to a noticeable electromechanical behaviour resulting from an electrokinetic phenomenon, known as the streaming potentials (Netti & Ambrosio, 2002; Bazant, 2011).

Without external loading, the positive mobile ions attracted by the PGs distribute symmetrically in the solution. When cartilage is compressed, interstitial fluid carrying positive ions is displaced

relative to the fixed PG molecules entrapped in the collagen network, leading to a transient perturbation in the electrical field of the tissue (Lai et al., 2000). This charge separation phenomenon induces an electrical field along the fluid streamlines, called streaming potentials (Garon et al., 2002). The charged PGs are mainly responsible for the streaming potential effect which plays an important biomechanical role in controlling the dynamical stiffness of the articular cartilage (Netti & Ambrosio, 2002). In OA, the collagen network breaks down and the concentration of fixed PG decreases, resulting in abnormally low streaming potentials.

Many studies have been conducted to simultaneously compare the streaming potentials and the biomechanical properties between normal and degraded cartilage samples *in vitro,* either in confined or unconfined conditions (Légaré et al., 2002b; Chen, Nguyen, & Sah, 1997; Kim, Bonassar, & Grodzinsky, 1995; Garon et al., 2002; Frank et al., 1987). Under oscillatory compression, streaming potential amplitude and stiffness of articular cartilage were proportional to loading frequency, in a range from 0.01 Hz to 10 Hz and at a constant imposed strain. When loading frequency was lower than 0.01Hz, owing to the low interstitial fluid velocity, the streaming potentials were barely detectable (Lee et al., 1981).

Streaming potentials amplitude and stiffness were investigated on normal and enzymatically digested bovine cartilage disks (Frank et al., 1987). The results showed that both streaming potential amplitude and dynamic stiffness decreased with time following enzymatic digestion, suggesting that streaming potential is a sensitive index for detecting the degradation of the cartilage matrix.

The streaming potential response of the cartilage in confined compression and creep configuration was measured experimentally in normal and PG-depleted tissue by Chen et al. (1997). The measured response indicated a relatively linear relationship between the changes in potential amplitude and compressive stress both in normal and degraded cartilage disks. In addition, a change in potential amplitude during compression time was also observed, even though the theoretical model predicted a constant potential level during 10 seconds period. For normal cartilage, the potential amplitude decreased by about 45 percent after 10 seconds of loading. The digested sample exhibited reduction of amplitude too, while the variation was less marked than the normal one.

Spatially resolved streaming potentials were measured in normal and degraded cartilage disks with a linear array of eight microelectrodes. The electrodes were placed on cartilage disks, from the centre to the periphery and with an inter-electrode interval of 300 μm (Garon et al., 2002). Radial profiles of streaming potentials demonstrated that the absolute streaming potential values were maximal at the disk center, decreasing monotonically along the radial position across the disk. These findings agreed with previous predictions that streaming potential amplitude is proportional to the internal hydrostatic fluid pressure in which peak pressure occurs at the disk center and decreases gradually to a minimum at the disk periphery (Kim et al., 1995). The potential gradient increased from the center to the edge of the disk. The spatially resolved streaming potential profiles were compared between normal and cultured samples degraded by cytokine interleukin-1α, they showed that streaming potential amplitude decreases as a function of the culture time. The experimental data confirmed that, with low GAG concentration, the stiffness of degraded cartilage was significantly lower than the normal cartilage, even after only one day of culture. The radial streaming potential profile also exhibited frequency dependence as in previous studies.

Although streaming potentials have been exhaustively studied with isolated cartilage samples in a laboratory setting, one report using a porcine *ex vivo* model showed that the electrical potential within the cartilage matrix extends outside the cartilage tissue (Schmidt-Rohlfing et al., 2002). The surrounding soft tissues of the joint samples were removed while the capsule was left intact until the insertion of the gold-plated electrodes. Experimental data demonstrated that an approximately linear relation might exist between the applied force and the detected electrical signal; and no delay was observed between them. With a loading frequency ranging between 0.036 Hz and 1.4 Hz, there was no change of electrical potential amplitude while the applied force was maintained at a constant level, exhibiting frequency independent properties under low loading frequency. With a loading force of 287 N, the peak to peak amplitude detected outside of the cartilage tissue was around 45 mV between two electrodes 1.5 cm apart, which was about ten times smaller than the values obtained inside the cartilage matrix.

In summary, these *in vitro* and *ex vivo* studies highlight the ability of the streaming potential method to assess cartilage function and quality. The spatially resolved streaming potential profile fits the prediction of the biphasic model describing cartilage response to loading.

2.6.2 Arthro-BST

The Arthro-BST (Biomomentum Inc., Laval, Québec, Canada), is an arthroscopic device measuring the streaming potential of articular cartilage, that was designed for the non-destructive evaluation of cartilage quality (Figure 2.9) (Garon, 2007).

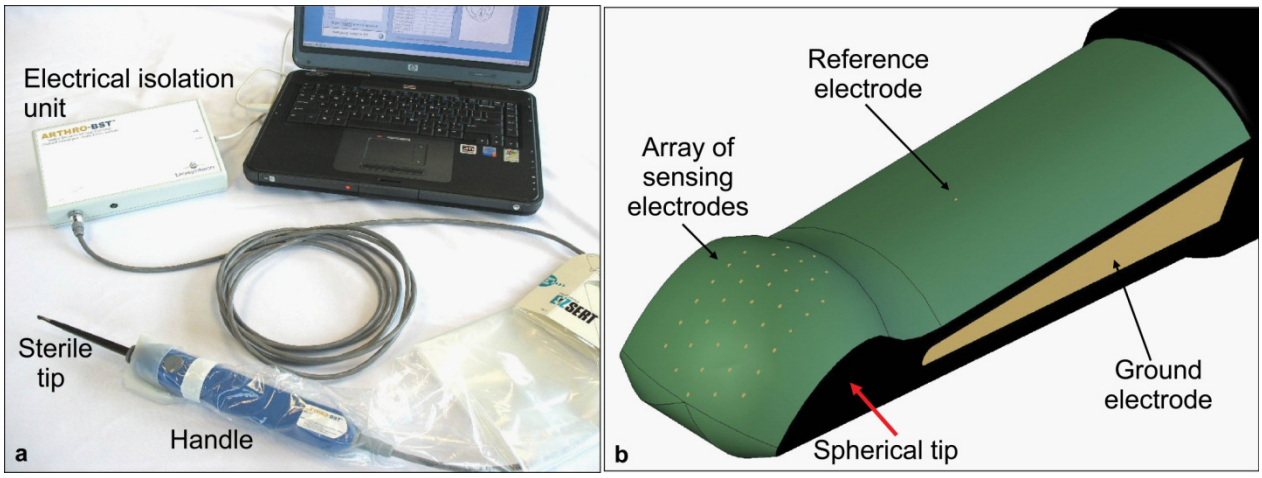

Figure 2.9: a) The Arthro-BST device for measuring cartilage streaming potentials. b) The microelectrodes matrix on the sterile tip of Arthro-BST (Changoor, 2011).

It consists of a hand-held arthroscopic probe with a sterile tip and other associated electronics that collects and processes the streaming potential signals. A spherical indenter on the tip of the probe (r = 3.175 mm) comprises an array of 37 gold microelectrodes (5 microelectrodes/mm^2) and is used to manually compress the cartilage surface. The device provides a quantitative parameter (QP) that reflects the electromechanical properties of the cartilage (Sim, 2013). High QP values indicate cartilage degeneration with weak electromechanical properties, and low QP values indicate normal cartilage.

The correlations of QP with histological, biochemical and biomechanical properties of cartilage were recently evaluated (Sim et al., 2014). The results revealed that the electromechanical QP strongly correlated with both the Mankin score (Makin histological-histochemical grading system) and the PLM score (polarized light microscopy qualitative score), which reflect tissue quality and collagen architecture accurately. It also correlated with biomechanical properties of

human cartilage samples including fibril modulus, matrix modulus and log of permeability. However, the QP correlated weakly with GAG and water content.

The Arthro-BST is a major breakthrough in clinical diagnosis and evaluation of cartilage quality. It provides a simple, non-destructive and highly sensitive method by which cartilage function can be mapped over the articular surfaces during standard arthroscopic surgery (Changoor, 2011).

2.6.3 First electroarthrography studies

EAG consists of recording electrical potentials on the knee surface while the joint is undergoing compressive loading. Préville et al. (2013) were the first to demonstrate that the signals arising from the streaming potentials in compressed articular cartilage can be measured from the surface of the knee in human subjects. Disposable electrodes were placed at eight different sites around the knee joint and the loading of the knee was achieved by voluntary shifting of the subject's weight from one leg to the other. The EAG recordings were performed on two groups of subjects: 20 asymptomatic subjects, 20 patients with bilateral OA who had a unilateral total knee replacement (TKR). Both the OA and the TKR knee were analyzed. The average EAG values at each electrode site for these three groups were compared (Figure 2.10).

The mean EAG potentials overlying the TKR were statistically null and different from those of the other two groups, which supported the hypothesis that the EAG signals are generated by compressed articular cartilage, and not by other sources such as muscles, tendons, ligaments, bones, skin, etc. The intergroup comparison showed that the amplitude of the potential for the asymptomatic group was greater than that of OA group, thus demonstrating that the degradation of cartilage is reflected on the EAG amplitudes. Also, the amplitude of the EAG depended on the location of the electrodes. The highest EAG values were observed over the joint line of the knee, and the values were higher on the medial side than on the lateral side, which is consistent with the higher loads in the medial compartment of the joint.

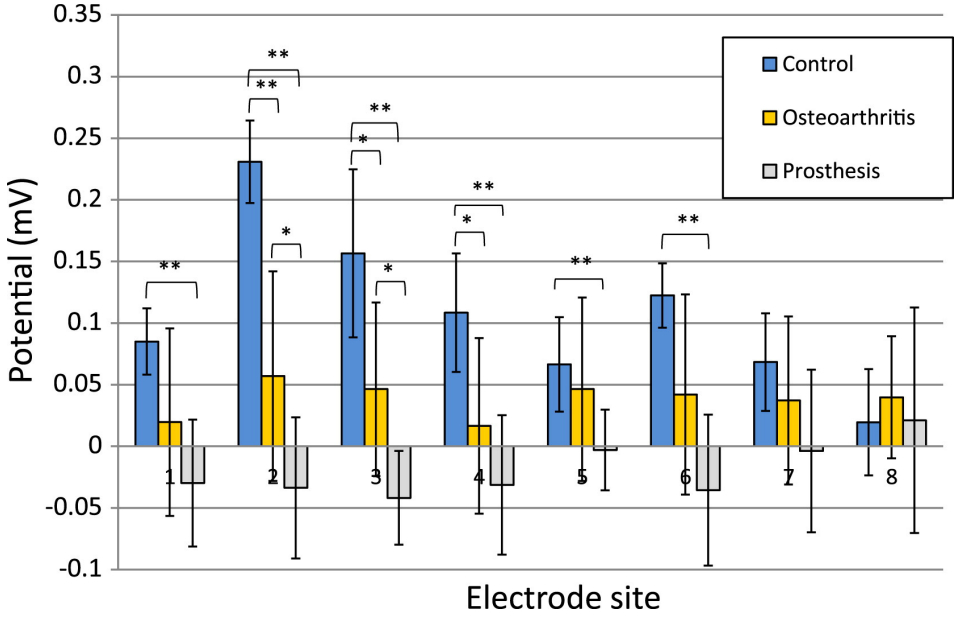

Figure 2.10: Mean values of EAG signals at eight electrode sites. On the medial side, electrodes (#2 and #3) were placed over the joint line determined by palpation, two more electrodes were placed above (#1) and below (#4) these first two electrodes. Electrode placement was similar on the lateral side. *P*-values: ** indicates $P < 0.01$, * indicates $P < 0.05$ (Préville et al., 2013).

Han et al. (2014) developed computer models of the human knee to investigate the generation of the EAG signals and to contribute to the development of interpretation criteria. The knee was modeled as a volume conductor composed of different regions characterized by specific electrical conductivities and the source was modeled as an impressed current density in different sections of the articular cartilage (Figure 2.11). The Finite Element Method was used to compute the potential distribution produced by these current sources in two knee models with a realistic geometry. For both models, maximum potentials could be observed on both side of the knee along the joint line, with higher potentials on the medial side, which was in agreement with the previous clinical results. Also, different localized cartilage defects stimulated as a reduced current density produced specific potential distributions. Therefore, equipotential map of EAG signal around the knee displayed potential ability to localize the degeneration.

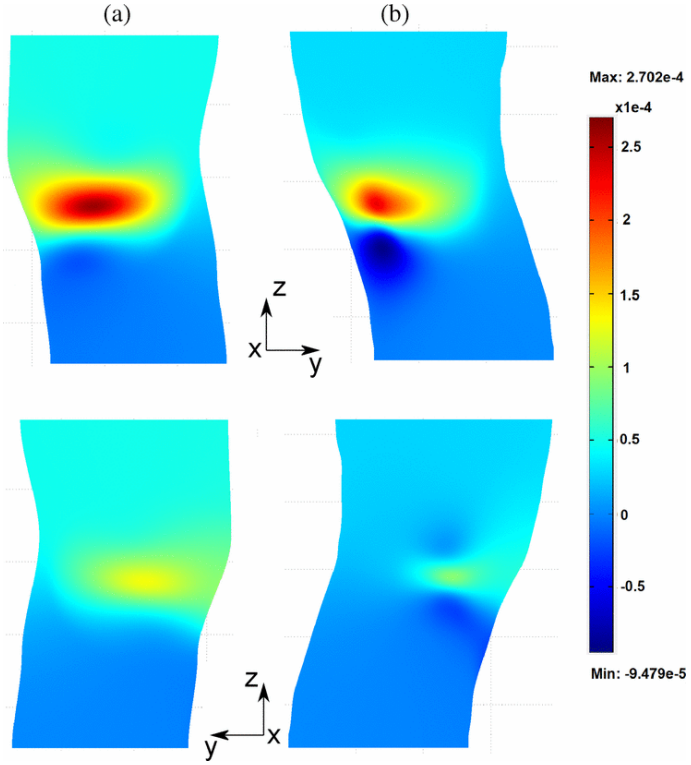

Figure 2.11: Simulated electric potential distribution over the knee surface with (A) general geometry and (B) specific subject geometry models. The upper row represents the medial side of the knee and the lower row of the lateral side (Han et al., 2014).

Recently, the EAG technique has been applied in animal studies. The EAG signals acquired *in vitro* from the distal forelimbs of one horse exhibiting natural cartilage degradation (ICRS grade 2) and one horse with normal cartilage (ICRS grade 0) indicated that the EAG was sensitive to cartilage degradation and reflected direct measurements of cartilage streaming potentials with the Arthro-BST probe (Changoor, 2013). The EAG signals were also measured successfully in three live horses during loading with the instrumented forelimb positioned on a floor-mounted force plate, a significant correlation was detected between the EAG coefficients acquired during *in vivo* and *in vitro* assessment with the Arthro-BST probe on the same fetlock (Changoor et al., 2014).

To summarize the development of the EAG technique, *in vitro* studies have initially shown that a decrease in the amplitude of the streaming potentials measured directly on the cartilage surface is an indicator of cartilage degeneration (Frank et al., 1987; Garon et al., 2002; Légaré et al., 2002a). A clinical study, computer simulations and animal studies have demonstrated that these

load-induced electric potentials can be also detected at the surface of the knee and that they are correlated with cartilage quality (Préville et al., 2013; Han et al., 2014; Changoor et al., 2014). Now, to clinically use the EAG method to characterize cartilage degeneration, the mechanisms determining the EAG signals within an individual need further investigation to contribute to the development of new optimized measurement protocols with improved repeatability.

2.6.4 Postural control

As discussed previously, mechanical loading of the cartilage was achieved by simply changing from a bipedal to a unipedal stance durin àg thew linical EAG measurement. The resultant force acting on the cartilage is influenced by all force vectors generating from the muscles, ligaments and ground reaction force (Fleming et al., 2001). Even though the body seems to be relatively still in bipedal condition, the mechanics of this activity is more dynamic and complicated (Kutzner et al., 2010). Hence, it is necessary considering the mechanisms by which an individual maintains balance during relaxed bipedal and unipedal stance.

During bipedal standing, the feet support the individual's body weight so that upright standing can be well maintained. The center of mass (COM) of the body must be positioned somewhere over the area bounded by the outline of the plantar aspects of both feet and the area directly between the feet. Evaluation of COM requires kinematic information of all body segments displacement during postural control (Winter et al., 1998).

The center of pressure (COP) which can be measured by force plate takes into account the location and magnitudes of all the ground reaction force vectors and might provide useful information regarding the postural control (Winter, 1995). The net COP of individual is available using one force plate. To reach the net COP of each limb, two force plates are required. In standing condition, the shift of net COP can be explained as a result of coordination of the following two mechanisms: an inverted pendulum model (ankle strategy) in the anterior-posterior (A/P) direction, dominated by ankle muscles, and bilateral limb loading model (hip strategy) in the medial-lateral (M/L) direction, dominated by hip abductor/adductor muscles (Winter et al., 1996). Basically, the net COP in A/P direction is totally under ankle control, which is synchronized with the COP of one limb. However, the net COP in M/L direction is also controlled by the load/unload fraction of body weight. Therefore, the COP in M/L direction of one limb is out-of-phase along with the net COP in M/L direction (Winter, 1995).

CHAPTER 3 ARTICLE 1: MECHANICAL LOADING OF KNEE ARTICULAR CARTILAGE INDUCED BY MUSCLE CONTRACTION CAN BE ASSESSED BY MEASURING ELECTRICAL POTENTIALS AT THE SURFACE OF THE KNEE

Lin Zhu, Michael D. Buschmann and Pierre Savard

Submitted to the Journal of Biomechanics in September 2015

Revised manuscript submitted in December 2015

Accepted in December 2015

Institut de génie biomédical, École Polytechnique de Montréal, Montréal, Québec, Canada

Corresponding author:

Pierre Savard
Institute of biomedical engineering
École Polytechnique de Montréal
CP 6079 succ. Centre-ville
Montréal, Québec, Canada.
Telephone: 1-514-340-4711 ext 4186
Fax: 1-514-340-4611
E-mail: pierre.savard@polymtl.ca

Keywords

Knee joint, Muscles, Contact force, Cartilage, Streaming potentials, Electroarthrography

Author's contribution

Lin Zhu	Data acquisition, data analysis, statistical analysis, literature review, drafting and critical revision of the manuscript
Michael D. Buschmann	Study conception and design, critical revision of the manuscript
Pierre Savard	Study conception and design, critical revision of the manuscript. Accepts responsibility for the integrity of the work as a whole

3.1 Abstract

Electroarthrography (EAG) consists of recording electrical potentials on the knee surface that originate from streaming potentials within articular cartilage while the joint is undergoing compressive loading. The aim was to investigate how the contraction of specific leg muscles affects the contact force of the knee joint and, in turn, the EAG values.

For six normal subjects, voluntary isometric muscle contractions were repeatedly conducted to activate four leg muscle groups while the subject was lying on his back. Two EAG signals were recorded on the medial and lateral sides of the knee, as well as four EMG signals (gastrocnemius, hamstring, quadriceps, tensor fascia latae), and the signal from a force plate fixed against the foot according to the direction of the force.

The EAG and force signals were very well correlated: the median of the correlation coefficients between an EAG signal and the corresponding force signal during each loading cycle was 0.91, and 86% of the correlation coefficients were statistically significant (p <5%). Isolated muscle contraction was possible for the gastrocnemius and hamstring, but not always for the quadriceps and tensor fascia latae. Using the clinical loading protocol which consists of a one-legged stance, the quadriceps and hamstring EMGs showed minimal activity; loading cycles with increased EAG amplitude were associated with higher EMG activity from the gastrocnemius, which is involved in antero-posterior balance.

These results document the role of the EAG as a "sensor" of the knee contact force and contribute to the development of clinical loading protocols with improved reproducibility.

3.2 INTRODUCTION

Articular cartilage is a hydrated soft tissue covering the subchondral bone which provides a low friction, wear-resistant joint surface (Netti and Ambrosio, 2002). Cartilage degeneration, known as osteoarthritis (OA), can cause pain, stiffness, and loss of mobility of the joint. Techniques based on clinical symptoms, imaging and biomarkers, are currently applied to diagnose OA (Bijlsma et al., 2011). Cartilage degradation can develop over decades and methods are currently lacking for detecting early stage OA, which could help prevent, or even reverse cartilage degradation (Chu et al., 2012).

The extracellular matrix of articular cartilage is composed of proteoglycan trapped in a collagen network. Due to its negatively charged glycosaminoglycan (GAG) side chains, proteoglycan attracts mobile cations in the fluid (Kim et al., 1995). Under equilibrium conditions, excess cations distribute around GAGs symmetrically. When mechanically loaded, interstitial fluid flow drags the excess cations and separates them from the fixed negatively charged proteoglycan groups, thereby generating an electrical field. This load-induced electrical field, called streaming potentials, could serve as a sensitive indicator of collagen integrity and proteoglycan loss (Buschmann and Grodzinsky, 1995; Frank et al., 1987; Armstrong et al., 1984). It has been shown in vitro that the sensitivity of these electromechanical characteristics to early stages of degradation is higher than purely mechanical, biochemical or histological properties (Garon et al., 2002; Légaré et al., 2002; Buschmann et al., 1999; Bonassar et al., 1995). Recently, a novel non-invasive technique called electroarthrography (EAG) was proposed to assess articular cartilage and diagnose OA by measuring load-induced electrical potentials at the surface of the knee. The knee is mechanically loaded as the upright subject shifts his weight from one leg to the other. A clinical study comparing normal subjects, OA patients and patients with total knee replacement, modeling studies and animal studies has supported the hypothesis that EAG signals originate only from articular cartilage and reflect the forces applied to the cartilage and its state of degradation (Préville et al., 2013; Han et al., 2014; Changoor et al., 2014).

The amplitude of the streaming potentials depends on cartilage integrity, but also on the loading conditions. Direct measurement of the knee joint contact force has long been impracticable due to technical limitations. Computer simulations have thus been carried out to calculate the contact force using musculoskeletal models (Shelburne et al., 2005; Adouni et al., 2012). With the development of instrumented knee implants, in vivo loading measurement became applicable. It was found that the contact force measured in vivo during a one-legged weight bearing stance, which is similar to the EAG loading technique, ranged from 2 to 3 times the body weight (Kutzner et al., 2010). Being aware of the possible role of muscle forces, we hypothesized that muscle contraction can modify the contact force and, in turn, the EAG values. The aim of this study was to test this hypothesis so as to document the role of the EAG as a “sensor” of the knee contact force and also, to contribute to the development of new EAG loading protocols with improved reproducibility.

3.3 Methods

Six healthy subjects without any relevant injuries were recruited to participate in this study (Table 3.1). The experimental protocol was approved by the Research Ethics Board of our institution. Before the experiments, each subject was instructed with respect to the experimental protocol and signed an informed consent form.

Table 3.1: Characteristics of the subjects

Subject	Gender	Weight (kg)	Height (cm)	Age
1	M	78	165	43
2	F	52	158	21
3	M	83.6	188	63
4	F	60	166	29
5	M	77	185	32
6	F	64	173	20
Mean±SD		69.1±12.3	172.5±11.9	34.7±16.2

To characterize the relationship between muscle contraction and EAG, voluntary isometric muscle contractions were conducted to activate specific leg muscles while the subject was lying on his back, this position ensured that the knee was minimally loaded. Electromyogram signals (EMG) were recorded to document specific muscle activities while a force plate was used to measure the force applied by the foot. The stability of the knee being predominantly maintained by the quadriceps, hamstring and gastrocnemius (Winby et al., 2009), these three muscle groups were investigated (Figure 3.1). We also investigated the tensor fasciae latae (TFL), which is activated to keep balance when the opposite foot is lifted (Saladin, 2004). Prior to the recordings, the subjects practiced voluntary contractions. During the recordings, the subject repeated each contraction ten times for averaging purposes; each isometric contraction lasted for 1-2 seconds, followed by a 10 second rest period to avoid cumulative fatigue. Finally, a knee loading protocol similar to the clinical protocol used previously was applied (Préville et al., 2013), with the erect subject shifting his weight from a two-legged stance to a one-legged stance.

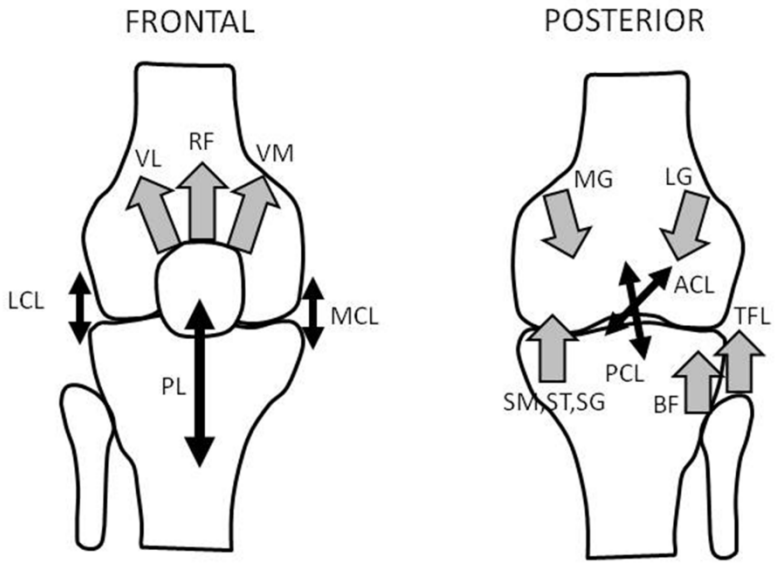

Figure 3.1: Schematic representation of some forces acting on the knee joint. The base of the gray arrows indicates the approximate insertion point of the muscles, whereas the arrows point in the direction of the acting force. The thinner double arrows represent the ligaments. Frontal view: vastus lateralis (VL), rectus femoris (RF), vastus medialis (VM), tensor fasciae latae (TFL), patella tendon (PT), lateral collateral ligament (LCL), medial collateral ligament (MCL). Posterior view: medial gastrocnemius (MG), lateral gastrocnemius (LG), biceps femoris (BF), semimembranous (SM), semitendinosus (ST), anterior cruciate ligament (ACL), posterior cruciate ligament (PCL).

An 8-channel wireless acquisition system (Bioradio 150, Clevemed Medical Inc.) was used to measure 2 EAG, 5 EMG and 1 force signal. The EAG and force signals were amplified with DC coupling whereas the EMG signals were amplified with AC coupling; the sampling rate was 600 Hz with a resolution of 16 bits. The EMG bipolar electrodes were positioned according to the SENIAM standard (Hermens et al., 2000) over the gastrocnemius medialis (GM) and the gastrocnemius lateralis (GL) from the calf, the biceps femoris long head (BF) from the hamstring, the rectus femoris (RF) from the quadriceps, and the TFL on the line from the anterior spina iliaca superior to the lateral femoral condyle in the proximal 1/6. Five pairs of electrodes with an

inter-electrode distance of 35mm were thus positioned, parallel to the direction of muscle fibers. As for the EAG measurements, two electrodes were positioned on the lateral and medial sides of the knee over the joint line which was determined by palpation; a reference electrode was placed over the middle of the tibia and a ground electrode was placed just below. Self-adhesive electrodes (Red Dot, 3M) were used and the skin under the electrode was prepared with an abrasive paste (Nuprep) to reduce the skin-electrode impedance. A force plate (FP-BTA, Vernier) measured the force applied by the foot during muscle contraction, and its position varied according to each muscle.

Signal processing was carried out using user-written software (Matlab). First, the EAG and force signals were low-pass filtered (5 Hz) to reduce noise and 60 Hz interference. Second, the DC drift of the EAG signals originating from electrode and amplifier offset potentials was eliminated by subtracting from the measured signals the baseline defined by a third order polynomial for each cycle. For the EMG signals, the average of the two signals from the gastrocnemius was first computed. The four EMG signals were then high-pass filtered (20 Hz) and fully rectified. A low-pass filter (5 Hz) was finally used to compute the envelope.

The following statistical procedures were applied. The Pearson's correlation coefficients between the EAG signal and the concomitant force signal were computed using all the samples during each contraction cycle. A total of 480 correlation coefficients were thus computed. Also, average values during each cycle for the EAG, EMG and force signals were computed during the time interval for which the force signal was above 90% of the maximum force observed during the cycle. The values from the 10 cycles were then averaged, representing each of the eight channels for each subject. A one way analysis of variance with the muscle group as a factor was applied for each of the eight variables to test the influence of the muscle group. A post hoc Student's *t* test was then used to compare specific variables. Statistical significance was tested at the $p<0.05$ level.

3.4 RESULTS

Representative EAG, EMG and force measurements during the isolated contraction of each of the four muscle groups are shown in Figures 3.2 to 3.5. The contraction of the gastrocnemius is shown in Figure 3.2.

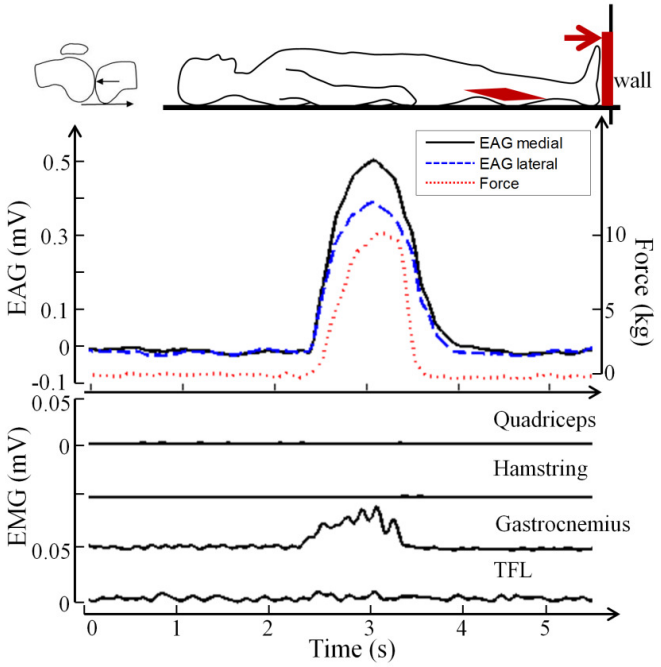

Figure 3.2: Representative data for gastrocnemius contraction. Top left, in the sagittal plane: the lower arrow illustrates the direction of muscle force acting on the condyles of the femur and the top arrow represents the resulting contact force on the cartilage. Top right: outline of the supine subject in the sagittal plane; the red rectangle shows the position of the force plate; the elongated diamond represents the contracted muscle; the red arrow indicates the direction of the force applied by the forefoot on the force plate. Middle panel: medial and lateral EAG signals (left scale), and force signal (right scale). Bottom panel: EMG envelope signals for the four muscle groups (scale: 0.05 mV).

The force plate was fixed against the sole of the foot (Figure 3.2, top right). The supine subjects slowly pointed their forefoot away so that a force was applied by the plantar flexion of the foot

and then came back to the initial position after 1-2 seconds. The medial and lateral heads of the gastrocnemius develop from the medial and lateral condyles of the femur separately. Thus, when the gastrocnemius is contracted, the muscle group pulls the femur toward the tibia, which increases the contact force acting on the cartilage (Figure 3.2, top left). The EAG and force signals increase and decrease simultaneously with the EMG signal (Figure 3.2, middle). The bottom panel of Figure 3.2 shows that an EMG signal was only observed in the gastrocnemius channel.

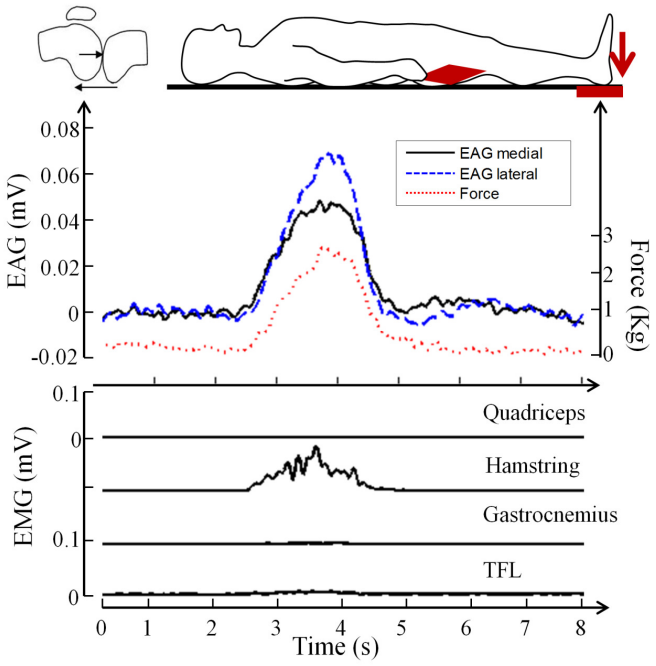

Figure 3.3: Representative data for hamstring contraction. Top left, in the sagittal plane: the lower arrow illustrates the direction of muscle force acting on the tibia and fibula, and the top arrow represents the resulting contact force on the cartilage. The rest of the format is similar to that of Figure 3.2, but the scales are different.

Data acquired during the contraction of the hamstring is shown in Figure 3.3. The force plate was placed on the table, under the heel (Figure 3.3, top right). The subjects slowly pressed their heel down on the force plate by contracting the posterior part of the thigh. When the hamstring

muscles (ST, SM, BF) are contracted, they exert a force on the tibia and the head of the fibula which pulls the tibial plateau against the femoral condyles (Figure 3.3 top left). The EAG and force signals increase and decrease with the EMG signal (Figure 3.3, middle). The bottom panel of Figure 3.3 shows that an EMG signal was only observed in the hamstring channel.

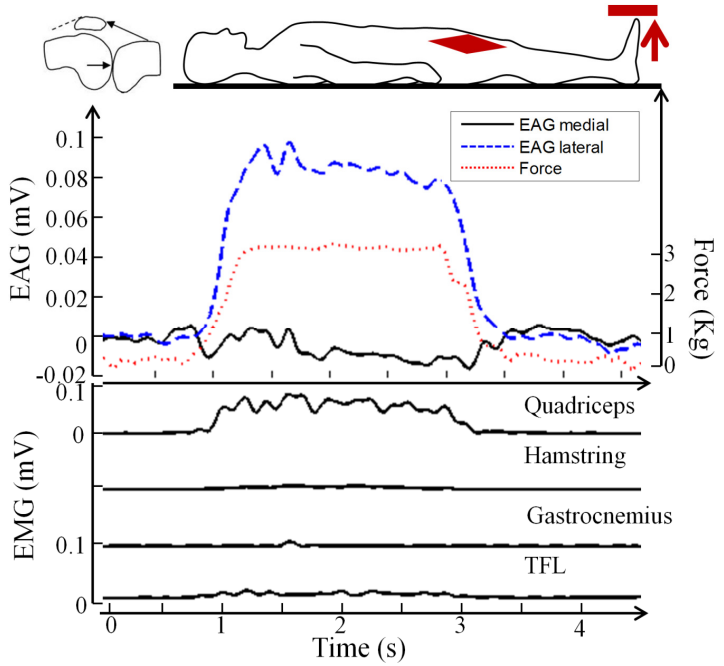

Figure 3.4 : Representative data for quadriceps contraction. Top left: the top arrow illustrates the direction of muscle force acting on the tibial tuberosity of the tibia via the patellar tendon, and the lower arrow represents the resulting contact force on the cartilage in the sagittal plane. The rest of the format is similar to that of Figure 3.2, but the scales are different.

Isolated contraction of the quadriceps generated the data shown in Figure 3.4. The force plate was fixed above the great toe (Figure 3.4 top right). The subjects tensed the quadriceps, trying to raise the leg and pushing upward with their great toe against the force plate. The rectus femoris and the other muscles from the quadriceps insert to the tuberosity of the tibia through the patellar tendon. When in tension, the quadriceps exerts force on the tibia which pulls the tibial plateau against the femoral condyles (Figure 3.4 top left). The bottom panel of Figure 3.4 show that the EMG signal

could be observed not only in the quadriceps channel but also, with lesser amplitude, in the TFL channel. Subjects found it difficult to achieve isolated contraction of the quadriceps in this exercise; the majority of contractions also involved the TFL. The EAG signal from the lateral side and the force signal showed similar patterns as the EMG signal. However, the EAG from the medial side of the knee showed much smaller values during contraction (Figure 3.4 middle panel).

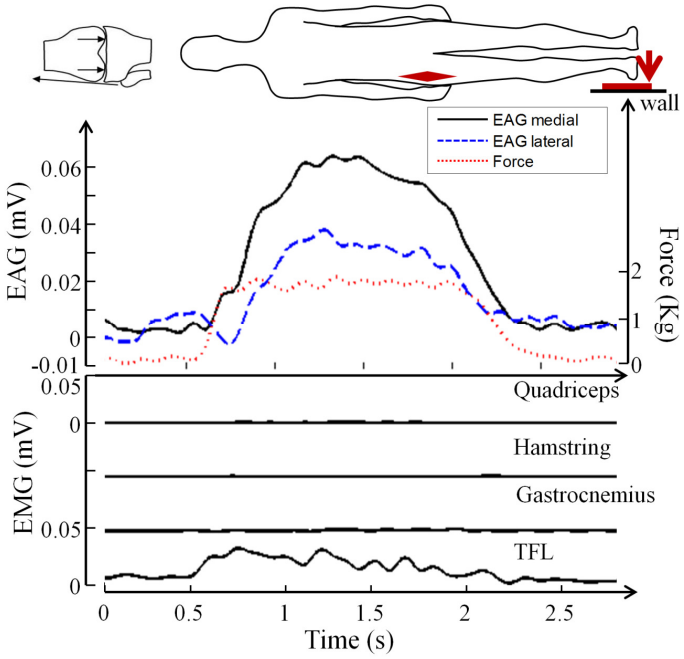

Figure 3.5 : Representative data for contraction of the tensor fasciae latae (TFL). Top left, in the frontal plane: the lower arrow illustrates the direction of muscle force acting on the lateral condyle of the tibia via the iliotibial band, and the top arrows represent the resulting contact force on the cartilage. Top right: outline of the supine subject in the frontal plane (shown from above). The rest of the format is similar to that of Figure 3.2, but the scales are different.

Data for an isolated TFL contraction is shown in Figure 3.5. The force plate was placed in a vertical position and fixed against the lateral side of the measured foot (Figure 3.5 top right). The subjects then pressed the lateral side of their foot against the force plate. In this procedure, the subjects needed to activate the TFL, which is inserted between the two layers of the iliotibial tract

and which connects to the lateral condyle of the tibia. Hence, the TFL contraction pulls the tibia against the femoral condyles and increases the contact force (Figure 3.5, top left). In the bottom panel of Figure 3.5C, we observe that the ascent and descent of the EAG and force signals are in accordance with the EMG signal from the TFL. In this example, the EMG signals from the other three muscles are absent. However, most subjects found it hard to exclusively contract the TFL and the quadriceps was frequently involved in this exercise.

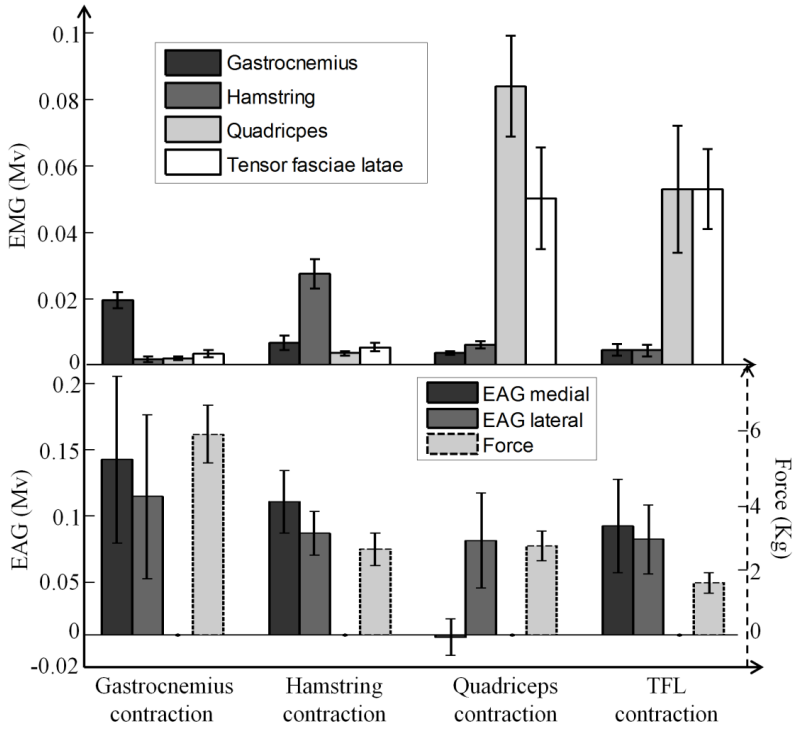

Figure 3.6 : Statistics for the EAG, EMG and force signals recorded during contraction of each of the four muscle groups (6 subjects). Top panel: mean and standard error of the four EMG channels. Bottom panel: mean and standard error of the EAG and force signals.

The mean and standard error of the averaged values of the EAG, EMG and force signals for the six subjects are presented in Figure 3.6, showing that EAG signals can be detected during the contraction of all four muscle groups. The EMG values show that isolated contractions were

achieved for the gastrocnemius and the hamstring, whereas the quadriceps and the TFL were jointly activated. Thus, during the gastrocnemius contraction, the average EMG amplitude for the gastrocnemius was significantly higher than for the other channels ($p<0.01$). Similarly, the EMG for the hamstring was higher during the hamstring contraction ($p<0.01$). For the quadriceps contraction, the means of quadriceps and TFL EMGs were not statistically different, but higher than for the other two channels ($p<0.01$ and $p<0.05$ respectively). As for the TFL, the EMG values of both quadriceps and TFL were identical and larger than for the other two channels ($p<0.05$). The force applied on the force plate was the greatest during gastrocnemius contraction ($p<0.05$), whereas the TFL generated the weakest force ($p<0.05$). The mean amplitudes of the EAG signals from the medial and lateral sides were not statistically different for the different muscle groups. The EAG amplitudes for the different muscle groups showed no statistically significant differences.

During muscle contraction, we found that noise due to motion of lead wires, pressure on the electrodes, deformation of the skin under the electrodes or electrical interference could occasionally contaminate the EAG signals. To assess these noise sources, we computed the correlation coefficients between an EAG signal and the force signal for all the samples during each loading cycle. We found that the EAG and force signals were very well correlated: the median of all the correlation coefficients was 0.91 and 86% of the correlation coefficients were statistically significant ($p<0.05$).

Finally, to assess the role of muscle contraction on EAG signals generated with the clinical loading protocol (Préville et al., 2013), we monitored the EMG and force signals in parallel with the EAG signals during a similar protocol. To mechanically load the knee, the subjects stood on both legs, then transferred their body weight to their instrumented leg and finally returned to the two-legged stance. Thus, the knee was initially pre-loaded by half of the body weight and then further loaded to full body weight. The force plate was placed under the foot of the instrumented leg to record the ground reaction force. Another plate having the same thickness was placed under the opposite foot to maintain balance. The positions of all the electrodes were the same as during the muscle contraction experiments. An example of the results is shown in Figure 3.7, where large variations of the EAG signals can be observed during the successive loading cycles,

with the peak amplitude of the medial EAG ranging between 0.25 mV (4th cycle) and 0.9 mV (10th cycle).

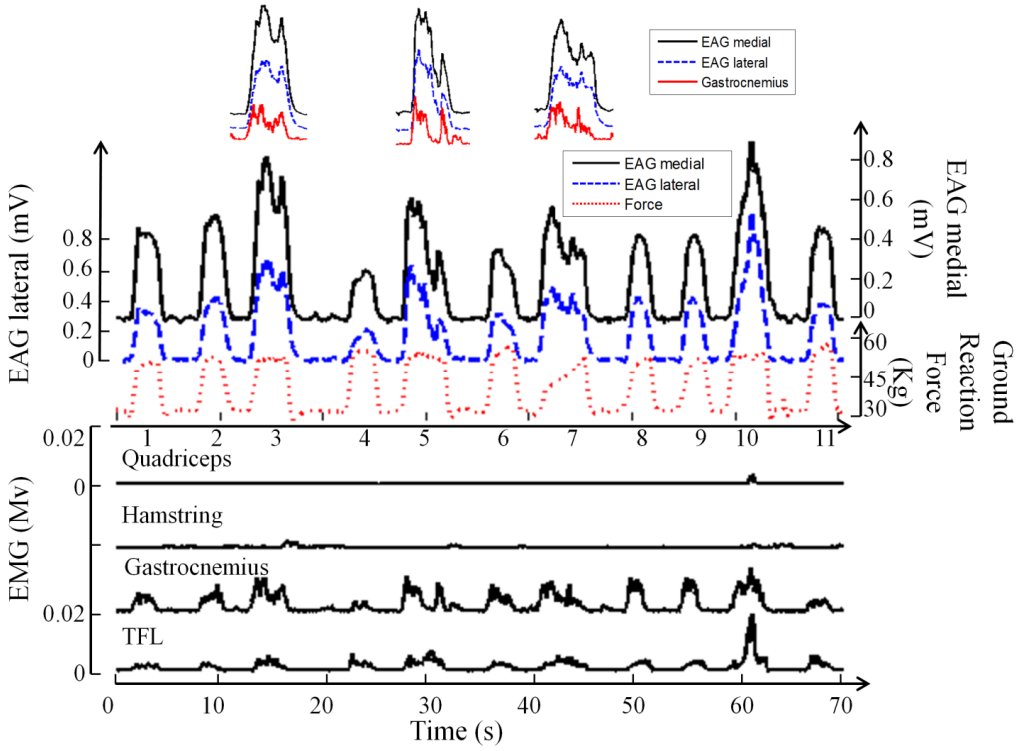

Figure 3.7 : The EAG, EMG and ground reaction force signals recorded on an erect subject during eleven successive loading cycles. During a loading cycle, the subject stood on both legs, then transferred his body weight on the instrumented leg and finally returned to the two-legged stance. The number of each loading cycle is shown below the ground reaction force signal. The top panel shows the EAG and gastrocnemius EMG signals corresponding to the loading cycles 3, 5 and 7.

In contrast, the change of the ground reaction force during each loading cycle (about half the body weight) showed a much smaller variability with values ranging between 30 and 35 kg. Therefore, another source of EAG variation was involved. The activity of the gastrocnemius as monitored by its EMG had an obvious impact on the amplitude of the EAG. During cycle 4, the EMG of gastrocnemius was low and the EAG amplitude was the lowest (Figure 3.7). During the

cycles 3, 5 and 7, the waveforms of the EAG signals showed characteristic notches which did not appear in the force channel but corresponded very well with the notches seen in the gastrocnemius EMG (top of Figure 3.7). During cycle 10, the subject recruited not only the gastrocnemius, but also the TFL to maintain balance, and the EAG values were the largest due to the involvement of more muscle groups. The cycles 1, 2, 8, 9 exhibited similar EAG values and also similar EMG values for the gastrocnemius. The EMG signals from the quadriceps and hamstring muscles showed almost no activity during the entire exercise whereas the TFL was always activated during the one-legged stance, with an occasional peak during the 10^{th} cycle.

3.5 Discussion

The results of this study show that electrical potentials can be generated at the surface of the knee by the isometric contraction of different muscle groups of the leg in supine subjects, and that these EAG signals are well correlated with the different force signals measured at the foot of the instrumented leg. Data from this study supported our hypothesis that muscle contraction acting across the knee joint increases the contact force of the joint, compresses the articular cartilage and generates streaming potentials that can be measured at the knee surface. EAG can thus be considered as a "sensor" of the knee contact force. Low frequency electrical activity from muscles do not affect the EAG because the DC components of electromyograms are much smaller than the AC components (Trimmel et al., 1989) and there is no significant increase in the AC components of the EAG reflecting EMG activity during loading.

Many studies on the effects of isometric muscle contraction on the human knee kinematics have been published. The contact force of the tibiofemoral joint is reported to increase as quadriceps, hamstring or gastrocnemius muscle force are applied (Zavatsky et al., 1994; Liu and Maitland, 2000). The contraction force of the TFL is transmitted across the knee by the iliotibial tract (Paré et al., 1981). However, quantification of the contact force is challenging. In isolated muscle contraction, the contact force of knee depends on the knee flexion angle, muscle force, insertion point of the muscle, lever-arm and inclination of the muscle (O'Connor, 1993).

Additionally, not only the contact force, but also the contact pattern of the tibiofemoral joint can be changed during muscle contraction. In full extension, with isolated quadriceps or

gastrocnemius contractions, the knee undergoes anterior tibial translation (Li et al., 1999; Fleming et al., 2001). Conversely, posterior tibial translation is observed during isolated hamstring contraction (Höher et al., 1999). Loading of the iliotibial band, receiving the insertion of the TFL, translates the tibia in the posterior direction relative to the femur (Kwak et al., 2000). It is noteworthy that isolated quadriceps contraction can result in a significant lateral translation of the tibia (Li et al., 1999; Höher et al., 1999). This may explain why the amplitude of the medial EAG during quadriceps contraction remains relatively constant. Overall, if muscle contraction produces a force component parallel to the tibia plateau, antero-posterior or rotational translation is expected.

In principle, the cruciate ligaments are loaded to balance the shear force on the tibia plateau induced by isometric muscle contraction (O'Connor, 1993; Pandy and Shelburne, 1997). Anteriorly directed force was assumed to load the anterior cruciate ligament; and posteriorly directed force loaded the posterior cruciate ligament (Zavatsky et al., 1994). Near extension, the muscle groups all meet the tibia at small angles. Therefore we consider the shearing force on the tibial plateau to be relatively small compared to the force applied perpendicularly to the tibia (Shelburne and Pandy, 1997).

During the one-legged stance loading protocol, body weight was not exerted axially, but rather medially. To prevent tilting of the femur, a lateral force is essential. Therefore, the TFL, as well as the gluteus maximus, are involved through the iliotibial band (Maquet, 1976). This was reflected on the EMG signals from the TFL observed during successive loading cycles (Fig. 7, bottom tracing). Moreover, the mechanics of this apparently simple stance are complex and dynamic. The centre of mass can be also subjected to antero-posterior movements. When the centre of mass moves anteriorly to the ankle joint, an ankle joint plantarflexion moment must be produced by the gastrocnemius and soleus muscles to maintain the balance (Winter, 1995). Again, this was reflected on the EMG signals from the gastrocnemius observed during the successive loading cycles (Fig. 7).

One possible solution to minimize the variability of the EAG signals measured during the one-legged stance loading protocol would involve stabilizing the subject during the weight transfer. For example, placing the two feet closer to each other can reduce the medial-lateral movements.

Also, the subject could lean lightly his contralateral shoulder against a wall to replace the support provided by the TFL contraction. In this way, the dynamic movements in both the medial-lateral and antero–posterior directions could be reduced, and hence the muscle activities involved in maintaining balance and their action on the EAG.

Although this study gave valuable results, it has some limitations. Firstly, it was not possible to measure muscle force directly using the EMG. The EMG does not necessarily reflect the total force generated by the muscle and can be influenced by different factors such as electrode position and alignment (Al, 1997). The contact force on the knee joint is also influenced by additional factors including muscle strength, muscle lever-arm and type of contraction. Hence, the force plate which was used to monitor the force against the foot gave only an indirect estimation of the contact force. Secondly, using surface EMG, we could mainly monitor the superficial large muscle groups. Thirdly, the subjects did not attain maximal voluntary contraction force to avoid the involvement of other muscles. Therefore, the generated EMG amplitudes and the forces were relatively small. If the subject increased the contraction strength as much as possible, EMG values would be detected on all channels and the EAG values were much higher than the values generated by isolated muscle contraction.

Due to the difficulties of measuring *in vivo* contact forces in the knee joint, mathematical models or cadaver samples have been widely used. Few experiments were conducted *in vivo* (Kutzner et al., 2010). In this article, we showed that the EAG is sensitive to the contraction of the muscles acting across the knee joint. The EAG signal could potentially be used as an intrinsic sensor reflecting the contact force in the knee joint. In addition, by controlling this contact force through understanding and measuring sources of contact forces, it should be possible to derive an assessment of intrinsic cartilage electromechanical activity reflecting its structure and function.

3.6 Conflict of interest

The co-inventors of EAG (P. Savard, M. Buschmann and J. Hardin) have obtained a U.S. Patent for this technology. A Collaborative Research and Development (CRD) Grant was obtained jointly from the Canadian Natural Sciences and Engineering Research Council and Biomomentum Inc. (Laval, QC, Canada).

3.7 Acknowledgements

This work was supported by the Canadian Institutes of Health Research (Operating grant number: APP37148), the Canadian Natural Sciences and Engineering Research Council (Grant number: CRDPJ 445265-12) and the China Scholarship Council (Number: 2009625035). The study sponsors were not involved in the study design, in the collection, analysis and interpretation of data; in the writing of the manuscript; and in the decision to submit the manuscript for publication.

3.8 References

Adouni, M., Shirazi-Adl, A., Shirazi, R., 2012. Computational biodynamics of human knee joint in gait: from muscle forces to cartilage stresses. J. Biomech. 45, 2149–2156.

Al, H., 1997. The relationship between electromyogram and muscle force. Sportverletz. Sportschaden Organ Ges. Orthopadisch-Traumatol. Sportmed. 11, 79–86.

Armstrong, C.G., Lai, W.M., Mow, V.C., 1984. An Analysis of the Unconfined Compression of Articular Cartilage. J. Biomech. Eng. 106, 165–173.

Bijlsma, J.W., Berenbaum, F., Lafeber, F.P., 2011. Osteoarthritis: an update with relevance for clinical practice. The Lancet 377, 2115–2126.

Bonassar, L.J., Jeffries, K.A., Paguio, C.G., Grodzinsky, A.J., 1995. Cartilage degradation and associated changes in biomechanical and electromechanical properties. Acta Orthop. 66, 38–44.

Buschmann, M.D., Grodzinsky, A.J., 1995. A molecular model of proteoglycan-associated electrostatic forces in cartilage mechanics. J. Biomech. Eng. 117, 179–192.

Buschmann, M.D., Kim, Y.-J., Wong, M., Frank, E., Hunziker, E.B., Grodzinsky, A.J., 1999. Stimulation of Aggrecan Synthesis in Cartilage Explants by Cyclic Loading Is Localized to Regions of High Interstitial Fluid Flow. Arch. Biochem. Biophys. 366, 1–7.

Changoor, A., Brett, W., Hoba, M., Garon, M., Quenneville, E., Gordon, K., Savard, P., Buschmann, M.D., Hurtig, M.B., Trout, D.R., 2014. Electroarthrography, a non-invasive

streaming potential-based method, measures cartilage quality in live horses. Osteoarthritis and Cartilage 22, S88–S89.

Chu, C.R., Williams, A.A., Coyle, C.H., Bowers, M.E., 2012. Early diagnosis to enable early treatment of pre-osteoarthritis. Arthritis Res. Ther. 14, 212.

Fleming, B.C., Renstrom, P.A., Ohlen, G., Johnson, R.J., Peura, G.D., Beynnon, B.D., Badger, G.J., 2001. The gastrocnemius muscle is an antagonist of the anterior cruciate ligament. J. Orthop. Res. 19, 1178–1184.

Frank, E.H., Grodzinsky, A.J., Koob, T.J., Eyre, D.R., 1987. Streaming potentials: a sensitive index of enzymatic degradation in articular cartilage. J. Orthop. Res. 5, 497–508.

Garon, M., Légaré, A., Guardo, R., Savard, P., Buschmann, M.D., 2002. Streaming potentials maps are spatially resolved indicators of amplitude, frequency and ionic strength dependant responses of articular cartilage to load. J. Biomech. 35, 207–216.

Han, Q., Buschmann, M.D., Savard, P., 2014. The forward problem of electroarthrography: modeling load-induced electrical potentials at the surface of the knee. IEEE Trans. Biomed. Eng. 61, 2020–2027.

Hermens, H.J., Freriks, B., Disselhorst-Klug, C., Rau, G., 2000. Development of recommendations for SEMG sensors and sensor placement procedures. J. Electromyogr. Kinesiol. 10, 361–374.

Höher, J., Vogrin, T.M., Woo, S.L., Carlin, G.J., Arøen, A., Harner, C.D., 1999. In situ forces in the human posterior cruciate ligament in response to muscle loads: a cadaveric study. J. Orthop. Res. 17, 763–768.

Kim, Y.J., Bonassar, L.J., Grodzinsky, A.J., 1995. The role of cartilage streaming potential, fluid flow and pressure in the stimulation of chondrocyte biosynthesis during dynamic compression. J. Biomech. 28, 1055–1066.

Kutzner, I., Heinlein, B., Graichen, F., Bender, A., Rohlmann, A., Halder, A., Beier, A., Bergmann, G., 2010. Loading of the knee joint during activities of daily living measured in vivo in five subjects. J. Biomech. 43, 2164–2173.

Kwak, S.D., Ahmad, C.S., Gardner, T.R., Grelsamer, R.P., Henry, J.H., Blankevoort, L., Ateshian, G.A., Mow, V.C., 2000. Hamstrings and iliotibial band forces affect knee kinematics and contact pattern. J. Orthop. Res. 18, 101–108.

Légaré, A., Garon, M., Guardo, R., Savard, P., Poole, A.R., Buschmann, M.D., 2002. Detection and analysis of cartilage degeneration by spatially resolved streaming potentials. J. Orthop. Res. 20, 819–826.

Li, G., Rudy, T.W., Sakane, M., Kanamori, A., Ma, C.B., Woo, S.L.-Y., 1999. The importance of quadriceps and hamstring muscle loading on knee kinematics and in-situ forces in the ACL. J. Biomech. 32, 395–400.

Liu, W., Maitland, M.E., 2000. The effect of hamstring muscle compensation for anterior laxity in the ACL-deficient knee during gait. J. Biomech. 33, 871–879.

Maquet, D.P.G.J., 1976. Biomechanical Treatment of Osteoarthritis of the Knee, in: Biomechanics of the Knee. Springer Berlin Heidelberg, pp. 129–210.

Netti, P.A., Ambrosio, L., 2002. Articular Cartilage, in: Barbucci, R. (Ed.), Integrated Biomaterials Science. Springer US, pp. 381–402.

O'Connor, J.J., 1993. Can muscle co-contraction protect knee ligaments after injury or repair? J. Bone Joint Surg. Br. 75, 41–48.

Pandy, M.G., Shelburne, K.B., 1997. Dependence of cruciate-ligament loading on muscle forces and external load. J. Biomech. 30, 1015–1024.

Paré, E.B., Stern, J.T., Schwartz, J.M., 1981. Functional differentiation within the tensor fasciae latae. A telemetered electromyographic analysis of its locomotor roles. J. Bone Joint Surg. Am. 63, 1457–1471.

Préville, A.-M., Lavigne, P., Buschmann, M.D., Hardin, J., Han, Q., Djerroud, L., Savard, P., 2013. Electroarthrography: a novel method to assess articular cartilage and diagnose osteoarthritis by non-invasive measurement of load-induced electrical potentials at the surface of the knee. Osteoarthr. Cartil. 21, 1731–1737.

Saladin, K.S., 2004. Anatomy & Physiology: The Unity of Form and Function. McGraw-Hill Higher Education.

Shelburne, K.B., Pandy, M.G., 1997. A musculoskeletal model of the knee for evaluating ligament forces during isometric contractions. J. Biomech. 30, 163–176.

Shelburne, K.B., Torry, M.R., Pandy, M.G., 2005. Muscle, ligament, and joint-contact forces at the knee during walking. Med. Sci. Sports Exerc. 37, 1948–1956.

Trimmel, M., Streicher, F., Groll-Knapp, E., Haider, M., 1989. The electromyographic DC potential as a correlate of muscular activity. Eur. J. Appl. Physiol. 58, 459–465.

Winby, C.R., Lloyd, D.G., Besier, T.F., Kirk, T.B., 2009. Muscle and external load contribution to knee joint contact loads during normal gait. J. Biomech. 42, 2294–2300.

Winter, D.A., 1995. A.B.C. (anatomy, Biomechanics and Control) of Balance During Standing and Walking. Waterloo Biomechanics.

Zavatsky, A.B., Beard, D.J., O'Connor, J.J., 1994. Cruciate ligament loading during isometric muscle contractions. A theoretical basis for rehabilitation. Am. J. Sports Med. 22, 418–423.

CHAPTER 4 ARTICLE 2: ELECTRICAL POTENTIALS MEASURED ON THE SURFACE OF THE KNEE REFLECT THE CHANGES OF THE CONTACT FORCE IN THE KNEE JOINT PRODUCED BY POSTURAL SWAY

by

Lin Zhu[1], Martin Garon[2], Éric Quenneville[2], Michael D. Buschmann[1] and Pierre Savard[1]

Submitted to the Gait & Posture in January 2016

[1] Institut de génie biomédical, Polytechnique Montréal, Montréal, Québec, Canada

[2] Biomomentum inc., Laval, Québec, Canada

Corresponding author:

Pierre Savard
Institute of biomedical engineering
École Polytechnique de Montréal
CP 6079 succ. Centre-ville
Montréal, Québec, Canada, H3C 3A7

Telephone: 1-514-340-4711 ext 4186
Fax: 1-514-340-4611
E-mail: pierre.savard@polymtl.ca

Keywords: Unipedal balance; knee joint; contact force; cartilage; electroarthrography.

Author's contribution

Lin Zhu	Data acquisition, data analysis, statistical analysis, literature review, drafting and critical revision of the manuscript
Martin Garon	Data acquisition system design, building experimental protocol, critical revision of the manuscript
Éric Quenneville	Data acquisition system design, building experimental protocol, critical revision of the manuscript
Michael D. Buschmann	Study conception and design, critical revision of the manuscript
Pierre Savard	Study conception and design, critical revision of the manuscript. Accepts responsibility for the integrity of the work as a whole

Highlights

- Electrical potentials can be measured on the knee surface during mechanical loading
- Postural sway during unipedal stance alters the joint contact force and potentials
- Ground reaction force and center of pressure displacement predict potentials

4.1 Abstract

Electroarthrography (EAG) is a novel technique for recording potentials on the knee surface during loading. We hypothesized that EAG can be used during unipedal stance as a "sensor" of the knee joint contact force due to body weight and muscle forces associated with postural balance. Twenty normal subjects (10 male, 10 female; age 29±10.5 yrs.; mass 68.8±14.2 kg; height 172.6±11.4 cm) mechanically loaded their knee by transferring their body weight from a bipedal stance to a unipedal stance, and back to a bipedal stance; this loading cycle was repeated 10 times on two different days. During loading, EAG potentials were recorded with 4 electrodes placed on the medial and lateral sides of the knee, over the joint line; the ground reaction force (GRF) and the antero-posterior and medial-lateral displacements of the center of pressure (COP) were measured with a force plate. Two electromechanical models predicting the EAG signal from the GRF alone, or from the GRF plus the COP displacements were computed by linear regression. The mean relative error between the four EAG signals and the predicted signals ranged from 24% to 49% for the GRF model, and from 15% to 35% for the GRF+COP model, this reduction was significant at 3 electrode sites ($p<0.05$). The GRF+COP model also improved the repeatability of the parameters estimated on the first and second days when compared to the GRF model. In conclusion, EAG reflects changes in the contact force of the knee joint due to postural sway during unipedal stance that can be predicted by the GRF and COP displacements.

4.2 Introduction

Electroarthrography (EAG) is a novel technology which consists of recording electrical potentials using electrodes applied on the surface of the knee during mechanical loading of the knee joint. A clinical study comparing normal subjects, osteoarthritis patients and patients with total knee replacement [1], a finite element modelling study [2] and animal studies [3][4] have supported

the hypothesis that EAG signals reflect the forces applied to the cartilage and its state of degradation. These EAG signals are generated by the relative displacement of ions against the fixed charge density within the cartilage that is induced by the hydrostatic pressure gradient during compression, this displacement produces “streaming potentials” that can be recorded directly on the cartilage surface and that are decreased in degraded cartilage [5][6][7].

To mechanically load the knee during the EAG recordings, the subjects stand on both legs, then slowly transfer their body weight to their instrumented leg and finally return to the bipedal stance. Variations of the EAG signals can be observed during loading as well as during successive loading cycles, which suggests that the cartilage is compressed not only by the body weight applied on the leg during the weight transfer. Indeed, measurements using instrumented knee implants have shown that the knee contact force measured *in vivo* during a unipedal weight bearing stance, which is similar to the loading technique used during the EAG measurements, range from 2 to 3 times the body weight [8]. This additional force can be attributed to the muscular activity developed by postural balance [9][10][11].

Direct assessment of these muscle forces is challenging. Since postural sway is closely related to muscle activity, monitoring the displacement of the centre of pressure (COP) of the subjects during the unipedal stance can provide useful information [12][13]. In biomechanics, the COP refers to the location of the vertical ground reaction force (GRF) vector which can be directly measured with a force platform [11]. It has been suggested that COP is particularly relevant to the biomechanical study of balance and postural control [14][15] and that COP excursions can be used as a good indicator of the postural stability of individuals [16].

We hypothesized that the EAG can be used during the unipedal stance in normal subjects as a “sensor” of the knee joint contact force, which would include the part of the body weight supported by the knee as well as muscle forces associated with postural sway and the displacement of the COP. Two electromechanical models predicting the EAG signal as a function of the ground reaction force and the orthogonal displacements of the COP were thus built to investigate the source of the EAG variations. Accounting for these variations can ultimately contribute to the development of optimized EAG measurement protocols with improved repeatability for the clinical assessment of cartilage degradation.

4.3 Methodology

4.3.1 Experiments

Twenty healthy volunteers without any relevant orthopedic injuries (10 male, 10 female; with age 29±10.5 y.o.; weight 68.8±14.2 kg; height 172.6±11.4 cm) were recruited. The experimental protocol was approved by the Research Ethics Board of Polytechnique Montréal. Before the experiments, each subject was informed of the experimental protocol and then signed an informed consent form.

Self-adhesive disposable electrodes (3M Red Dot) were used to measure the EAG signals from both sides of the knee of the dominant leg which was determined by the one-two step test: two electrodes were placed side by side on the medial side and two on the lateral side over the joint line which was determined by palpation (Figure 4.1). The reference electrode was positioned over the middle of the tibia and a ground electrode was placed below it. Before placing the electrodes, hair was shaved if necessary, and the skin under the electrode was cleaned with an abrasive paste (Nuprep) to reduce the skin-electrode impedance. An 8-channel portable wireless acquisition system (Bioradio 150, Clevemed Medical Inc., Cleveland, OH) was used to digitize the 4 EAG signals. These EAG signals and the 4 force signals described in the following paragraph were recorded simultaneously on a personal computer using custom designed software (LabView). A test-retest protocol was performed by having all the subjects complete the same measurement sequence on a subsequent day to evaluate the EAG repeatability.

During the EAG measurements, a Nintendo Wii Balance Board (WBB) was placed under the foot of the instrumented leg to record the GRF. The WBB has been increasingly used as a force plate for assessing postural control because it is inexpensive, portable and accurate [17], it exhibits excellent test-retest reliability for COP assessment and is being used to estimate standing balance in a clinical setting [18][19]. The WBB has four uniaxial vertical force transducers located at the four corners and the COP can be calculated (cm) along the anterior-posterior axis ($COP_{A/P}$), as well as along the medial-lateral axis ($COP_{M/L}$) with the following equations:

$$COP_{A/P} = \frac{L}{2}\frac{\left((TR+TL)-(BR+BL)\right)}{TR+TL+BR+BL} \tag{4.1}$$

$$COP_{M/L} = \frac{W}{2}\frac{((TR+BR)-(TL+BL))}{TR+TL+BR+BL} \quad (4.2)$$

Where the board dimensions are L = 43.3 cm and W = 22.8 cm, and TR, TL, BR and BL are the forces (kg) measured at the four corners of the WBB using the nomenclature shown in Figure 4.1.

A wooden board with the same height was placed under the other foot to help maintain balance during weight shifting. The subjects initially stood motionless on both legs, with their feet shoulder-width apart. Then, they slowly transferred their body weight on the instrumented leg to compress the cartilage. Finally, the subjects went back to the initial position. During this process, the subjects tried to keep their balance as best as possible. Each loading cycle lasted about 10 seconds. Ten loading cycles were repeated for averaging purposes.

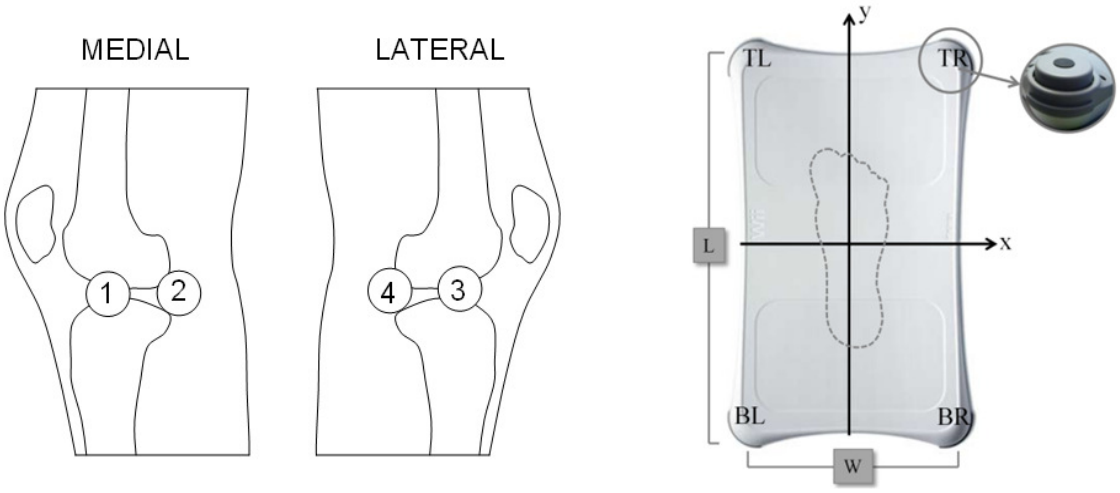

Figure 4.1 : Left panel: position of the 4 electrodes on the surface of the knee. Right panel: coordinate system and force transducers of the Wii Balance Board. The foot was placed within the dashed outline and the COP was calculated using the centre of board as the origin. Four transducers at each corner are identified as top left (*TL*), top right (*TR*), bottom left (*BL*) and bottom right (*BR*). The A/P movement corresponds with the *y* axis, and the M/L movement corresponds with the *x* axis.

Signal processing was carried out on a personal computer using user-written software (Matlab). The EAG and force signals were initially filtered with a low-pass filter having a cut-off frequency of 5 Hz to eliminate electromyographic interference. Then, the DC drift of both EAG and force signals, due to electrode polarization and amplifier offset potentials, was eliminated by subtracting from the measured signals a third degree polynomial manually fitted to each signal at the beginning and end of the loading cycle. This procedure was repeated for all the ten loading cycles.

4.3.2 Modeling

Standing on both feet in a symmetrical standing position, each knee supports the part of the body weight which is above, approximately 43% of the total body weight for each knee. When shifting to the unipedal stance, the loaded knee supports approximately 93% of the body weight [20]. If we consider this change as the only additional knee contact force and source of the EAG signals, the measured signal at any given time, $EAG(t)$, can be modeled as the linear combination of the streaming potential resulting from the ground reaction force $GRF(t)$ and a random error term ε.

$$EAG(t) = EMR * GRF(t) + \varepsilon \tag{4.3}$$

We refer to this equation as the GRF model. There is no constant term or linear drift in this equation because the baseline correction procedure shifted the signal so that the first and last points are always null. The amplitude of the EAG potential is assumed to be proportional to the ground reaction force, hence the coefficient *EMR* is defined as an *electromechanical ratio* (μV/kg) which describes the ability of the cartilage to generate a certain potential for a given ground reaction force. This coefficient should thus reflect the quality of the cartilage [5][6][7]. Finally, the *EMR* was estimated by linear regression using all the *EAG* and *GRF* samples recorded during a loading cycle.

A more complex model that takes into account the additional knee contact forces produced by the muscular activity necessary for postural control was developed. These muscular forces were estimated by the displacement of the COP as shown in Figure 4.2. In the sagittal plane, when the center of mass is anterior to the ankle joint, an ankle joint plantarflexion moment must be produced by the contraction of the gastrocnemius in order to maintain balance. This

plantarflexion moment causes the $COP_{A/P}$ to move anteriorly to counterbalance the tendency of leaning further forward [21]. Since the gastrocnemius muscles pull on the condyles of the femur when contracting, this produces a muscular force *M* acting on the articular joint which is added to *W*, the part of the body weight supported by the knee, and thus increases *R*, the resultant knee contact force. Finally, this also increases the streaming potentials generated by the compression of the cartilage. Thus, the $COP_{A/P}$ displacements can be used to assess the changes in the force from the calf muscles which can reach up to 6.2 times the body weight in unipedal balance [22].

In the coronal plane (Figure 4.2B), since the center of mass is located medially with respect to the knee joint, a lateral muscular force *M*, generated by the tensor fasciae latae and gluteus maximus muscles and pulling on the iliotibial band which is anchored on the lateral condyle of the tibia, is essential to maintain the equilibrium. The resultant force acting on cartilage, *R*, is the combination of supported body weight *W* and muscle force *M*. If the compression is equally distributed on the weight-bearing surface, the resultant force is approximately twice that of the body weight [20]. The $COP_{M/L}$ is controlled by the invertors and evertors of the foot, e.g., tibialis posterior and peronei [11]. The displacements of the $COP_{M/L}$ reflect changes in the resultant knee contact force and the EAG amplitude.

The second model, referred to as the GRF+COP model, is a linear combination of the streaming potential resulting from the ground reaction force $GRF(t)$, and the muscular forces assessed by the displacements of the COP along both antero-posterior and medial-lateral axes.

$$EAG(t) = EMR\ GRF(t) + \beta\ COP_{A/P}(t) + \gamma\ COP_{M/L}(\mathrm{t}) + \varepsilon \tag{4.4}$$

The coefficients *EMR,* β and γ are estimated by multiple linear regression using all the *EAG*, *GRF*, $COP_{A/P}$ and $COP_{M/L}$ samples recorded during a loading cycle. The coefficients β and γ express the ability of the cartilage to generate a certain potential for a given displacement of the COP, but they also depend on the subject's weight and the lever arm between the insertion point of the tendon and the axis of the knee joint in the appropriate plane. Since this distance is specific to each subject and not readily available, the estimated β and γ values were not retained in our analysis to characterize the cartilage quality which is more directly related to the *EMR* coefficient.

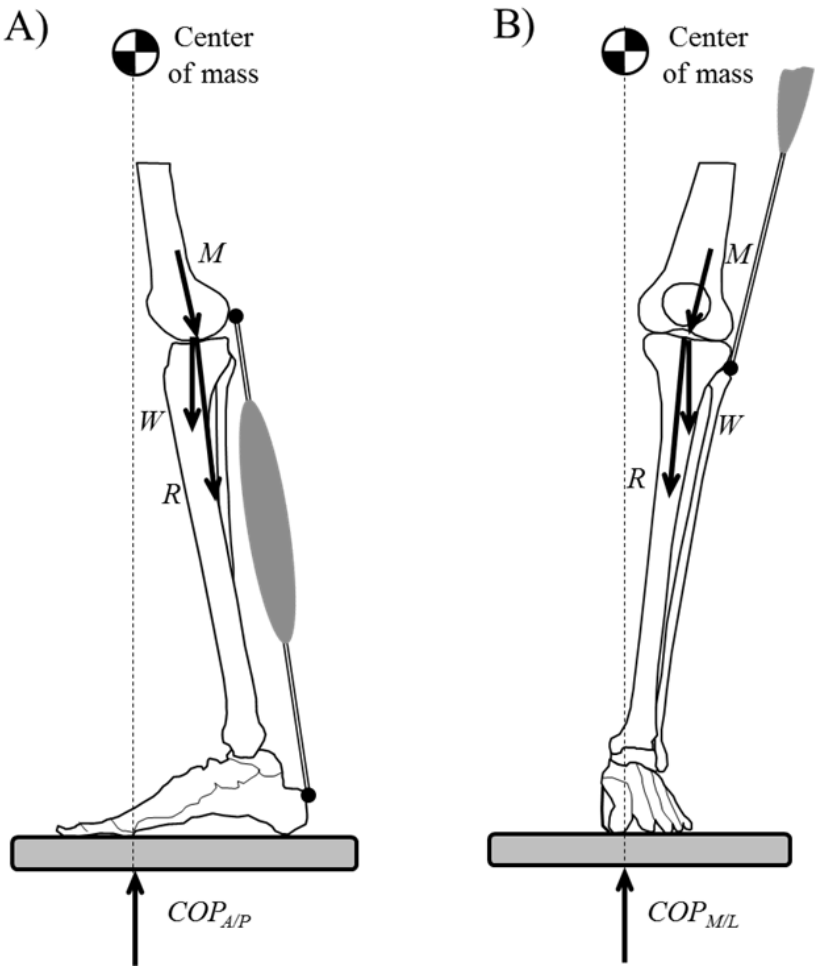

Figure 4.2 : Conceptual 2D models representing static knee loading during the one-legged stance. The gray rectangle represents the force plate under the foot. A) Sagittal plane: *W*, part of the body weight supported by the knee; *M*, force generated by the gastrocnemius muscles and pulling on the condyles of the femur to maintain equilibrium; *R*, resultant of *W* and *M* forces passing through the mechanical axis; the black arrow under the force plate represents the position of the center of pressure along the antero-posterior axis, $COP_{A/P}$. B) Coronal plane: *W* and *R*, same as above; *M*, force generated by the tensor fasciae latae and gluteus maximus muscles and pulling on the iliotibial band which is anchored on the lateral condyle of the tibia to maintain equilibrium; the black arrow under the force plate represents the position of the center of pressure along the medial-lateral axis, $COP_{M/L}$.

Finally, the average relative error (RE) between a measured EAG signal and the modeled signal during a loading cycle comprising N samples was computed to evaluate the reconstruction accuracy with the two proposed models. Herein, a lower RE implies a better estimation.

$$\mathrm{RE} = \sum_1^N \frac{|\mathrm{EAG} - \widehat{\mathrm{EAG}}|}{|\mathrm{EAG}|} * \frac{100\%}{N} \tag{4.5}$$

4.4 Results

Signals recorded during a loading cycle are presented in Figure 4.3. For each of the 4 EAG signals that are shown (in black), the parameters of eqs. (4.3) and (4.4) were first computed by linear regression and then applied to the corresponding GRF and COP signals to compute the predicted EAG values for the two models. During the loading cycle, we observe that the GRF changes from about half the body weight to the whole body weight, and then return to about half of the body weight. Meanwhile, the COP moves in both A/P and M/L directions. All the 4 EAG signals increase during loading, reflecting the electrical currents flowing away from the zones of compression and toward the electrodes [2]. The EAG signals also show local maxima at the beginning and end of the loading cycle. These local maxima are not seen in the signals computed with the GRF model. However, they are well reproduced with the GRF+COP model which incorporates the COP displacements. Indeed, we observe that the local maxima in the EAG signals correspond to those of the COP in A/P direction. The relative errors between the modeled EAG signals computed with the simple GRF model and the measured EAG signals are 11.9%, 11.9%, 12.5% and 16.7%, for the four channels, respectively. The relative errors decreased to 8.9%, 9.1%, 9.3% and 12.3% with the GRF+COP model.

The average EMR and RE of the ten loading cycles were calculated for each subject and each EAG channel. The mean and standard error of these averaged values were then computed for the 20 subjects and shown in Figure 4.4. The EMR estimated with the GRF model is abbreviated as EMR/GRF, whereas the EMR estimated with the GRF+COP model is abbreviated as EMR/GRF+COP. There is no statistically significant difference between the EMR/GRF and the EMR/GRF+COP for all the four EAG channels, which signifies that most of the EAG signals can

be attributed to GRF change. However, the absolute values of the EMR/GRF are slightly greater than the EMR/GRF+COP, which suggest that the EMR is overestimated because of the part of the EAG which is generated by the contractile force of muscles for postural control is incorporated into the estimated EMR.

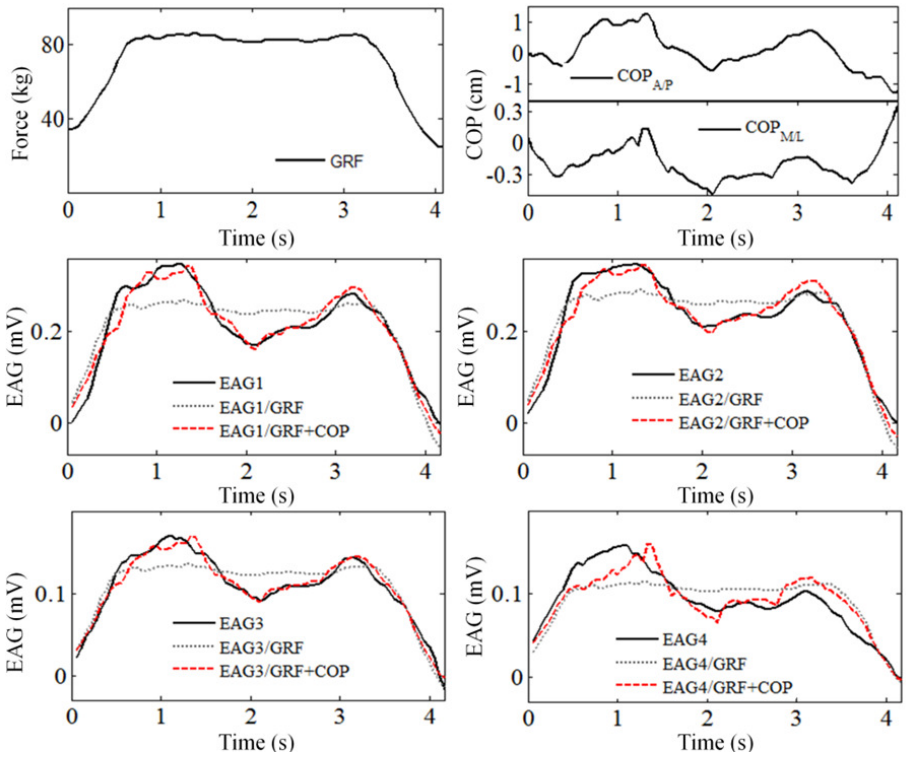

Figure 4.3 : Representative EAG signals and the corresponding signals predicted by the two models during a loading cycle. Top left: ground reaction force collected by the force plate under the instrumented leg. Top right: center of pressure displacements along the A/P and M/L directions. Middle left to bottom right: the 4 measured EAG signals (black line), and their corresponding modeled ones; EAG 1 and EAG2 were recorded on the medial side of the knee, whereas EAG3 and EAG4 were recorded on the lateral side. The gray dotted lines represent the EAGs computed from the ground reaction force using the GRF model. The dashed red lines represent the EAGs computed from the ground reaction force and the center of pressure displacements along the A/P and M/L directions with the GRF+COP model.

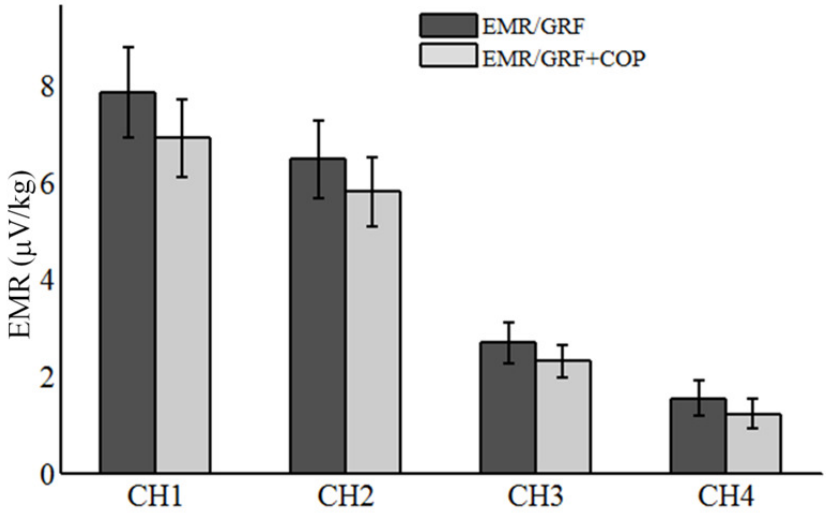

Figure 4.4 : The mean and standard error of the electromechanical ratios estimated with the GRF and GRF+COP models for 20 subjects. CH1 and CH2 are the EAG channels from the medial side of the knee, CH3 and CH4 are from the lateral side.

Similarly, the RE estimated with the GRF model is abbreviated as RE/GRF, and the RE estimated with the GRF+COP model is abbreviated as RE/GRF+COP. Figure 4.5 shows that the RE/GRF is significantly higher than the RE/GRF+COP for electrode sites 1, 2 and 4. The RE decreases by about 10% for all four channels when using the GRF+COP model. The relative errors are lower on the medial side (CH1 and CH2) than on the lateral side (CH3 and CH4), because the EAG amplitude and the signal-to-noise ratio are higher.

For the test-retest analysis, the intraclass correlation coefficients (ICC) were computed between the estimated EMRs of the first and second days for each electrode site and for each EAG model using a repeated measurement model with the statistical software SAS (Table 4.1). The GRF+COP model increased the ICC, and thus improved the repeatability, when compared to the GRF model. The EAG signals from the medial side of the knee also showed a better repeatability because of their higher signal-to-noise ratio.

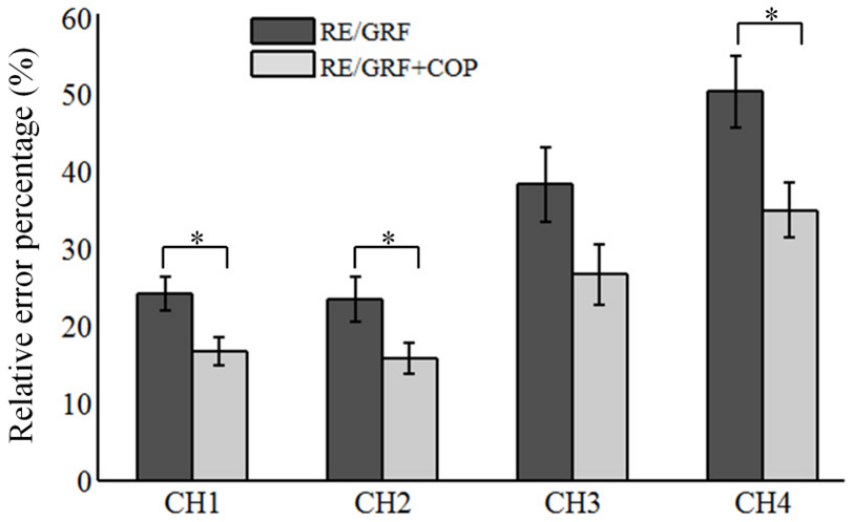

Figure 4.5 : The mean and standard error of the relative errors computed between the measured EAG and the modeled signals using the GRF and GRF+COP models for 20 subjects. CH1 and CH2 indicate the EAG channels from the medial side of the knee, and CH3 and CH4 are from the lateral side. The asterisk * signifies $p < 0.05$.

Table 4.1 : Intraclass correlation coefficient (ICC) between the EMRs obtained on the first and second days for the two models

ICC between the EMRs of day1 and day2	CH1	CH2	CH3	CH4
Based on the GRF model	0.667	0.697	0.553	0.418
Based on the GRF+COP model	0.732	0.757	0.564	0.435

4.5 Discussion

As previously mentioned, the contact force of the knee joint measured *in vivo* can reach up to 2 to 3 times the body weight during the unipedal weight bearing stance [8]. The load on the knee would be highly underestimated if only body weight is considered. Even in static conditions,

muscle activity is required to maintain equilibrium. Even though the body seems to be relatively still in the A/P direction during the body weight shifting protocol, the subjects constantly alter the contractile force of the ankle joint plantarflexors and dorsiflexors in order to maintain balance [23]. Moreover, although the range of COP displacement in M/L direction is small due to anatomical limitations, the invertors and evertors cannot work independently, which requires the collaboration of the plantarflexors and dorsiflexors. For example, if the gastrocnemius muscles are activated to move the COP anteriorly, they also move the COP laterally [22]. Therefore, the inclusion in the electromechanical model of the COP displacement in the M/L direction is essential.

There are several advantages for incorporating the COP displacements into the electromechanical model. First, the COP can be easily measured during the EAG recordings with the addition of a force plate. Second, the COP displacement can better estimate the overall muscle activity which is specific to postural control than surface electromyography (EMG), which is less sensitive to the activity of deeper muscles [24], and has an indirect relationship with the developed force. Finally, the electromechanical ratio between the EAG potentials and the ground reaction force which is computed with the GRF+COP model is inherently less sensitive to the muscle activity produced by postural sway which is a significant source of variation. This ratio thus shows a better reproducibility than the ratio computed with the simpler GRF model. This is an important advantage for the clinical application of the EAG technique for the detection of cartilage degradation.

In this work, we proposed two electromechanical models to explore the origin of the EAG signals. The results showed that the electrical potentials obtained at the surface of the knee during a unipedal stance are well correlated with the displacements of the center of pressure which reflect the changes in the contact force of the knee joint. This was observed at all the four electrode sites on both the medial and lateral sides of the knee. The greater EMR values observed on the medial side than on the lateral side can be due to the larger hydrostatic pressure in the medial compartment [25]. The contact force is not only attributed to body weight, but also to the muscle activity produced for postural control during the unipedal stance. The local maxima that often appear on the EAG signals at the onset and offset of a loading cycle and which were initially attributed to noise have now been explained by the time-varying muscular forces during

postural sway. The proposed electromechanical GRF+COP model improves the reproducibility of the EAG measurements and can contribute to the development of a clinically applicable technique to assess the intrinsic properties of cartilage and detect its degradation.

4.6 Acknowledgements

This work was supported by the Canadian Institutes of Health Research (Operating grant number: APP37148), the Canadian Natural Sciences and Engineering Research Council (Grant number: CRDPJ 445265-12) and the China Scholarship Council (Scholarship number: 2009625035). The study sponsors were not involved in the decision to submit the manuscript for publication.

4.7 References

[1] A.-M. Préville, P. Lavigne, M. D. Buschmann, J. Hardin, Q. Han, L. Djerroud, and P. Savard, "Electroarthrography: a novel method to assess articular cartilage and diagnose osteoarthritis by non-invasive measurement of load-induced electrical potentials at the surface of the knee," *Osteoarthr. Cartil. OARS Osteoarthr. Res. Soc.*, vol. 21, no. 11, pp. 1731–1737, Nov. 2013.

[2] Q. Han, M. D. Buschmann, and P. Savard, "The forward problem of electroarthrography: modeling load-induced electrical potentials at the surface of the knee," *IEEE Trans. Biomed. Eng.*, vol. 61, no. 7, pp. 2020–2027, Jul. 2014.

[3] A. Changoor, M. Hoba, M. Garon, E. Quenneville, K. Gordon, M. D. Buschmann, P. Savard, and M. B. Hurtig, "Electroarthrography provides a non-invasive streaming potential-based method for detecting natural and trypsin-induced cartilage degeneration in equine fetlock joints," *Osteoarthritis Cartilage*, vol. 21, p. S103, Apr. 2013.

[4] A. Changoor, W. Brett, M. Hoba, M. Garon, E. Quenneville, K. Gordon, P. Savard, M. D. Buschmann, M. B. Hurtig, and D. R. Trout, "Electroarthrography, a non-invasive streaming potential-based method, measures cartilage quality in live horses," *Osteoarthritis Cartilage*, vol. 22, pp. S88–S89, Apr. 2014.

[5] A. Légaré, M. Garon, R. Guardo, P. Savard, A. R. Poole, and M. D. Buschmann, "Detection and analysis of cartilage degeneration by spatially resolved streaming

potentials," *J. Orthop. Res. Off. Publ. Orthop. Res. Soc.*, vol. 20, no. 4, pp. 819–826, Jul. 2002.

[6] A. C. Chen, T. T. Nguyen, and R. L. Sah, "Streaming potentials during the confined compression creep test of normal and proteoglycan-depleted cartilage," *Ann. Biomed. Eng.*, vol. 25, no. 2, pp. 269–277, Apr. 1997.

[7] M. Garon, A. Légaré, R. Guardo, P. Savard, and M. D. Buschmann, "Streaming potentials maps are spatially resolved indicators of amplitude, frequency and ionic strength dependant responses of articular cartilage to load," *J. Biomech.*, vol. 35, no. 2, pp. 207–216, Feb. 2002.

[8] I. Kutzner, B. Heinlein, F. Graichen, A. Bender, A. Rohlmann, A. Halder, A. Beier, and G. Bergmann, "Loading of the knee joint during activities of daily living measured in vivo in five subjects," *J. Biomech.*, vol. 43, no. 11, pp. 2164–2173, Aug. 2010.

[9] K. B. Shelburne, M. R. Torry, and M. G. Pandy, "Muscle, ligament, and joint-contact forces at the knee during walking," *Med. Sci. Sports Exerc.*, vol. 37, no. 11, pp. 1948–1956, Nov. 2005.

[10] M. Adouni, A. Shirazi-Adl, and R. Shirazi, "Computational biodynamics of human knee joint in gait: from muscle forces to cartilage stresses," *J. Biomech.*, vol. 45, no. 12, pp. 2149–2156, Aug. 2012.

[11] D. Winter, "Human balance and posture control during standing and walking," *Gait Posture*, vol. 3, no. 4, pp. 193–214, Dec. 1995.

[12] P. G. Morasso and M. Schieppati, "Can Muscle Stiffness Alone Stabilize Upright Standing?," *J. Neurophysiol.*, vol. 82, no. 3, pp. 1622–1626, Sep. 1999.

[13] K. Masani, M. R. Popovic, K. Nakazawa, M. Kouzaki, and D. Nozaki, "Importance of Body Sway Velocity Information in Controlling Ankle Extensor Activities During Quiet Stance," *J. Neurophysiol.*, vol. 90, no. 6, pp. 3774–3782, Dec. 2003.

[14] D. A. Winter, F. Prince, J. S. Frank, C. Powell, and K. F. Zabjek, "Unified theory regarding A/P and M/L balance in quiet stance," *J. Neurophysiol.*, vol. 75, no. 6, pp. 2334–2343, Jun. 1996.

[15] N. Jamshidi, M. Rostami, S. Najarian, M. B. Menhaj, M. Saadatnia, and F. Salami, "Differences in center of pressure trajectory between normal and steppage gait," *J. Res. Med. Sci. Off. J. Isfahan Univ. Med. Sci.*, vol. 15, no. 1, pp. 33–40, 2010.

[16] A. Ruhe, R. Fejer, and B. Walker, "The test–retest reliability of centre of pressure measures in bipedal static task conditions – A systematic review of the literature," *Gait Posture*, vol. 32, no. 4, pp. 436–445, Oct. 2010.

[17] H. L. Bartlett, L. H. Ting, and J. T. Bingham, "Accuracy of force and center of pressure measures of the Wii Balance Board," *Gait Posture*, vol. 39, no. 1, pp. 224–228, Jan. 2014.

[18] R. A. Clark, A. L. Bryant, Y. Pua, P. McCrory, K. Bennell, and M. Hunt, "Validity and reliability of the Nintendo Wii Balance Board for assessment of standing balance," *Gait Posture*, vol. 31, no. 3, pp. 307–310, Mar. 2010.

[19] J. M. Leach, M. Mancini, R. J. Peterka, T. L. Hayes, and F. B. Horak, "Validating and calibrating the Nintendo Wii balance board to derive reliable center of pressure measures," *Sensors*, vol. 14, no. 10, pp. 18244–18267, 2014.

[20] D. P. G. J. Maquet, "Biomechanical Treatment of Osteoarthritis of the Knee," in *Biomechanics of the Knee*, Springer Berlin Heidelberg, 1976, pp. 129–210.

[21] D. A. Winter, *A.B.C. (anatomy, Biomechanics and Control) of Balance During Standing and Walking*. Waterloo Biomechanics, 1995.

[22] K. J. Kim, E. Uchiyama, H. B. Kitaoka, and K. N. An, "An in vitro study of individual ankle muscle actions on the center of pressure," *Gait Posture*, vol. 17, no. 2, pp. 125–131, Apr. 2003.

[23] D. A. Winter. (2009), *Biomechanics and Motor Control of Human Movement, Fourth Edition*.[Online]. Available: http://ca.wiley.com/WileyCDA/WileyTitle/productCd-0470398183.html

[24] T. A. Kuiken, M. M. Lowery, and N. S. Stoykov, “The effect of subcutaneous fat on myoelectric signal amplitude and cross-talk,” Prosthet. Orthot. Int., vol. 27, no. 1, pp. 48–54, Apr. 2003.

[25] F. Johnson, S. Leitl, and W. Waugh, “The distribution of load across the knee. A comparison of static and dynamic measurements,” J. Bone Joint Surg. Br., vol. 62, no. 3, pp. 346–349, Aug. 1980.

CHAPTER 5 ARTICLE 3: DECREASE OF THE ELECTRICAL POTENTIALS MEASURED ON THE SURFACE OF THE KNEE AND PRODUCED BY CARTILAGE COMPRESSION DURING SUCCESSIVE LOADING CYCLES

by

Lin Zhu[1], Martin Garon[2], Éric Quenneville[2], Michael D. Buschmann[1] and Pierre Savard[1]

Submitted to the Journal of Biomechanics in March 2016

[1] Institut de génie biomédical, Polytechnique Montréal, Montréal, Québec, Canada

[2] Biomomentum inc., Laval, Québec, Canada

Corresponding author:

Pierre Savard
Institute of biomedical engineering
École Polytechnique de Montréal
CP 6079 succ. Centre-ville
Montréal, Québec, Canada, H3C 3A7

Telephone: 1-514-340-4711 ext 4186
Fax: 1-514-340-4611
E-mail: pierre.savard@polymtl.ca

Keywords

Knee joint, Cartilage, Streaming potentials, Electroarthrography, Hysteresis

Author's contribution

Lin Zhu	Data acquisition, data analysis, statistical analysis, literature review, drafting and critical revision of the manuscript
Martin Garon	Data acquisition system design, building experimental protocol, critical revision of the manuscript
Éric Quenneville	Data acquisition system design, building experimental protocol, critical revision of the manuscript
Michael D. Buschmann	Study conception and design, critical revision of the manuscript
Pierre Savard	Study conception and design, critical revision of the manuscript. Accepts responsibility for the integrity of the work as a whole

5.1 Abstract

Electroarthrography (EAG) is a new technique for measuring electrical potentials appearing on the knee surface during loading that reflects cartilage quality and joint contact force. Our objective was to investigate the evolution of EAG signals during successive loading cycles. A first study was conducted on 20 standing subjects who shifted their body weight to achieve knee loading. Their EAG signals were recorded during 10 successive loading cycles and during a subsequent sequence of 10 cycles recorded after a 15 min exercise period. Multiple linear regression models estimated the electro-mechanical ratio (EMR) interpreting the ability of cartilage to generate a certain potential for a given ground reaction force by taking into account this force and the center of pressure displacements during unipedal stance. The results showed that the EMR values slowly decreased with successive cycles: during the initial sequence, the correlation coefficients between EMR values and sequence numbers were significant at 3 of the 4 electrode sites ($p < 0.05$); for the post-exercise sequence, the EMR values still decreased and were significantly lower than during the initial sequence ($p<0.001$) To eliminate the possible involvement of muscle contraction in this decrease, a passive loading protocol was applied for 6 supine subjects. The results also showed that the EAG values decreased during successive cycles while the electromyogram signals from 4 muscle groups remained stable. We conclude that the reduction of EMR values does not arise from muscle activity and habituation of the stretch reflex, but from the electromechanical properties of cartilage.

5.2 Introduction

Electroarthrography (EAG) refers to a novel technique for measuring the load-induced streaming potentials at the surface of knee that are generated by articular cartilage. Streaming potentials, an electromechanical phenomenon, arises from the movement of electrolyte ions in the liquid phase relative to charge groups that are fixed to the cartilage extracellular matrix (ECM) under dynamic compression (Paolo A. Netti, 2007). *In vitro* studies have shown that streaming potentials can indicate cartilage degeneration (Frank, et al. 1987; Garon et al., 2002; Légaré et al., 2002). We previously demonstrated in simulations, animal studies and a clinical study that load-induced electric potentials can also be detected at the surface of the knee and can potentially be used for

the non-invasive assessment of cartilage quality (Préville et al., 2013; Han et al., 2014; Changoor et al., 2014).

Although a test-retest protocol demonstrated that EAG measurements are repeatable (Préville et al., 2013), some variability can still be observed in the EAG amplitude within individuals, which can hinder its clinical application for cartilage quality assessment. During *in vivo* EAG measurements, joint loading is achieved by having the subjects slowly shift their weight from a bipedal stance to a unipedal stance. The regulation of balance during weight shifting involves continuous muscular activities by which the knee contact force can also be influenced (Adouni et al., 2012). The resultant contact force that has been measured *in vivo* is thus two to three times the body weight during a one-legged stance (Kutzner et al., 2010). By monitoring electromyograms (EMG) of the knee flexor and extensor muscles during EAG measurements, we also observed that knee flexors and extensors, especially gastrocnemius, were activated during weight shifting to maintain balance (Zhu et al., 2016). Thus, muscular activities that are inevitable in body sway can contribute to the variation of the EAG measurements.

To reduce the muscular contribution to the contact force of the knee joint, a new passive loading protocol is proposed here (Figure 5.1A). Instead of directly loading the knee in an upright position, an external force is applied perpendicular to the tibia in supine subjects. The shear force produces hyperextension of the knee angle and strains the collateral ligaments and the anterior cruciate ligament, thus increasing the contact force in the knee joint (Moglo and Shirazi, 2005). We hypothesize that minimal muscular activity will be induced with this loading protocol and that the load-induced EAG signals will be proportional to the applied loading force.

Loading sequences consist of six to ten cycles for averaging purposes (Préville et al., 2013; Changoor et al., 2014). To our knowledge, no previous studies have investigated the evolution of the EAG signals during successive loading cycles. Therefore, a temporal analysis of the EAG signals was carried out using both the weight shifting protocol (WSP) and the passive hyperextension loading protocol (PHLP). By this study, we hope to improve the understanding the EAG signals and contribute to the development of reliable EAG techniques for cartilage quality assessment.

5.3 Methodology

The experimental protocol was approved by the Research Ethics Board of Polytechnique Montréal. Before the experiments, each subject was informed of the experimental protocol and then signed an informed consent form. The WSP study comprised 20 subjects (10 males, 10 females), with age 28.5±10.7 y.o., height 172.7±11.4 cm, weight 67.5±14.4 kg; the subsequent PHLP study comprised six subjects (3 males, 3 females), with age 34.7±16.2 y.o., height 172.5± 11.9 cm, weight 69.1±12.3 kg. None of the participants reported any history of knee injury or symptomatic abnormalities.

Self-adhesive recessed disposable electrodes (Red Dot™, 3M) were used to measure the EAG signals from the surface of the knee. The electrodes were positioned over the joint line of the knee on the dominant leg (Préville et al., 2013). The joint line was determined by palpation. Four electrodes for the WSP study and two electrodes for the PHLP study were distributed over the medial and lateral sides. As described in a following section, the need to record electromyograms for the PHLP technique reduced the number of available EAG channels. A reference electrode was positioned at the middle of the frontal tibia and a ground electrode was placed just below it. Skin preparation with an abrasive paste (Nuprep) was performed at all electrode sites to minimize epidermal impedance before placing the electrodes. Hair was shaved if necessary.

5.3.1 Weight shifting protocol

For the WSP study, the subjects were informed not to do any strenuous physical exercise before the experiments. The subjects stood barefoot with their feet shoulder-width apart, keeping their legs straight and their eyes fixed ahead to eliminate any excess motion. To mechanically load the cartilage, the subjects swung slowly to transfer all their body weight to the measured leg in a controlled manner for 3~4s. Then, they came back to the initial position with the body weight equally distributed on both legs. Data were collected for 3 s prior to and after the loading. A Nintendo Wii Balance Board (WBB) was placed under the foot of the measured knee to record the four vertical forces at the corners of the board. A wooden plate with the same height was placed under the other foot to maintain normal balance. Each subject was given the opportunity to practice the weight shifting procedure before EAG capture began, with usually 3 to 5 cycles.

When the subjects became adept with the protocol, 10 consecutively loading sequences were recorded. Hereafter, to determine whether the results could be reproduced and investigate the possible role of prior physical activity, the subjects continued the weight shifting exercise for about 15 minutes. Once this exercise was completed, 10 more consecutive loading sequences were documented.

5.3.2 Passive hyperextension loading protocol

Knee loading was achieved during the PHLP study while the subjects were lying on their back (Figure 5.1 A). Specifically, the operator slowly pressed the tibia at the tuberosity level by the thumb and index fingers for several seconds, and then released. The foot was not constrained during loading but the subjects maintained a constant vertical orientation of the foot. To characterize the relationship between the applied force and the EAG signals, a force plate (FP-BTA, Vernier software and technology, LLC) was placed on a table under the heel of the measured leg to record the force transferred to the heel. The table did not extend under the leg of the subjects. The loading procedure was repeated only five times for each subject so as to better reproduce the manual loading. To detect possible muscle activity from the leg during the PHLP study, electromyography (EMG) signals were also recorded. Five pairs of electrodes (Red Dot™, 3M) with an inter-electrode distance of 35 mm were positioned parallel to the muscle fibers according to SENIAM standard (Hermens, et al., 2000). Five sites were chosen on the gastrocnemius medialis (GM) and the gastrocnemius lateralis (GL) from the calf, the biceps femoris long head (BF) of the hamstring, the rectus femoris (RF) in the middle of the front thigh and the tensor fasciae latae (TFL) on the line from the anterior spina iliac superior to the lateral femoral condyle.

5.3.3 Data acquisition and processing

The EAG, EMG and force signals were recorded simultaneously with a portable 8-channel wireless acquisition system (Bioradio 150, Clevemed Medical Inc., Cleveland, OH). The EAG and force signals were amplified with DC coupling whereas the EMG signals were amplified with AC coupling. The sampling rate was 600 Hz with a resolution of 16 bits. Signal processing was carried out on a personal computer using user-written software (Matlab). All digitalized

EAG and force signals were initially low-pass filtered with a 5 Hz cut-off frequency to reduce possible high frequency components, such as EMG, noise and 60 Hz interference. Afterwards, the DC drift of both EAG and force signals, originating from electrode polarization and amplifier offset potential, was corrected. Note that the drift due to electrode polarization prevents recordings longer than about 5 to 10 s. To correct this drift, the operator manually selected points prior to and after each loading cycle by examining the force signals. A third degree polynomial was used to reconstruct the baseline based on the selected values and subtracted from the filtered EAG and force signals respectively. This procedure was repeated for all the loading cycles. As for the EMG signals from the PHLP data, the average of the two EMG signals from the gastrocnemius was first computed. The four EMG signals were then high-pass filtered (20 Hz) and fully rectified. A low-pass filter with cut-off frequency of 5 Hz was finally used to compute the EMG envelope.

5.3.4 WSP modeling

Initially, EAG analysis involved only the amplitude of the measured potentials during loading (Préville et al., 2013). Since streaming potentials are associated with loading conditions, the term *electro-mechanical ratio* (EMR: μV/kg) was later brought to describe the ability of the cartilage to generate a certain potential for a given force (Schmidt-Rohlfing et al., 2002 ;Changoor et al., 2013). The knee joint contact force that compresses the cartilage during WSP loading is difficult to measure. It incorporates not only the ground reaction force (GRF) (Kutzner et al., 2010), but also the muscle forces that maintain the balance of the subject. Thus, when the center of mass of an upright subject moves anteriorly, the tendons of the gastrocnemius muscles pull on the condyles of the femur to maintain balance, which increases the knee contact force (Figure 5.1B). Similarly, when the center of mass moves medially, a force generated by the tensor fasciae latae and gluteus maximus muscles pulls on the iliotibial band which is anchored on the lateral condyle of the tibia, which again increases the contact force (Figure 5.1C). The centre of pressure (COP) is a good indicator to estimate the balance of individuals in posture control (Winter, et al., 1996) and its displacement is associated to the muscle forces acting across the knee joint. Therefore, an electromechanical model was developed to predict the EAG signal from the GRF and the COP displacements. These displacements (cm) can be calculated from the WBB data along the

anterior-posterior axis ($COP_{A/P}$), as well as along the medial-lateral axis ($COP_{M/L}$) with the following equations:

$$COP_{A/P} = \frac{L}{2}\frac{\left((TR+TL)-(BR+BL)\right)}{TR+TL+BR+BL} \tag{5.1}$$

$$COP_{M/L} = \frac{W}{2}\frac{((TR+BR)-(TL+BL))}{TR+TL+BR+BL} \tag{5.2}$$

Where the board dimensions are $L = 43.3$ cm and $W = 22.8$ cm, and *TR* (top right), *TL* (top right), *BR* (bottom right) and *BL* (bottom left) represent the forces (kg) measured by four sensors at each corner of the WBB. Finally, the EAG signal measured at a given time $EAG(t)$ can be modelled as linear combination of the ground reaction force $GRF(t)$, and the muscular forces represented by the displacements of the COP along both antero-posterior and medial-lateral directions.

$$EAG(t) = EMR \cdot GRF(t) + \beta \cdot COP_{A/P}(t) + \gamma \cdot COP_{M/L}(\mathrm{t}) + \varepsilon \tag{5.3}$$

The coefficients *EMR,* β and γ are estimated by multiple linear regression using all the *EAG, GRF,* $COP_{A/P}$ and $COP_{M/L}$ samples recorded during a loading cycle. The coefficient ε represents random noise and there is no constant term in this equation since the baseline correction was applied to both EAG and GRF signals. The coefficients β and γ express the ability of the cartilage to generate a certain potential for a given displacement of the COP, but they also depend on the subject's weight and the lever arm between the insertion point of the tendon and the axis of the knee joint in the appropriate plane. Since this distance is specific to each subject and not readily available, the estimated β and γ values were not retained in our analysis to characterize the cartilage quality which is more directly related to the *EMR* coefficient.

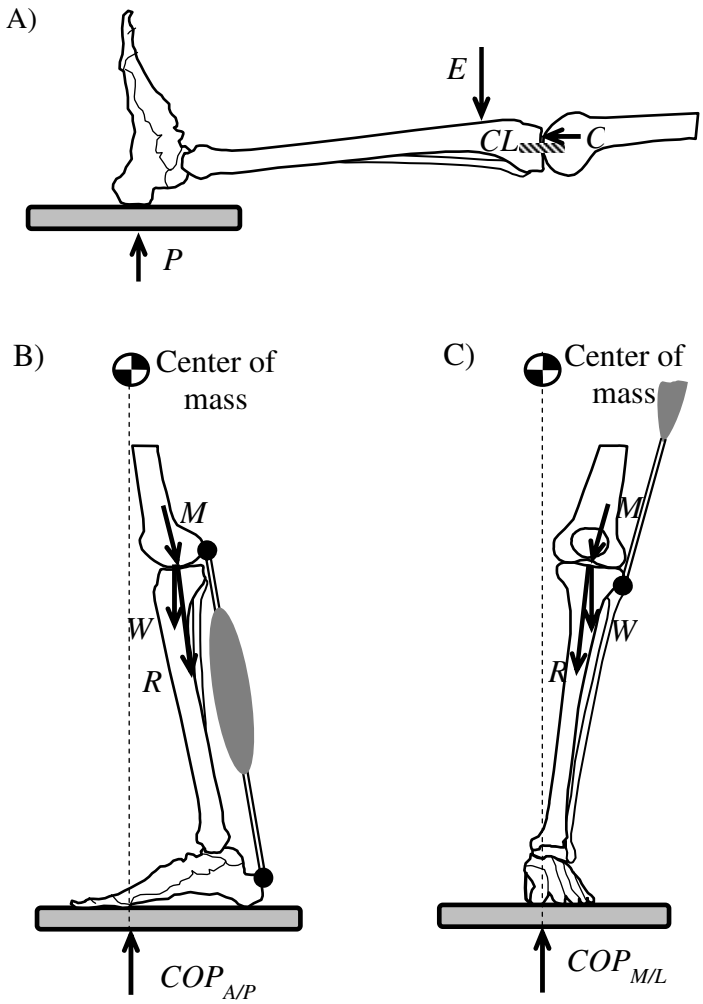

Figure 5.1: Knee loading during hyperextension (top) and unipedal stance (bottom). The gray rectangles represent the force plate. A) Sagittal plane: *E*, manually applied external force on supine subjects; *P*, measured force; *C*, joint contact force; *CL*, collateral ligament. B) Sagittal plane: *W*, part of the body weight supported by the knee; *M*, force by the gastrocnemius pulling on the condyles of the femur to maintain equilibrium; *R*, resultant of *W* and *M* passing through the mechanical axis; $COP_{A/P}$, position of the center of pressure along the antero-posterior axis, C) Coronal plane: *W* and *R*, same as above; *M*, force generated by the tensor fasciae latae and gluteus maximus muscles and pulling on the iliotibial band which is anchored on the lateral condyle of the tibia to maintain equilibrium; $COP_{M/L}$, the position of the center of pressure along the medial-lateral axis.

5.4 Results

Measured and modeled EAG signals obtained during the weight shifting protocol are shown in Figure 5.2.

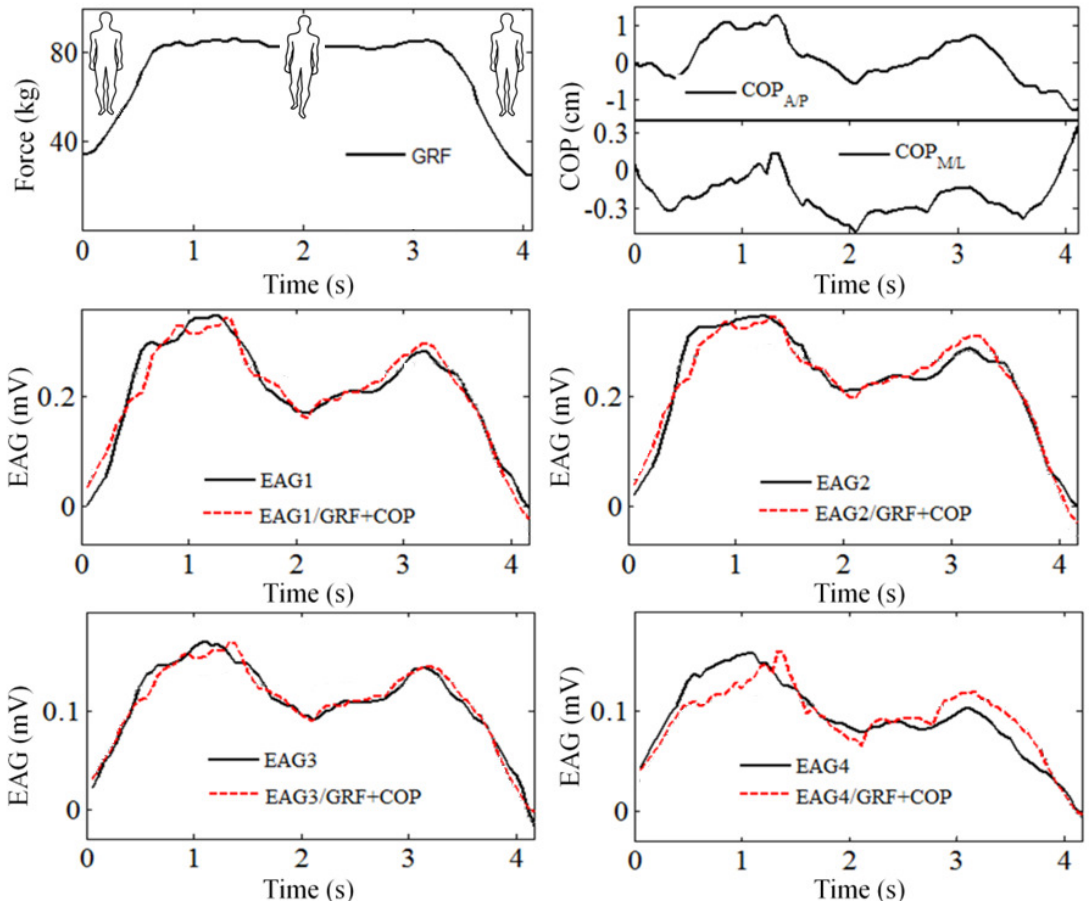

Figure 5.2: Measured and modeled EAG signals during a loading cycle with the weight shifting protocol. Top left: ground reaction force as the subject goes from a bipedal stance to a unipedal stance, and back to a bipedal stance. Top right: center of pressure displacements in the anteroposterior ($COP_{A/P}$) and mediolateral ($COP_{M/L}$) directions. Middle left to bottom right: measured and modeled EAG signals at the four electrode sites (EAG1, anteromedial; EAG2, posteromedial; EAG3, anterolateral; EAG4, posterolateral). The black line indicates the measured EAG signal, and the dashed red line shows the modelled signal based on the GRF and COP displacements.

As the subject went from a bipedal stance to a unipedal stance, the GRF changed from about half the body weight to the whole body weight, and then back during unipedal stance. The measured EAG signals at the four electrode sites showed broad positive deflexions during loading, but their shape did not exactly reflect the GRF signal. The EAG signals showed smaller positive deflexions at the beginning and end of the loading cycle which were not present in the GRF signal, but which were similar to the anterior COP displacement. Thus, both GRF and COP displacements signals are taken into account by the electromechanical model. For each of the four EAG signals, the parameters of eq. (5.3) were first computed by linear regression during each loading cycle and the model was then applied to the corresponding GRF and COP signals to compute the predicted EAG values. The modelled signals reproduced adequately the measured EAG signals. This procedure was applied to all loading cycles of all subjects to estimate their EMRs.

The mean EMRs of 20 subjects during successive WSP loading cycles are plotted in Figure 5. 3 for the four channels. The electromechanical ratio (EMR) estimated with the individualized models slowly decreased during successive loading cycles. During the initial loading sequence as well as during the post-exercise sequence, the trend lines between the mean EMR values and the successive loading cycles were all negative. The corresponding correlation coefficients between the EMR values and the sequence number were statistically significant ($p<0.05$) for three of the four signals during the initial sequence, but were not significant during the post-exercise sequence because of a slower decrease. After the 15 min exercise period, the mean EMRs at the four electrode sites were significantly lower ($p<0.001$) (Table 5.1).

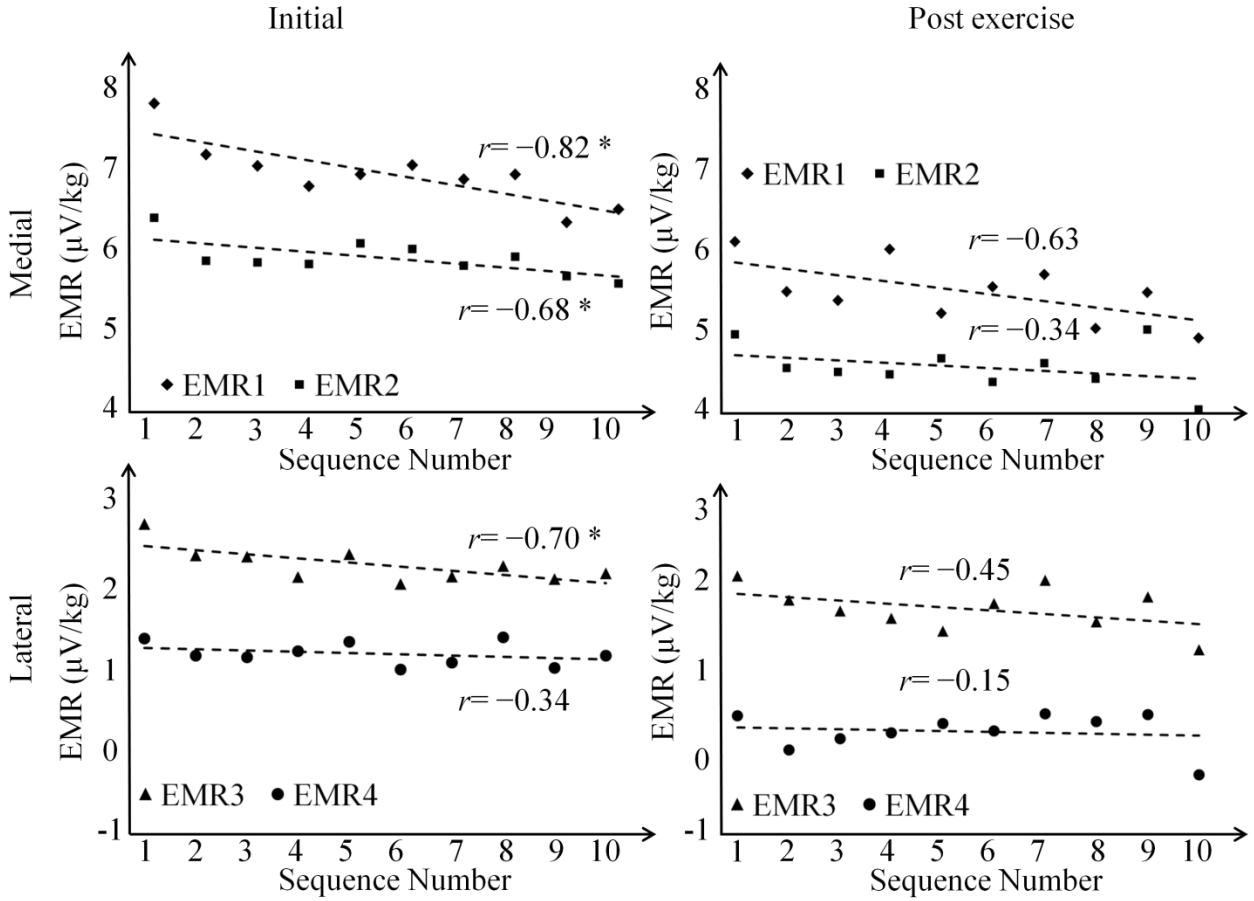

Figure. 5.3: Evolution of the electromechanical ratio (EMR) observed during successive loading cycles with the weight shifting protocol. Each symbol represents the average EMR (N=20 subjects) as a function of the sequence number of the loading cycle. The EMRs corresponding to the four electrode sites are represented by diamonds (EMR1, anteromedial), squares (EMR2, posteromedial), triangles (EMR3, anterolateral) and dots (EMR4, posterolateral). The dashed lines indicate the linear trend line and *r* shows the corresponding correlation coefficient between the EMR values and the sequence number, which is marked by a star if significant ($p<0.05$). The left panel shows data from the initial loading sequence, whereas the right panel shows a subsequent sequence recorded after a 15 min exercise period. All the EMRs were significantly lower after the exercise period ($p<0.001$)

Table 5.1: The electromechanical ratios obtained with the weight shifting protocol during the initial and post-exercise sequences at the four electrode sites.

	EMR1 (μV/kg)	EMR2 (μV/kg)	EMR3 (μV/kg)	EMR4 (μV/kg)
Initial Mean ± SD	6.91±0.42	5.81±0.24	2.30±0.22	1.22±0.14
Post exercice Mean ± SD	5.61±0.43	4.56±0.32	1.61±0.25	0.23±0.21
Paired *t*-test significance	< 0.001	< 0.001	< 0.001	< 0.001

Figure 5.4 illustrates the passive hyperextension loading protocol (panel A) and shows the corresponding EAG, force and EMG signals recorded in a representative subject. When the tibia was externally loaded, the medial and lateral EAG signals increased simultaneously with the signal from the force plate under the heel (Figure 5.4B). The EAG from the medial side was higher than the lateral side. As expected during this passive loading, the EMG signals from the four muscle groups remained relatively silent during loading (Figure 5.4C). To further evaluate the effect of PHLP on muscle activity, the means of the EMG envelopes for all the points during the loading phase and as well as prior to the loading were computed separately for all EMG signals and all subjects. Paired *t*-test analysis showed that there was no significant difference between the mean EMG values before and during loading for all the EMG channels.

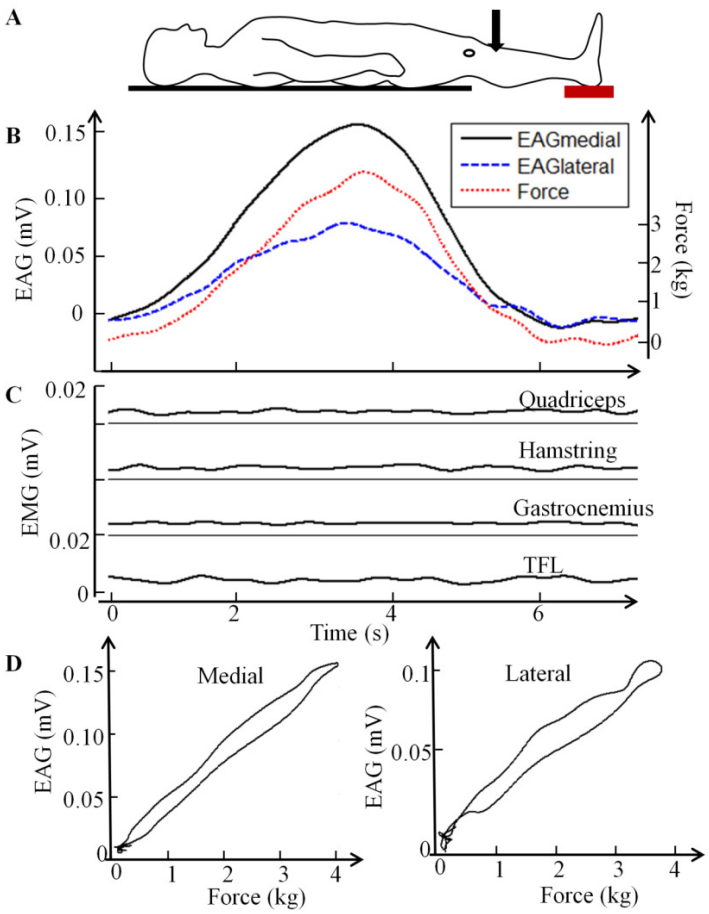

Figure 5.4: Representative data obtained during one loading cycle with the passive hyperextension loading protocol (PHLP). A: outline of the supine subject in the sagittal plane; the rectangle shows the position of the force plate; the black dot represents the position of the EAG electrode on the lateral side; the black arrow indicates the direction and position of the manually applied force on the tibia. B: medial and lateral EAG signals (left scale), and force signal (right scale). C: EMG envelope signals for the four muscle groups (scale: 0.02 mV). D: medial (left) and lateral (right) EAG signals versus the measured force during the loading cycle showing hysteresis with the loading phase producing higher potentials than the unloading phase.

The relationship between the measured EAG signals and the force signal showed excellent linearity with the PHLP (Figure 5.4D). However, some hysteresis was observed: the unloading path was lower than the loading path for both the medial and lateral EAGs. An electromechanical ratio was then computed between each EAG signal and the corresponding

force signal measured under the heel using a simple linear regression model for all the loading sequences. This EMR also decreased slowly during successive loading cycles (Figure 5.5). The trend lines between the mean EMR values measured on the lateral and medial sites and the successive loading cycles were negative. The correlation coefficient between the EMR values and the sequence number was statistically significant ($p<0.05$) for the lateral site but not for the medial site. However, the correlation coefficient between the sum of the values from both sites and the sequence number was statistically significant ($p<0.05$). This sum can correct for small rotations of the foot that could alter the balance between medial and lateral loading.

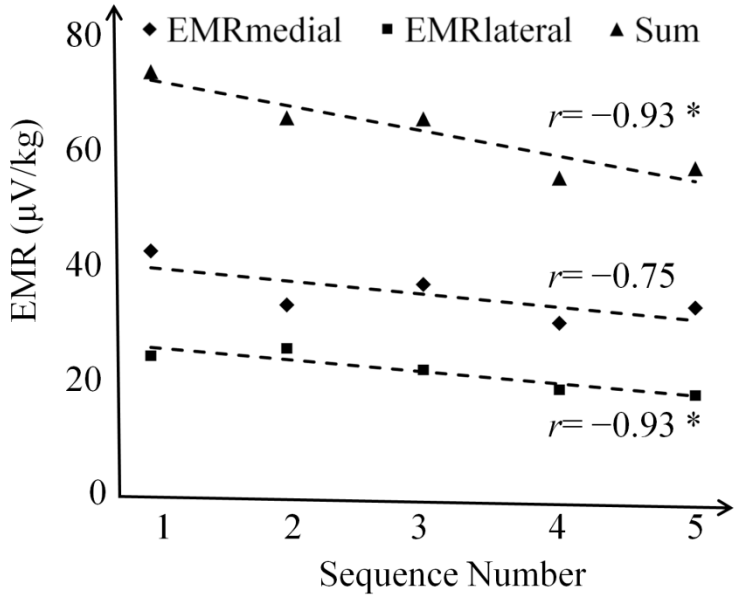

Figure 5.5: Temporal evolution of the electromechanical ratio (EMR) observed during successive loading cycles with the passive hyperextension loading protocol. Each symbol represents the average EMR (N=6 subjects) as a function of the sequence number of the loading cycle. The EMRs corresponding to the two electrode sites are represented by diamonds (medial) and squares (lateral) the triangles are the sum of both signals. The dashed lines indicate the linear trend line and *r* shows the corresponding correlation coefficient between the EMR values and the sequence number, which is marked by a star if significant ($p<0.05$).

5.5 Discussion

The results of this study have shown that the EMR values decreased significantly with successive loading cycles during the initial WSP sequence. After the exercise period, the EMR values were significantly lower than during the initial sequence and also decreased more slowly, suggesting a levelling of the EMR values. The EAG amplitude involves the electromechanical properties of articular cartilage, but also the force of compression acting on articular cartilage. A previous study has shown that the contraction of specific leg muscles that increases the knee contact force also generates EAG signals, and that WSP cycles with increased EAG amplitude are associated with higher EMG activity from the gastrocnemius muscles, which are involved in antero-posterior balance (Zhu et al, 2016). Habituation of the stretch reflex (Jackson et al., 2009; Laudani et al., 2009) could thus decrease the knee contact force during successive WSP loading cycles and explain the EMR decrease. The electromechanical model (eq. 5.3) can compensate for the part of the knee contact force that is generated by muscular activity involved in maintaining balance, but not for all muscle activity. To suppress the possible involvement of all muscles in the EMR decrease, a novel passive loading technique was then developed for which no significant differences were detected in the EMG of four muscle groups before and during loading. A significant EMR decrease was still observed with this PHLP technique. This suggests that the EMR decrease involves the electromechanical properties of articular cartilage, and not the compression force.

The measurement of the electromechanical properties of isolated cartilage samples during repetitive loading periods followed by recovery periods has not yet been reported to our knowledge, and the effects of sinusoidal loading have been documented for few cycles only (Légaré et al., 2002; Garon et al., 2002; Iatridis et al., 2009). However, streaming potentials have been recorded during stress relaxation following ramp loading (Garon et al., 2002), which suggests that cumulative effects can alter the electrical responses to repetitive loading cycles.

The time dependant biomechanical properties of cartilage samples have been well documented. For example, bovine articular cartilage takes approximately 30 minutes to return to its full thickness from a 17.5% compressive strain, as interstitial fluid flows back slowly within the poroelastic medium following compression (Courtland, et al. 2003; Mansour, 2003). During

repetitive and physiologically realistic loading, with each loading period followed by a twice longer recovery period similar to our protocol, the total strain of cartilage measured *in vitro* increased logarithmically due to the delayed recovery of cartilage thickness (Barker and Seedhom, 2001). This can be attributed to the decrease of permeability due to the diminishing pore size under dynamic loading, the so-called strain-dependent permeability effect: the lower the permeability, the harder it is to force the fluid out of the solid matrix to prevent further loss of fluid (Lu and Mow, 2008). This can also explain the observed EMR decrease as the electrical potentials are associated with the movement of counterions in the fluid.

Our results revealed that hysteresis is also present in the EAG measurements (Figure 5.4D). Hysteresis is another biomechanical characteristic of poroelastic materials with a stress-strain path during unloading that does not follow that developed during loading. The difference of the two curves results from energy dissipation due to internal friction in the material (Edelsten et al., 2010; Pal, 2014). Previous studies have reported hysteresis under physiological loading of cartilage specimens for both stress-strain curves (Abdel-Sayed, et al., 2014; Kelm, 2002) and stress-streaming potential curves (Garon et al., 2001).

The new passive hyperextension loading is quite different from the posterior tibial loading technique which generates posterior tibial translation, but in knee specimens (Höher et al., 1998; Butler et al., 1980; Carlin et al., 1996). It is also different from the loading technique of Fleming et al (2001) which is applied in human subjects, but on the flexed knee. The passive hyperextension loading is very simple to implement, but it is biomechanically complex since it can involve multiple structures from the entire leg. Its main effect is the hyperextension of the knee. Moglo and Shirazi (2005) have shown with a non linear finite element model that passive knee joint extension increases the total axial contact force by straining the lateral and medial collateral ligaments, as well as the anterior cruciate ligament, but not the posterior cruciate ligament. The ligaments being involved, their viscoelastic behavior could also explain some of the time-dependent effects observed with the PHLP (Ciarletta & Amar, 2010).

In this study, we investigated the evolution of the EAG signals during successive loading cycles using two loading protocols. By observing the mean EMRs of all subjects over successive loading cycles, we concluded that the EMR decreased with repeated cycles due to the

electromechanical properties of articular cartilage, instead of muscle contractile activity and possible habituation of the stretch reflex. In addition, we introduced and validated the feasibility of a new passive loading protocol with minimal muscle activation.

Our study may be useful for the further improvement of EAG measurement protocols. Thus, the results suggest that refraining from all physical activity before EAG measurements should be controlled in future studies since the loading of just a few steps can significantly reduce the amplitude of the EAG signals. Also, both loading protocols could be further investigated. During WSP loading, the angle of the knee could be controlled or measured as some subjects may be in a natural state of hyperextension that increases the EAG signals while other subjects may have a null or positive angle of flexion. For the PHLP, a biomechanical model of the leg could be developed to investigate the relationship between the applied force and the distribution of the contact forces in the knee joint under different conditions such as the angle of the foot.

5.6 Acknowledgements

This work was supported by the Canadian Institutes of Health Research (Operating grant number: APP37148), the Canadian Natural Sciences and Engineering Research Council (Grant number: CRDPJ 445265-12) and the China Scholarship Council. The study sponsors were not involved in the collection and analysis of data, and in the decision to submit the manuscript for publication.

5.7 References

Abdel-Sayed, P., Moghadam, M. N., Salomir, R., Tchernin, D., Pioletti, D. P. (2014). Intrinsic viscoelasticity increases temperature in knee cartilage under physiological loading. *Journal of the Mechanical Behavior of Biomedical Materials*, *30*, 123–130. http://doi.org/10.1016/j.jmbbm.2013.10.025

Adouni, M., Shirazi-Adl, A., Shirazi, R. (2012). Computational biodynamics of human knee joint in gait: from muscle forces to cartilage stresses. *Journal of Biomechanics*, *45*(12), 2149–2156. http://doi.org/10.1016/j.jbiomech.2012.05.040

Amis, A. A., Bull, A. M. J., Gupte, C. M., Hijazi, I., Race, A., Robinson, J. R. (2003). Biomechanics of the PCL and related structures: posterolateral, posteromedial and

meniscofemoral ligaments. *Knee Surgery, Sports Traumatology, Arthroscopy: Official Journal of the ESSKA*, *11*(5), 271–281. http://doi.org/10.1007/s00167-003-0410-7

Barker, M. K., Seedhom, B. B. (2001). The relationship of the compressive modulus of articular cartilage with its deformation response to cyclic loading: does cartilage optimize its modulus so as to minimize the strains arising in it due to the prevalent loading regime? *Rheumatology*, *40*(3), 274–284. http://doi.org/10.1093/rheumatology/40.3.274

Bartel, D. L., Davy, D. T., Keaveny, T. M. (2006). *Orthopaedic Biomechanics: Mechanics and Design in Musculoskeletal Systems*. Pearson/Prentice Hall.

Butler, D. L., Noyes, F. R., Grood, E. S. (1980). Ligamentous restraints to anterior-posterior drawer in the human knee. A biomechanical study. *The Journal of Bone and Joint Surgery*, *62*(2), 259–270.

Carlin, G. J., Livesay, G. A., Harner, C. D., Ishibashi, Y., Kim, H. S., Woo, S. L. (1996). In-situ forces in the human posterior cruciate ligament in response to posterior tibial loading. *Annals of Biomedical Engineering*, *24*(2), 193–197.

Changoor, A., Brett, W., Hoba, M., Garon, M., Quenneville, E., Gordon, K., … Trout, D. R. (2014). Electroarthrography, a non-invasive streaming potential-based method, measures cartilage quality in live horses. *Osteoarthritis and Cartilage*, *22*, S88–S89. http://doi.org/10.1016/j.joca.2014.02.172

Changoor, A., Hoba, M., Garon, M., Quenneville, E., Gordon, K., Buschmann, M. D., … Hurtig, M. B. (2013). Electroarthrography provides a non-invasive streaming potential-based method for detecting natural and trypsin-induced cartilage degeneration in equine fetlock joints. *Osteoarthritis and Cartilage*, *21*, S103. http://doi.org/10.1016/j.joca.2013.02.217

Ciarletta, P., and Amar, M. B. (2010). Hysteretic Behavior of Ligaments and Tendons: Microstructural Analysis of Damage, Softening and Non-Recoverable Strain. In K. Garikipati & E. M. Arruda (Eds.), *IUTAM Symposium on Cellular, Molecular and Tissue Mechanics* (pp. 31–43). Springer Netherlands. Retrieved from http://link.springer.com/chapter/10.1007/978-90-481-3348-2_3

Courtland, H.-W., Wright, G. M., Root, R. G., DeMont, M. E. (2003). Comparative equilibrium mechanical properties of bovine and lamprey cartilaginous tissues. *Journal of Experimental Biology*, *206*(8), 1397–1408. http://doi.org/10.1242/jeb.00264

Edelsten, L., Jeffrey, J.E., Burgin, L.V., Aspden, R.M. (2010). Viscoelastic deformation of articular cartilage during impact loading. *Soft Matter*, *6*(20), 5206–5212. http://doi.org/10.1039/C0SM00097C

Fleming, B. C., Renstrom, P.A., Beynnon, B.D., Engstrom, B., Peura, G.D., Badger, G.J., Johnson, R.J. (2001). The effect of weight bearing and external loading on anterior cruciate ligament strain. *Journal of Biomechanics*, 34:163-170.

Frank, E. H., Grodzinsky, A. J., Koob, T. J., Eyre, D. R. (1987). Streaming potentials: a sensitive index of enzymatic degradation in articular cartilage. *Journal of Orthopaedic Research: Official Publication of the Orthopaedic Research Society*, *5*(4), 497–508. http://doi.org/10.1002/jor.1100050405

Garon, M., Guardo, R., Buschmann, M. D. (2001). Estimation and sensitivity to cartilage degradation of electromechanical coupling coefficients derived using spatially resolved streaming potentials. Transactions of the Orthopaedic Research Society, 26, 420.

Garon, M., Légaré, A., Guardo, R., Savard, P., Buschmann, M. D. (2002). Streaming potentials maps are spatially resolved indicators of amplitude, frequency and ionic strength dependant responses of articular cartilage to load. *Journal of Biomechanics*, *35*(2), 207–216.

Gollehon, D. L., Torzilli, P. A., Warren, R. F. (1987). The role of the posterolateral and cruciate ligaments in the stability of the human knee. A biomechanical study. *The Journal of Bone and Joint Surgery. American Volume*, *69*(2), 233–242.

Han, Q., Buschmann, M. D., Savard, P. (2014). The forward problem of electroarthrography: modeling load-induced electrical potentials at the surface of the knee. *IEEE Transactions on Bio-Medical Engineering*, *61*(7), 2020–2027. http://doi.org/10.1109/TBME.2014.2312104

Hermens, H. J., Freriks, B., Disselhorst-Klug, C., Rau, G. (2000). Development of recommendations for SEMG sensors and sensor placement procedures. *Journal of Electromyography and Kinesiology*, *10*(5), 361–374. http://doi.org/10.1016/S1050-6411(00)00027-4

Höher, J., Harner, C. D., Vogrin, T. M., Baek, G. H., Carlin, G. J., Woo, S. L. (1998). In situ forces in the posterolateral structures of the knee under posterior tibial loading in the intact and posterior cruciate ligament-deficient knee. *Journal of Orthopaedic Research: Official Publication of the Orthopaedic Research Society*, *16*(6), 675–681. http://doi.org/10.1002/jor.1100160608

Höher, J., Vogrin, T. M., Woo, S. L., Carlin, G. J., Arøen, A., Harner, C. D. (1999). In situ forces in the human posterior cruciate ligament in response to muscle loads: a cadaveric study. *Journal of Orthopaedic Research: Official Publication of the Orthopaedic Research Society*, *17*(5), 763–768. http://doi.org/10.1002/jor.1100170522

Iatridis, J.C., Furukawa, M., Stokes, I.A.F., Gardner-Morse, M.G., Laible, J.P. (2009). Spatially resolved streaming potentials of human intervertebral disk motion segments under dynamic axial compression. J. Biomech, 131(3), 031006.

Jackson, N. D., Gutierrez, G. M., Kaminski, T. (2009). The effect of fatigue and habituation on the stretch reflex of the ankle musculature. *Journal of Electromyography and Kinesiology: Official Journal of the International Society of Electrophysiological Kinesiology*, *19*(1), 75–84. http://doi.org/10.1016/j.jelekin.2007.06.016

Kelm, L. N. (2002). *Hysteretic response of articular cartilage to cyclic loading* (Thesis). Rice University. Retrieved from https://scholarship.rice.edu/handle/1911/17515

Kutzner, I., Heinlein, B., Graichen, F., Bender, A., Rohlmann, A., Halder, A., Bergmann, G. (2010). Loading of the knee joint during activities of daily living measured in vivo in five subjects. *Journal of Biomechanics*, *43*(11), 2164–2173. http://doi.org/10.1016/j.jbiomech.2010.03.046

Laudani, L., Wood, L., Casabona, A., Giuffrida, R., De Vito, G. (2009). Effects of repeated ankle plantar-flexions on H-reflex and body sway during standing. Journal of

Electromyography and Kinesiology, 19(1), 85–92. http://doi.org/10.1016/j.jelekin.2007.06.012

Légaré, A., Garon, M., Guardo, R., Savard, P., Poole, A. R., Buschmann, M. D. (2002). Detection and analysis of cartilage degeneration by spatially resolved streaming potentials. *Journal of Orthopaedic Research: Official Publication of the Orthopaedic Research Society*, *20*(4), 819–826. http://doi.org/10.1016/S0736-0266(02)00002-5

Li, G., Gil, J., Kanamori, A., Woo, S. L. (1999). A validated three-dimensional computational model of a human knee joint. *Journal of Biomechanical Engineering*, *121*(6), 657–662.

Lu, X. L., Mow, V. C. (2008). Biomechanics of articular cartilage and determination of material properties. *Medicine and Science in Sports and Exercise*, *40*(2), 193–199. http://doi.org/10.1249/mss.0b013e31815cb1fc

Mansour, J. M. (2003). Biomechanics of cartilage. *Kinesiology: The Mechanics and Pathomechanics of Human Movement*, 66–79.

Markolf, K. L., Slauterbeck, J. R., Armstrong, K. L., Shapiro, M. S., Finerman, G. A. (1997). A biomechanical study of replacement of the posterior cruciate ligament with a graft. Part II: Forces in the graft compared with forces in the intact ligament. *The Journal of Bone and Joint Surgery. American Volume*, *79*(3), 381–386.

Moglo, K. E., Shirazi-Adl, A. Cruciate coupling and screw-home mechanism in passive knee joint during extension-flexion. (2005). *Journal of Biomechanics*, 38:1075-1083.

Pal, S. (2014). *Design of Artificial Human Joints and amp Organs*. Boston, MA: Springer US. Retrieved from http://link.springer.com/10.1007/978-1-4614-6255-2

Paolo A. Netti, L. A. (2007). Articular Cartilage, 381–402. http://doi.org/10.1007/0-306-47583-9_12

Préville, A.-M., Lavigne, P., Buschmann, M. D., Hardin, J., Han, Q., Djerroud, L., Savard, P. (2013). Electroarthrography: a novel method to assess articular cartilage and diagnose osteoarthritis by non-invasive measurement of load-induced electrical potentials at the

surface of the knee. *Osteoarthritis and Cartilage / OARS, Osteoarthritis Research Society*, *21*(11), 1731–1737. http://doi.org/10.1016/j.joca.2013.07.003

Schmidt-Rohlfing, B., Schneider, U., Goost, H., Silny, J. (2002). Mechanically induced electrical potentials of articular cartilage. *Journal of Biomechanics*, *35*(4), 475–482.

Weightman, B. O., Freeman, M. a. R., Swanson, S. a. V. (1973). Fatigue of Articular Cartilage. *Nature*, *244*(5414), 303–304. http://doi.org/10.1038/244303a0

Winter, D. A., Prince, F., Frank, J. S., Powell, C., Zabjek, K. F. (1996). Unified theory regarding A/P and M/L balance in quiet stance. *Journal of Neurophysiology*, *75*(6), 2334–2343.

Zhu, L., Buschmann, M. D., Savard, P. (2016). Mechanical loading of knee articular cartilage induced by muscle contraction can be assessed by measuring electrical potentials at the surface of the knee. Journal of Biomechanics, 49(3), 338–343. http://doi.org/10.1016/j.jbiomech.2015.12.033

CHAPTER 6 GENERAL DISCUSSION

OA, known as cartilage degeneration, is the most common knee disease. The early changes in cartilage tissue, associated with OA, include loss of PGs and degradation of the collagen fibril network (Buckwalter & Mankin, 1998). At the late stage of OA, cartilage tissue is mostly worn away; and subchondral bone is exposed. Basically, the earliest changes are reversible by changing loading conditions or by surgical intervention. It would be crucial to recognize the very early stage of cartilage degeneration (Kiviranta et al., 2007).

The electromechanical properties of articular cartilage have been investigated by many *in vitro* studies showing that the amplitude of electrical potentials of articular cartilage measured during compression reflects its integrity (Garon, 2007). The EAG technique, a non-invasive measurement of these electrical potentials, could potentially be a new diagnostic method for OA. This technique has several advantages, such as low cost, portable instrumentation, easy operation, signal analysis simplicity and possibility of early detection of OA in order to stop or reverse its progression. Our intention was to deepen our knowledge of EAG measurements and improve its reproducibility. Previous studies have shown that the electrical potentials detected on the surface of knee arise from the streaming potentials generated by compressed cartilage and that they are susceptible to cartilage degeneration. However, even though EAG measurements are repeatable, variability in the individual EAG amplitudes is still observed which could hamper its application as a diagnostic tool for OA. Our study is the first reported investigation on the variability of the EAG and constitute a basis for further development of the EAG techniques.

The preceding three chapters addressed the main research objectives of this thesis which focused on investigating the effects of muscle activity on the EAG measurements, the development of electromechanical models predicting the EAG signal and the temporal evolution of the EAG signals during successive loading cycles. Here, several points related to the thesis as a whole are discussed.

6.1 Effects of muscle activity on the EAG measurements

Theoretically, knee joint stability is maintained by the forces from the ligaments, muscles and body weight (Fleming et al., 2001). The resultant force acting on the cartilage is then influenced

by all these force vectors (Bartel et al., 2006b). With the development of instrumented knee implants, *in vivo* loading measurement became applicable. It has thus been demonstrated that the contact force measured *in vivo* is about 2 to 3 times the body weight during a one-legged stance (Kutzner et al., 2010), which indicates that the muscles and soft tissues have an effect even under static conditions.

Consequently, muscle activities were monitored during EAG measurements by surface EMG to investigate whether the muscle contractile force contributed to the variability of the contact force, and thus, the EAG values. Four muscle groups which act on the knee joint were chosen: quadriceps, hamstring, gastrocnemius and tensor fasciae latae. Specifically, the electrodes were positioned on the rectus femoris of the quadriceps muscle group and biceps femoris long head of the hamstring muscle group. We concluded that isometric muscle contraction can apply force on the tibiofemoral plateau and generate detectable EAG signals. For these experiments, it should be noted that the measured forces during contraction of different muscles are not comparable. For the gastrocnemius contraction, the force applied on the force plate was the greatest owing to the simplicity of this movement for applying force on the platform. Alternatively, the tensor fasciae latae generated the weakest force because of the extra effort that the subjects made to avoid the involvement of other muscles. Due to individual differences, the EMG amplitudes varied among subjects. It also varied among different muscle groups with one subject. Therefore, a large distribution of the amplitude of the EMG signals, and in turn, the EAG and force signal is expected.

During the weight shifting protocol, the EAG amplitude was well correlated with the EMG activity from the gastrocnemius muscles (Figure 3.7). Since during standing posture both feet carried about 50% of the body weight and the center of mass is projected about 7 cm in front of the ankle, each gastrocnemius muscle has to contract to counteract the half torque created by the body weight and causing a fall forward. By moving the total body weight on one foot, the gastrocnemius muscle of the weight bearing limb will have to develop twice the force. The increase of EMG activity from the gastrocnemius and of the EAG amplitude during the weight shifting can be largely explained by this phenomenon. In addition, the GRF across loading cycles should have been constant since the subject was supposed to transfer all the body weight to a single limb. However, the subject was not required to lift the non-instrumented leg and the toe of

this leg was still in contact with the floor to keep relative balance, thus, the GRF during unipedal stance might slightly change. In fact, during the weight shifting, not only the measured muscles but also other muscle groups, like tibialis anterior, peroneii, might be activated cooperatively to maintain body balance. But it was impracticable to record all the EMG signals from these muscle groups.

To further explain the effect of muscle contractile force during the usual weight shifting protocol, additional results during a loading cycle are presented in Figure 6.1. All the electrodes were kept at the same place as for the muscle contraction experiment. It is manifest that the EAG and ground reaction force signals increase and decrease simultaneously. However, the waveforms of the EAG and ground reaction force signals are not as similar as for the passive hyperextension loading protocol (Figure 5.4). The quadriceps and hamstring are not much involved, but the EMG signals from gastrocnemius and TFL increase during loading (Figure 6.1B). The relationship between the EAG signals and the ground reaction force signal are plotted (Figure 6. 1C). A hysteresis phenomenon appears like in Figure 5.4. However, unlike for the passive hyperextension loading protocol, the relationship between measured EAG signals and force signal exhibits nonlinearity. The EAG signals and ground reaction force are linearly related only during the early loading phase. When the subject transferred almost all his weight to the measured leg, muscle activity was needed to stop the swing and find a new balance. Therefore, the ground reaction force kept still but the EAG increased further over time during the late stage of shifting due to muscle activity. This example again shows how muscle activity impacts the EAG signals.

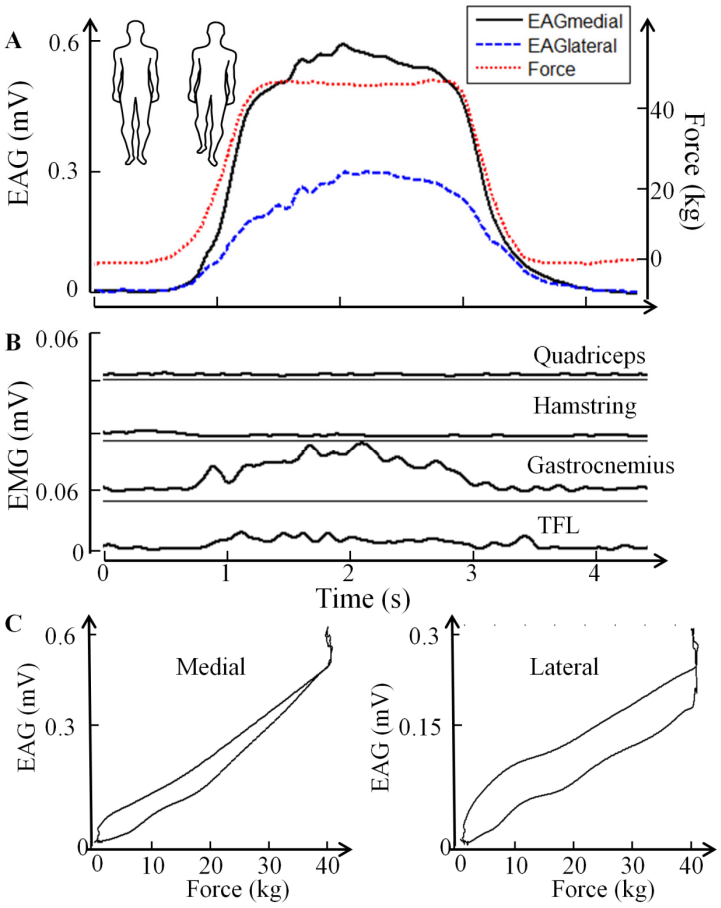

Figure 6.1: Representative data obtained during a loading cycle with the weight shifting protocol. A: medial and lateral EAG signals (left scale), and force signal (right scale); outline of the upright subject in the frontal plane was displayed at the left corner to demonstrate how the measured leg is loaded; B: EMG envelope signals for the four muscle groups (scale: 0.06 mV). C: medial EAG signal (left) and lateral EAG signal (right) versus the measured ground reaction force during the loading cycle.

6.2 Development of electromechanical models

During typical EAG measurements, mechanical joint loading is achieved by having the upright subject slowly shifts his body weight from a two legged stance to a one legged stance. Aforementioned, we concluded that muscles were involved during weight shifting and the corresponding contractile forces could induce variability of EAG values. Three strategies could be adopted to address this phenomenon:

1) Investigate and develop a loading protocol that reduces the muscular forces acting on the cartilage. For example, holding a horizontal bar can stabilize the subject and reduce the gastrocnemius activity. This activity should then be monitored with an EMG channel during the loading protocol. Possible problems with this approach could be subject compliance and the potential involvement of other muscle groups.

2) Investigate and develop a linear regression model where the dependent variable is the EAG signal, and the independent variable is the gastrocnemius EMG envelope at the same instant. The intercept between the regression line and the y-axis should give the EAG amplitude when no muscle force is applied. A possible problem is that the EMG amplitude shows intra-subject and inter-subject variability. In addition, the relationship between the EMG and muscle force is still unclear.

3) Investigate and develop a linear regression model where the dependent variable is the EAG, and the independent variables are the displacements of the center of pressure (COP) and the ground reaction force. Of note, cartilage is primarily compressed by the extra body weight applied to the measured leg resulting from weight shifting. The EAG signals should be proportional to the ground reaction forces (GRF) recorded by the force platform under the measured leg. However, in posture control, the regulation of balance during body shifting would involve continuous muscular activities, from which the knee contact force would also be increased (Shelburne, Torry, & Pandy, 2005b; Adouni et al., 2012). Studies of posture control during weight shifting demonstrated that COP movement in the anterior-posterior (A/P) direction was dominated by ankle joint plantar flexors and dorsi flexors; and that COP movement in the medial-lateral (M/L) direction was dominated by hip abductor and adductor muscles (D. Winter, 1995). Therefore, we hypothesized that the displacement of COP could reflect the alteration of joint contact force and we selected and investigated this strategy because of the clear relationship between the dependent and the independent variables.

This second study, as a continuation of our previous work, was undertaken by developing two linear regression models exploring the origin of the EAG signals: GRF model and GRF+COP model. Linear models were selected since streaming potentials recorded over a cartilage sample have shown an almost linear relationship with the magnitude of the applied force (Schmide-

Rohlfing et al., 2001). Our results revealed that ground reaction force and center of pressure displacement could predict electrical potentials obtained at the surface of the knee during weight shifting. With GRF+COP model, the relative errors between the reconstructed signal and measured signal were significantly lower on three out of four electrode sites comparing with the relative errors computed by GRF model. Actually, four models, including GRF model, GRF+$COP_{A/L}$ model, GRF +$COP_{M/L}$ model and GRF+ $COP_{A/L}$ +$COP_{M/L}$ model, were investigated to predict the measured EAG signals. Adding only $COP_{A/L}$ could already significantly improve the relative errors between the modelled and the measured signals. However, the model involving $COP_{A/L}$ and $COP_{M/L}$ provided more information about postural control.

Although this study gave valuable results, it has some limitations. For example, the force plate gave only an approximate location of the COP when compared with in shoe systems (Debbi et al., 2012). Parameters that could influence the EAG signals such as the knee joint kinematics, the relative joint-COP position, antagonistic muscles co-activity, muscles such as the hip adductor and adductor muscles, OA and other subject specific parameters may not be represented either by GRF nor by COP displacements. Also, the proposed regression equations were simple linear equations that did not include coupled terms or higher order terms that might improve the results. Despite these limitations, the inclusion of the COP displacements in the GRF+COP model did lower the relative error to about 15% on the medial side, where the electrode sites have a higher signal-to-noise ratio.

These results also suggest that the EMR estimated with the GRF+COP model could constitute a more reliable clinical estimator than the peak EAG values or the mean EAG values since it reduces the EAG variability due to body sway. Indeed, the EMR showed an improved reproducibility during a test-retest procedure when the COP displacements where included in the regression model. The resulting infraclass correlation coefficients with this EMR were excellent on the medial side where the signal-to-noise ratio is larger, and fair to good on the lateral side (Fleiss, 1986).

6.3 Evolution of the EAG signals

EAG loading sequences consist of 10 repetitive cycles for averaging purposes. The EMR of all loading cycles were computed using the two proposed models introduced in the previous section. A low but noticeable EMR variability was still present among each loading cycles within individual. This may confirm the existence of random measurement error, in which case one assumes that the parameter being measured is actually stable. On the other hand, it may also imply that the dispersion of EMR distribution is caused by another source of variability. Therefore, this last study aimed to investigate a possible temporal dispersion within subjects.

Articular cartilage is a highly anisotropic and heterogeneous material exhibiting time-dependent behaviour (Bartel et al., 2006b). The viscoelasticity is attributed to two types of mechanisms: flow-independent behaviour of the collagen-proteoglycan matrix and flow-dependent behaviour of the interstitial fluid flow through the matrix and the resistance of the matrix to this flow. The biomechanical behaviour of cartilage can be explained by the interaction of these two sources.

The permeability, which is inversely related to the resistance to fluid flow through the cartilage matrix, is extremely low for normal cartilage (Lu & Mow, 2008). High energy dissipation is taking place during compression inside the tissue. Hence, the loading curve and unloading curve do not follow the same path, which characterizes a hysteresis phenomenon. Under cyclic loading, the largest energy loss is observed at the first and second loading cycles. Afterward, the amount of hysteresis decreases with each subsequent cycle and eventually becomes nearly constant (Kelm, 2002). Hysteresis loops can be observed in EAG measurements for both loading protocols, shown in Figure 5.4 and Figure 6.1.

The extruded fluid encounters large drag-induced forces in the recovery process of articular cartilage due to its low permeability (Courtland et al., 2003). The repetitive loading would delay the recovery of cartilage; thus the total cartilage strain measured *in vitro* increases logarithmically (Barker & Seedhom, 2001). In addition, the permeability decreases with the increasing compressive strain due to the closing pores and increased repulsive force under dynamic loading, the so-called strain-dependent permeability effect (Bartel et al., 2006b; Mansour, 2003; Lu & Mow, 2008). The lower the permeability, the harder it is to force the fluid out of the solid matrix to prevent further loss of fluid; furthermore, the dynamic stiffness of cartilage increases. A

previous study has described that the stiffness tends to be stable after about ten loading cycles (Woo et al., 2000), but the values obtained are still different for subsequent cycles. When it comes to the EAG technique, the mechanism linking the EMR decrease with repetitive loading cycles and the increased stiffness remains to be determined.

To investigate the possible evolution of EAG signals during successive loading cycles, a novel passive hyperextension loading protocol was designed to reduce the involvement of muscle contraction. A force was manually applied over the tibia of the supine subjects so as to comfortably maintain the vertical angle of the foot. The mechanism of this loading was not discussed in detail due to its complexity. It is different from the *in situ* posterior tibial loading technique generating only posterior tibial translation as the femur and tibia are totally clamped (Höher et al., 1998; Carlin et al., 1996; Butler, Noyes, & Grood, 1980). When a posterior shear force is applied on the tibia in supine position, passive hyperextension is created. Finite element simulations demonstrated that collateral ligaments and anterior cruciate ligament are strained in hyperextension and that the total contact force increases correspondingly (Moglo & Shirazi-Adl, 2005). *In situ* passive hyperextension experiments also confirmed that the ACL is stretched first, coupled with relative tibial displacement when shear force was applied on both tibia and femur (Meyer, Baumer, & Haut, 2011). In PHLP, the main effect is hyperextension of the knee but tibial translation could also occur.

Near extension, although the PCL is tight, it does not contribute greatly to restraint because its fibres are aligned in a proximal-distal direction (Amis et al., 2003). In contrast, posterolateral structures including lateral collateral ligament and the popliteus complex plays an important role in intact knee to restrain the tibial posterior translation near extension (Höher et al., 1998). In addition, the posteromedial structures become tight and well-aligned to resist tibial posterior translation as the knee extends suggesting that the posteromedial structures also make a significant contribution to resisting tibial posterior translation (Höher et al., 1999). Taken together, posterolateral and posteromedial structures are responsible for posterior knee stability as the knee is extended (Amis et al., 2003).

Resulting from the greater mobility of the lateral compartment of the tibial plateau, some investigators have found that a posterior draw force could induce a coupled tibial external

rotation in the intact knee (Gollehon, Torzilli, & Warren, 1987). Although this external rotation is less than one degree normally, the EAG signals might be influenced by the secondary mechanisms during the loading (Höher et al., 1999). This limitation should be considered when applying PHLP clinically. Locking the tibia in neutral position could be one option. Therefore, resulting from the complex mechanism of PHLP, the relationship between applied force and contact force is not intuitively clear (Gollehon, Torzilli, & Warren, 1987).

CHAPTER 7 CONCLUSION AND RECOMMENDATIONS

7.1 Conclusion

The degeneration of articular cartilage is one of the most common markers of OA. This work was motivated by a growing need for clinically and economically effective methodologies for diagnosing knee osteoarthritis. Electroarthrography (EAG) is a non-invasive technology for recording electrical potentials on the knee surface that reflects the quality and contact force of the cartilage. Our study provided valuable information for the future development of EAG as a useful clinical tool by investigating the sources of variability of the EAG signals. First, EAG signals were shown to be sensitive to muscle contraction by evaluating the effects of specific *in vivo* muscle contractions in supine subjects. These results also showed that muscle contraction can explain the EAG variations during the weight shifting loading protocol. To compensate for the effects of muscle contraction, two linear regression models based on ground reaction force and center of pressure displacements were then developed to compute an *electro-mechanical ratio* (EMR). This EMR characterizes the ability of cartilage to generate a certain potential under a given load. Electromechanical modeling incorporating the center of pressure displacements enhanced the reproducibility of the EMR estimation. Finally, the temporal evolution of EAG during successive loading cycles was investigated using weight shifting and posterior tibial loading protocols. Both protocols showed a decrease of the EAG signals during successive loading cycles. By comparing the results of both protocols, we concluded that this decrease was not due to muscular effects such as the habituation of the stretch reflex, but to the poroelasticity of cartilage due to its flow-dependent and flow-independent properties. On a final note, both loading protocols described in this thesis could be the subject of further studies before being applied in the context of a widespread clinical assessment of cartilage quality.

7.2 Recommendations

This thesis presents an original contribution to our understanding of EAG variability and also generates new questions that could be explored in future studies, as described in the following paragraphs.

In daily activities, the muscles that can generate compressive forces in the knee joint become activated to maintain the balance of the subject. Electrical modeling has already been applied to compute the potential distributions generated on the surface of the knee by a given electrical source. However, biomechanical and electromechanical modeling of the EAG has never been developed. This type of modeling could be crucial to investigate factors such as muscle contraction and ligaments deformation. For example, ligaments can play an important role for knee loading during the hyperextension of the knee in upright subjects. Modelling can also be used to investigate the effects of specific cartilage defects.

Additional investigation to elucidate the mechanisms of posterior tibial loading would be beneficial. For a deep flexed knee joint, almost all the restraint is provided by the posterior cruciate ligament. However, in full extension, the restraint comes from the posterolateral and posteromedial structures of knee joint, and probably also from the contact force of the tibiofemoral plateau. A model that can quantify the relationship between the knee contact force and the applied force would be critical for the further application of this loading protocol.

Based on results to date, there is insufficient information about human factors such as age, past trauma, gender, height, weight, body mass index, etc. For example, the mechanical properties of the collagen network might change with age, and therefore the electrical behavior of cartilage. Assessing the EAG data on a larger number of subjects, it would be possible to determine which human factors are significant. In addition, for the possible clinical application of the EAG technique, it is necessary to build a database to quantify the EMR in osteoarthritis subjects and determine an EMR threshold to diagnose osteoarthritis according to the patient category.

As for future applications of the EAG technique, two aspects are the most interesting:

1) Studies with healthy subjects in the fields of kinesiology and biomechanics: the EAG can serve as a “natural sensor” to estimate the changes of the knee contact force in different circumstances like walking, running, posture maintenance, ascending and descending stairs, new types of running shoes, etc.

2) Detection and characterization of osteoarthritis: the studies could be initially limited to those for which the subjects are their own control to increase the statistical power of the test by eliminating inter-individual variation. For example, EAG changes in subjects undergoing a

clinical trial for new drugs or treatments, or the comparison between the EAG from a knee after ligament repair surgery versus the contralateral knee.

Finally, other joints such as the ankle could also be investigated with the EAG technique. The creativity is unlimited!

BIBLIOGRAPHY

Abdel-Sayed, P., Moghadam, M. N., Salomir, R., Tchernin, D., & Pioletti, D. P. (2014). Intrinsic viscoelasticity increases temperature in knee cartilage under physiological loading. *Journal of the Mechanical Behavior of Biomedical Materials*, *30*, 123–130. http://doi.org/10.1016/j.jmbbm.2013.10.025

A. Changoor, M. H. (2013). Electroarthrography provides a non-invasive streaming potential-based method for detecting natural and trypsin-induced cartilage degeneration in equine fetlock joints. *Osteoarthritis and Cartilage*, *21*, S103. http://doi.org/10.1016/j.joca.2013.02.217

Adouni, M., Shirazi-Adl, A., & Shirazi, R. (2012). Computational biodynamics of human knee joint in gait: from muscle forces to cartilage stresses. *Journal of Biomechanics*, *45*(12), 2149–2156. http://doi.org/10.1016/j.jbiomech.2012.05.040

Al, H. (1997). The relationship between electromyogram and muscle force. *Sportverletzung Sportschaden : Organ Der Gesellschaft Fur Orthopadisch-Traumatologische Sportmedizin*, *11*(3), 79–86.

Anatomy of knee joint | Aash Arthroscopy Center. (2011). Retrieved from http://aasharthroscopy.com/anatomy-of-knee-joint/

Anila Namboodiripad, P. C. (2014). Cystatin C: Its role in pathogenesis of OSMF. *Journal of Oral Biology and Craniofacial Research*, *4*(1), 42–46. http://doi.org/10.1016/j.jobcr.2014.02.004

Appleton, C. T. G., McErlain, D. D., Pitelka, V., Schwartz, N., Bernier, S. M., Henry, J. L., … Beier, F. (2007). Forced mobilization accelerates pathogenesis: characterization of a preclinical surgical model of osteoarthritis. *Arthritis Research & Therapy*, *9*(1), R13. http://doi.org/10.1186/ar2120

Arden, N., Blanco, F., Cooper, C., Guermazi, A., Hayashi, D., Hunter, D., … Reginster, J.-Y. (2015). *Atlas of Osteoarthritis*. Springer.

Armstrong, C. G., Lai, W. M., & Mow, V. C. (1984). An Analysis of the Unconfined Compression of Articular Cartilage. *Journal of Biomechanical Engineering*, *106*(2), 165–173. http://doi.org/10.1115/1.3138475

Barber, J. R. (2011). *Intermediate Mechanics of Materials* (Vol. 175). Dordrecht: Springer Netherlands. Retrieved from http://link.springer.com/10.1007/978-94-007-0295-0

Barbucci, R. (2007). *Integrated Biomaterials Science*. Springer Science & Business Media.

Barker, M. K., & Seedhom, B. B. (2001). The relationship of the compressive modulus of articular cartilage with its deformation response to cyclic loading: does cartilage optimize its modulus so as to minimize the strains arising in it due to the prevalent loading regime? *Rheumatology*, *40*(3), 274–284. http://doi.org/10.1093/rheumatology/40.3.274

Bartel, D. L., Davy, D. T., & Keaveny, T. M. (2006a). *Orthopaedic Biomechanics: Mechanics and Design in Musculoskeletal Systems*. Pearson/Prentice Hall.

Bartel, D. L., Davy, D. T., & Keaveny, T. M. (2006b). *Orthopaedic Biomechanics: Mechanics and Design in Musculoskeletal Systems*. Pearson/Prentice Hall.

Bartlett, H. L., Ting, L. H., & Bingham, J. T. (2014). Accuracy of force and center of pressure measures of the Wii Balance Board. *Gait & Posture*, *39*(1), 224–228. http://doi.org/10.1016/j.gaitpost.2013.07.010

Bazant, M. Z. (2011). Induced-Charge Electrokinetic Phenomena. In A. Ramos (Ed.), *Electrokinetics and Electrohydrodynamics in Microsystems* (pp. 221–297). Springer Vienna. Retrieved from http://link.springer.com/chapter/10.1007/978-3-7091-0900-7_7

Beecher, B., Martin, J., Pedersen, D., Heiner, A., & Buckwalter, J. (2007). Antioxidants Block Cyclic Loading Induced Chondrocyte Death. *The Iowa Orthopaedic Journal*, *27*, 1–8.

Bhosale, A. M., & Richardson, J. B. (2008). Articular cartilage: structure, injuries and review of management. *British Medical Bulletin*, *87*(1), 77–95. http://doi.org/10.1093/bmb/ldn025

Bijlsma, J. W., Berenbaum, F., & Lafeber, F. P. (2011a). Osteoarthritis: an update with relevance for clinical practice. *The Lancet*, *377*(9783), 2115–2126. http://doi.org/10.1016/S0140-6736(11)60243-2

Bijlsma, J. W., Berenbaum, F., & Lafeber, F. P. (2011b). Osteoarthritis: an update with relevance for clinical practice. *The Lancet*, *377*(9783), 2115–2126. http://doi.org/10.1016/S0140-6736(11)60243-2

Bijlsma, J. W. J., & Knahr, K. (2007). Strategies for the prevention and management of osteoarthritis of the hip and knee. *Best Practice & Research. Clinical Rheumatology*, *21*(1), 59–76. http://doi.org/10.1016/j.berh.2006.08.013

Blitterswijk, C. V., & Boer, J. D. (2014). *Tissue Engineering*. Academic Press.

Bombardier, C., Hawker, G., & Mosher, D. (2011). The impact of arthritis in Canada: today and the next 30 years.

Bonassar, L. J., Jeffries, K. A., Paguio, C. G., & Grodzinsky, A. J. (1995). Cartilage degradation and associated changes in biomechanical and electromechanical properties. *Acta Orthopaedica*, *66*(s266), 38–44. http://doi.org/10.3109/17453679509157645

Boskey, A., & Camacho, N. P. (2007). FT-IR Imaging of Native and Tissue-Engineered Bone and Cartilage. *Biomaterials*, *28*(15), 2465–2478. http://doi.org/10.1016/j.biomaterials.2006.11.043

Brandt, K. D., Dieppe, P., & Radin, E. L. (2008). Etiopathogenesis of osteoarthritis. *Rheumatic Diseases Clinics of North America*, *34*(3), 531–559. http://doi.org/10.1016/j.rdc.2008.05.011

Braun, H. J., & Gold, G. E. (2012). Diagnosis of osteoarthritis: imaging. *Bone*, *51*(2), 278–288. http://doi.org/10.1016/j.bone.2011.11.019

Brismar, B. H., Wredmark, T., Movin, T., Leandersson, J., & Svensson, O. (2002). Observer reliability in the arthroscopic classification of osteoarthritis of the knee. *The Journal of Bone and Joint Surgery. British Volume*, *84*(1), 42–47.

Bronner, F., & Farach-Carson, M. C. (2007). *Bone and Osteoarthritis*. Springer.

Buckwalter, J. A., & Mankin, H. J. (1997). Instructional Course Lectures, The American Academy of Orthopaedic Surgeons - Articular Cartilage. Part II: Degeneration and

Osteoarthrosis, Repair, Regeneration, and Transplantation*†. *J Bone Joint Surg Am*, *79*(4), 612–32.

Buckwalter, J. A., & Mankin, H. J. (1998). Articular cartilage repair and transplantation. *Arthritis & Rheumatism*, *41*(8), 1331–1342.

Buckwalter, J. A., Mankin, H. J., & Grodzinsky, A. J. (2005). Articular cartilage and osteoarthritis. *Instructional Course Lectures*, *54*, 465–480.

Buckwalter, J., Mow, V., & Ratcliffe, A. (1994). Restoration of Injured or Degenerated Articular Cartilage. *The Journal of the American Academy of Orthopaedic Surgeons*, *2*(4), 192–201.

Buschmann, M. D., & Grodzinsky, A. J. (1995). A molecular model of proteoglycan-associated electrostatic forces in cartilage mechanics. *Journal of Biomechanical Engineering*, *117*(2), 179–192.

Buschmann, M. D., Kim, Y.-J., Wong, M., Frank, E., Hunziker, E. B., & Grodzinsky, A. J. (1999). Stimulation of Aggrecan Synthesis in Cartilage Explants by Cyclic Loading Is Localized to Regions of High Interstitial Fluid Flow1. *Archives of Biochemistry and Biophysics*, *366*(1), 1–7. http://doi.org/10.1006/abbi.1999.1197

Carlin, G. J., Livesay, G. A., Harner, C. D., Ishibashi, Y., Kim, H. S., & Woo, S. L. (1996). In-situ forces in the human posterior cruciate ligament in response to posterior tibial loading. *Annals of Biomedical Engineering*, *24*(2), 193–197.

Centers for Disease Control and Prevention (CDC). (1996). Prevalence and impact of arthritis by race and ethnicity--United States, 1989-1991. *MMWR. Morbidity and Mortality Weekly Report*, *45*(18), 373–378.

Chaganti, R. K., & Lane, N. E. (2011). Risk factors for incident osteoarthritis of the hip and knee. *Current Reviews in Musculoskeletal Medicine*, *4*(3), 99–104. http://doi.org/10.1007/s12178-011-9088-5

Changoor, A. (2011). Electromechanical and Polarization Microscopy Evaluation of Cartilage Repair and Degeneration. Doctoral thesis, École Polytechnique de Montreal, Montreal, Canada

Changoor, A., Brett, W., Hoba, M., Garon, M., Quenneville, E., Gordon, K., … Trout, D. R. (2014). Electroarthrography, a non-invasive streaming potential-based method, measures cartilage quality in live horses. *Osteoarthritis and Cartilage*, *22*, S88–S89. http://doi.org/10.1016/j.joca.2014.02.172

Changoor, A., Hoba, M., Garon, M., Quenneville, E., Gordon, K., Buschmann, M. D., … Hurtig, M. B. (2013). Electroarthrography provides a non-invasive streaming potential-based method for detecting natural and trypsin-induced cartilage degeneration in equine fetlock joints. *Osteoarthritis and Cartilage*, *21*, S103. http://doi.org/10.1016/j.joca.2013.02.217

Chan, W. P., Lang, P., Stevens, M. P., Sack, K., Majumdar, S., Stoller, D. W., … Genant, H. K. (1991). Osteoarthritis of the knee: comparison of radiography, CT, and MR imaging to assess extent and severity. *American Journal of Roentgenology*, *157*(4), 799–806. http://doi.org/10.2214/ajr.157.4.1892040

Chen, A. C., Nguyen, T. T., & Sah, R. L. (1997). Streaming potentials during the confined compression creep test of normal and proteoglycan-depleted cartilage. *Annals of Biomedical Engineering*, *25*(2), 269–277.

Choi, J.-A., & Gold, G. (2011). MR Imaging of Articular Cartilage Physiology. *Magnetic Resonance Imaging Clinics of North America*, *19*(2), 249–282. http://doi.org/10.1016/j.mric.2011.02.010

Chu, C. R., Williams, A. A., Coyle, C. H., & Bowers, M. E. (2012). Early diagnosis to enable early treatment of pre-osteoarthritis. *Arthritis Research & Therapy*, *14*(3), 212. http://doi.org/10.1186/ar3845

Chu, C. R., Williams, A., Tolliver, D., Kwoh, K., Bruno, S., & Irrgang, J. J. (2010). Clinical Optical Coherence Tomography of Early Articular Cartilage Degeneration in Persons with Degenerative Meniscal Tears. *Arthritis and Rheumatism*, *62*(5), 1412–1420. http://doi.org/10.1002/art.27378

Ciarletta, P., & Amar, M. B. (2010). Hysteretic Behavior of Ligaments and Tendons: Microstructural Analysis of Damage, Softening and Non-Recoverable Strain. In K. Garikipati & E. M. Arruda (Eds.), *IUTAM Symposium on Cellular, Molecular and Tissue*

Mechanics (pp. 31–43). Springer Netherlands. Retrieved from http://link.springer.com/chapter/10.1007/978-90-481-3348-2_3

Comper, W. D. (1996). *Extracellular Matrix*. Amsterdam, CRC Press.

Coulson, M. (2014). *The Fitness Instructor's Handbook: A Complete Guide to Health and Fitness*. Bloomsbury Publishing.

Coumas, J. M., & Palmer, W. E. (1998). Knee arthrography. Evolution and current status. *Radiologic Clinics of North America*, *36*(4), 703–728.

Courtland, H.-W., Wright, G. M., Root, R. G., & DeMont, M. E. (2003). Comparative equilibrium mechanical properties of bovine and lamprey cartilaginous tissues. *Journal of Experimental Biology*, *206*(8), 1397–1408. http://doi.org/10.1242/jeb.00264

Crema, M. D., Roemer, F. W., Marra, M. D., Burstein, D., Gold, G. E., Eckstein, F., … Guermazi, A. (2011). Articular Cartilage in the Knee: Current MR Imaging Techniques and Applications in Clinical Practice and Research. *RadioGraphics*, *31*(1), 37–61. http://doi.org/10.1148/rg.311105084

C Y Huang, V. C. M. (2001). The Role of Flow-Independent Viscoelasticity in the Biphasic Tensile and Compressive Responses of Articular Cartilage. *Journal of Biomechanical Engineering*, *123*(5), 410–7. http://doi.org/10.1115/1.1392316

Debbi, E. M., Wolf, A., Goryachev, Y., Yizhar, Z., Luger, E., Debi, R., & Haim, A. (2012). In-shoe center of pressure: Indirect force plate vs. direct insole measurement. *The Foot*, *22*(4), 269–275. http://doi.org/10.1016/j.foot.2012.07.001

DeFrances, C. J., & Podgornik, M. N. (2006). 2004 National Hospital Discharge Survey. *Advance Data*, (371), 1–19.

Delakis, I., Xanthis, C., & Kitney, R. I. (2009). Assessment of the limiting spatial resolution of an MRI scanner by direct analysis of the edge spread function. *Medical Physics*, *36*(5), 1637–1642.

Dennis, D. A., Komistek, R. D., Hoff, W. A., & Gabriel, S. M. (1996). In vivo knee kinematics derived using an inverse perspective technique. *Clinical Orthopaedics and Related Research*, (331), 107–117.

Desrochers, J., Amrein, M. W., & Matyas, J. R. (2012). Viscoelasticity of the articular cartilage surface in early osteoarthritis. *Osteoarthritis and Cartilage*, *20*(5), 413–421. http://doi.org/10.1016/j.joca.2012.01.011

Drake, R. L., Vogl, W., & Mitchell, A. W. M. (2010). *Gray's Anatomy for Students*. Churchill Livingstone/Elsevier.

Eckstein, F., Cicuttini, F., Raynauld, J.-P., Waterton, J. C., & Peterfy, C. (2006). Magnetic resonance imaging (MRI) of articular cartilage in knee osteoarthritis (OA): morphological assessment. *Osteoarthritis and Cartilage*, *14, Supplement 1*, 46–75. http://doi.org/10.1016/j.joca.2006.02.026

Felson, D. T. (2013). Osteoarthritis as a disease of mechanics. *Osteoarthritis and Cartilage*, *21*(1), 10–15. http://doi.org/10.1016/j.joca.2012.09.012

Felson, D. T., Lawrence, R. C., Dieppe, P. A., Hirsch, R., Helmick, C. G., Jordan, J. M., … Fries, J. F. (2000). Osteoarthritis: new insights. Part 1: the disease and its risk factors. *Annals of Internal Medicine*, *133*(8), 635–646.

Flandry, F., & Hommel, G. (2011). Normal anatomy and biomechanics of the knee. *Sports Medicine and Arthroscopy Review*, *19*(2), 82–92. http://doi.org/10.1097/JSA.0b013e318210c0aa

Fleis J. The design and analysis of clinical experiments. New York: J Wiley & sons, 1986.

Fleming, B. C., Renstrom, P. A., Beynnon, B. D., Engstrom, B., Peura, G. D., Badger, G. J., & Johnson, R. J. (2001). The effect of weightbearing and external loading on anterior cruciate ligament strain. *Journal of Biomechanics*, *34*(2), 163–170. http://doi.org/10.1016/S0021-9290(00)00154-8

Fleming, B. C., Renstrom, P. A., Ohlen, G., Johnson, R. J., Peura, G. D., Beynnon, B. D., & Badger, G. J. (2001). The gastrocnemius muscle is an antagonist of the anterior cruciate

ligament. *Journal of Orthopaedic Research: Official Publication of the Orthopaedic Research Society*, *19*(6), 1178–1184.

Fleming, B. C., Renstrom, P. A., Beynnon, B. D., Engstrom, B., Peura, G. D., Badger, G. J., & Johnson, R. J. (2001). The effect of weightbearing and external loading on anterior cruciate ligament strain. Journal of biomechanics, 34(2), 163-170.

Frank, E. H., Grodzinsky, A. J., Koob, T. J., & Eyre, D. R. (1987). Streaming potentials: A sensitive index of enzymatic degradation in articular cartilage. *Journal of Orthopaedic Research*, *5*(4), 497–508. http://doi.org/10.1002/jor.1100050405

Frank, E. H., Grodzinsky, A. J., Koob, T. J., & Eyre, D. R. (1987). Streaming potentials: a sensitive index of enzymatic degradation in articular cartilage. *Journal of Orthopaedic Research: Official Publication of the Orthopaedic Research Society*, *5*(4), 497–508. http://doi.org/10.1002/jor.1100050405

Fukubayashi, T., & Kurosawa, H. (1980). The contact area and pressure distribution pattern of the knee. A study of normal and osteoarthrotic knee joints. *Acta Orthopaedica Scandinavica*, *51*(6), 871–879.

Garon, M. (2007). *Conception et validation d'une sonde arthroscopique pour l'évaluation des propriétés électromécaniques fonctionnelles du cartilage articulaire*. École polytechnique. Retrieved from http://www.biomomentum.com/docs/fr/Garon-2007a.pdf

Garon, M., Légaré, A., Guardo, R., Savard, P., & Buschmann, M. D. (2002). Streaming potentials maps are spatially resolved indicators of amplitude, frequency and ionic strength dependant responses of articular cartilage to load. *Journal of Biomechanics*, *35*(2), 207–216.

Gold, G. E., Chen, C. A., Koo, S., Hargreaves, B. A., & Bangerter, N. K. (2009). Recent Advances in MRI of Articular Cartilage. *AJR. American Journal of Roentgenology*, *193*(3), 628–638. http://doi.org/10.2214/AJR.09.3042

Gollehon, D. L., Torzilli, P. A., & Warren, R. F. (1987). The role of the posterolateral and cruciate ligaments in the stability of the human knee. A biomechanical study. *The Journal of Bone and Joint Surgery. American Volume*, *69*(2), 233–242.

Han, Q., Buschmann, M. D., & Savard, P. (2014). The forward problem of electroarthrography: modeling load-induced electrical potentials at the surface of the knee. *IEEE Transactions on Bio-Medical Engineering*, *61*(7), 2020–2027. http://doi.org/10.1109/TBME.2014.2312104

Hasler, E. M., Herzog, W., Wu, J. Z., Müller, W., & Wyss, U. (1999). Articular cartilage biomechanics: theoretical models, material properties, and biosynthetic response. *Critical Reviews in Biomedical Engineering*, *27*(6), 415–488.

Hayes, D. W., Brower, R. L., & John, K. J. (2001). Articular cartilage. Anatomy, injury, and repair. *Clinics in Podiatric Medicine and Surgery*, *18*(1), 35–53.

Hermens, H. J., Freriks, B., Disselhorst-Klug, C., & Rau, G. (2000). Development of recommendations for SEMG sensors and sensor placement procedures. *Journal of Electromyography and Kinesiology*, *10*(5), 361–374. http://doi.org/10.1016/S1050-6411(00)00027-4

Höher, J., Harner, C. D., Vogrin, T. M., Baek, G. H., Carlin, G. J., & Woo, S. L. (1998). In situ forces in the posterolateral structures of the knee under posterior tibial loading in the intact and posterior cruciate ligament-deficient knee. *Journal of Orthopaedic Research: Official Publication of the Orthopaedic Research Society*, *16*(6), 675–681. http://doi.org/10.1002/jor.1100160608

Höher, J., Vogrin, T. M., Woo, S. L., Carlin, G. J., Arøen, A., & Harner, C. D. (1999). In situ forces in the human posterior cruciate ligament in response to muscle loads: a cadaveric study. *Journal of Orthopaedic Research: Official Publication of the Orthopaedic Research Society*, *17*(5), 763–768. http://doi.org/10.1002/jor.1100170522

Hoshino, A., & Wallace, W. A. (1987). Impact-absorbing properties of the human knee. *The Journal of Bone and Joint Surgery. British Volume*, *69*(5), 807–811.

Hsu, R. W., Himeno, S., Coventry, M. B., & Chao, E. Y. (1990). Normal axial alignment of the lower extremity and load-bearing distribution at the knee. *Clinical Orthopaedics and Related Research*, (255), 215–227.

Huang, C.-Y., Stankiewicz, A., Ateshian, G. A., & Mow, V. C. (2005). ANISOTROPY, INHOMOGENEITY, AND TENSION-COMPRESSION NONLINEARITY OF HUMAN GLENOHUMERAL CARTILAGE IN FINITE DEFORMATION. *Journal of Biomechanics*, *38*(4), 799–809. http://doi.org/10.1016/j.jbiomech.2004.05.006

Hwang, J. (2010). Integration of cartilage and bone through a calcified cartilage interface to form a functional osteochondral graft. *eScholarship*. Retrieved from http://escholarship.org/uc/item/1g68z5mt

Iatridis, J. C., Furukawa, M., Stokes, I. A. F., Gardner-Morse, M. G., & Laible, J. P. (2009). Spatially resolved streaming potentials of human intervertebral disk motion segments under dynamic axial compression. *Journal of Biomechanical Engineering*, *131*(3), 031006. http://doi.org/10.1115/1.3005164

Inoue, R., Ishibashi, Y., Tsuda, E., Yamamoto, Y., Matsuzaka, M., Takahashi, I., … Toh, S. (2011). Medical problems and risk factors of metabolic syndrome among radiographic knee osteoarthritis patients in the Japanese general population. *Journal of Orthopaedic Science*, *16*(6), 704–709. http://doi.org/10.1007/s00776-011-0157-9

Jackson, A., & Gu, W. (2009). TRANSPORT PROPERTIES OF CARTILAGINOUS TISSUES. *Current Rheumatology Reviews*, *5*(1), 40. http://doi.org/10.2174/157339709787315320

James, C.-B., & Uhl, T. L. (2001). A Review of Articular Cartilage Pathology and the Use of Glucosamine Sulfate. *Journal of Athletic Training*, *36*(4), 413–419.

Jamshidi, N., Rostami, M., Najarian, S., Menhaj, M. B., Saadatnia, M., & Salami, F. (2010). Differences in center of pressure trajectory between normal and steppage gait. *Journal of Research in Medical Sciences : The Official Journal of Isfahan University of Medical Sciences*, *15*(1), 33–40.

Johnson, F., Leitl, S., & Waugh, W. (1980). The distribution of load across the knee. A comparison of static and dynamic measurements. *The Journal of Bone and Joint Surgery. British Volume*, *62*(3), 346–349.

Jones, A., Hopkinson, N., Pattrick, M., Berman, P., & Doherty, M. (1992). Evaluation of a method for clinically assessing osteoarthritis of the knee. *Annals of the Rheumatic Diseases*, *51*(2), 243–245.

Jordan, J. M., Helmick, C. G., Renner, J. B., Luta, G., Dragomir, A. D., Woodard, J., … Hochberg, M. C. (2007). Prevalence of knee symptoms and radiographic and symptomatic knee osteoarthritis in African Americans and Caucasians: the Johnston County Osteoarthritis Project. *The Journal of Rheumatology*, *34*(1), 172–180.

June, R. K., Neu, C. P., Barone, J. R., & Fyhrie, D. P. (2011). Polymer Mechanics as a Model for Short-Term and Flow-Independent Cartilage Viscoelasticity. *Materials Science & Engineering. C, Materials for Biological Applications*, *31*(4), 781–788. http://doi.org/10.1016/j.msec.2010.11.029

Kelm, L. N. (2002). *Hysteretic response of articular cartilage to cyclic loading* (Thesis). Rice University. Retrieved from https://scholarship.rice.edu/handle/1911/17515

Kim, K. J., Uchiyama, E., Kitaoka, H. B., & An, K. N. (2003). An in vitro study of individual ankle muscle actions on the center of pressure. *Gait & Posture*, *17*(2), 125–131.

Kim, Y. J., Bonassar, L. J., & Grodzinsky, A. J. (1995). The role of cartilage streaming potential, fluid flow and pressure in the stimulation of chondrocyte biosynthesis during dynamic compression. *Journal of Biomechanics*, *28*(9), 1055–1066.

Kiviranta, P., Töyräs, J., Nieminen, M. T., Laasanen, M. S., Saarakkala, S., Nieminen, H. J., Jurvelin, J. S. (2007). Comparison of novel clinically applicable methodology for sensitive diagnostics of cartilage degeneration. *European Cells & Materials*, *13*, 46–55; discussion 55.

Korhonen, R. K. (2003). Experimental Analysis and Finite Element Modeling of Normal and Degraded Articular Cartilage. Doctoral Dissertation, University of Kuopio, Kuopio.

Krishnan, R., Park, S., Eckstein, F., & Ateshian, G. A. (2003). Inhomogeneous Cartilage Properties Enhance Superficial Interstitial Fluid Support and Frictional Properties, But Do

not Provide a Homogeneous State of Stress. *Journal of Biomechanical Engineering*, *125*(5), 569–577.

K., R., & Saarakkal, S. (2011). Biomechanics and Modeling of Skeletal Soft Tissues. In V. Klika (Ed.), *Theoretical Biomechanics*. InTech. Retrieved from http://www.intechopen.com/books/theoretical-biomechanics/biomechanics-and-modeling-of-skeletal-soft-tissues

Kulowski, J. (1932). Flexion Contracture of the Knee. *J Bone Joint Surg Am*, *14*(3), 618–630.

Kumar, D., Manal, K. T., & Rudolph, K. S. (2013). Knee joint loading during gait in healthy controls and individuals with knee osteoarthritis. *Osteoarthritis and Cartilage*, *21*(2), 298–305. http://doi.org/10.1016/j.joca.2012.11.008

Kutzner, I., Heinlein, B., Graichen, F., Bender, A., Rohlmann, A., Halder, A., … Bergmann, G. (2010). Loading of the knee joint during activities of daily living measured in vivo in five subjects. *Journal of Biomechanics*, *43*(11), 2164–2173. http://doi.org/10.1016/j.jbiomech.2010.03.046

Kwak, S. D., Ahmad, C. S., Gardner, T. R., Grelsamer, R. P., Henry, J. H., Blankevoort, L., … Mow, V. C. (2000). Hamstrings and iliotibial band forces affect knee kinematics and contact pattern. *Journal of Orthopaedic Research: Official Publication of the Orthopaedic Research Society*, *18*(1), 101–108. http://doi.org/10.1002/jor.1100180115

Lafeber, F. P., Intema, F., Van Roermund, P. M., & Marijnissen, A. C. (2006). Unloading joints to treat osteoarthritis, including joint distraction: *Current Opinion in Rheumatology*, *18*(5), 519–525. http://doi.org/10.1097/01.bor.0000240366.54960.a1

Lai, W. M., Mow, V. C., Sun, D. D., & Ateshian, G. A. (2000). On the electric potentials inside a charged soft hydrated biological tissue: streaming potential versus diffusion potential. *Journal of Biomechanical Engineering*, *122*(4), 336–346.

Langelier, E., & Buschmann, M. D. (2003). Increasing strain and strain rate strengthen transient stiffness but weaken the response to subsequent compression for articular cartilage in unconfined compression. *Journal of Biomechanics*, *36*(6), 853–859.

Lanza, R., Langer, R., & Vacanti, J. P. (2011). *Principles of Tissue Engineering*. Academic Press.

Laubenthal, K. N., Smidt, G. L., & Kettelkamp, D. B. (1972). A quantitative analysis of knee motion during activities of daily living. *Physical Therapy*, *52*(1), 34–43.

Laudani, L., Wood, L., Casabona, A., Giuffrida, R., & De Vito, G. (2009). Effects of repeated ankle plantar-flexions on H-reflex and body sway during standing. *Journal of Electromyography and Kinesiology*, *19*(1), 85–92. http://doi.org/10.1016/j.jelekin.2007.06.012

Leach, J. M., Mancini, M., Peterka, R. J., Hayes, T. L., & Horak, F. B. (2014). Validating and calibrating the Nintendo Wii balance board to derive reliable center of pressure measures. *Sensors (Basel, Switzerland)*, *14*(10), 18244–18267. http://doi.org/10.3390/s141018244

Lee, R. C., Frank, E. H., Grodzinsky, A. J., & Roylance, D. K. (1981). Oscillatory Compressional Behavior of Articular Cartilage and Its Associated Electromechanical Properties. *Journal of Biomechanical Engineering*, *103*(4), 280–292. http://doi.org/10.1115/1.3138294

Légaré, A., Garon, M., Guardo, R., Savard, P., Poole, A. R., & Buschmann, M. D. (2002a). Detection and analysis of cartilage degeneration by spatially resolved streaming potentials. *Journal of Orthopaedic Research: Official Publication of the Orthopaedic Research Society*, *20*(4), 819–826. http://doi.org/10.1016/S0736-0266(02)00002-5

Légaré, A., Garon, M., Guardo, R., Savard, P., Poole, A. R., & Buschmann, M. D. (2002b). Detection and analysis of cartilage degeneration by spatially resolved streaming potentials. *Journal of Orthopaedic Research: Official Publication of the Orthopaedic Research Society*, *20*(4), 819–826. http://doi.org/10.1016/S0736-0266(02)00002-5

Li, G., Rudy, T. W., Sakane, M., Kanamori, A., Ma, C. B., & Woo, S. L.-Y. (1999). The importance of quadriceps and hamstring muscle loading on knee kinematics and in-situ forces in the ACL. *Journal of Biomechanics*, *32*(4), 395–400. http://doi.org/10.1016/S0021-9290(98)00181-X

Litwic, A., Edwards, M., Dennison, E., & Cooper, C. (2013). Epidemiology and Burden of Osteoarthritis. *British Medical Bulletin*, *105*, 185–199. http://doi.org/10.1093/bmb/lds038

Liu, W., & Maitland, M. E. (2000). The effect of hamstring muscle compensation for anterior laxity in the ACL-deficient knee during gait. *Journal of Biomechanics*, *33*(7), 871–879.

Loeuille, D. (2012). [When should MRI for knee or hip osteoarthritis should be performed?]. *La Revue Du Praticien*, *62*(5), 625–629.

Lorna Edelsten, J. E. J. (2010). Viscoelastic deformation of articular cartilage during impact loading. *Soft Matter*, *6*(20), 5206–5212. http://doi.org/10.1039/C0SM00097C

Lu, X. L., & Mow, V. C. (2008). Biomechanics of articular cartilage and determination of material properties. *Medicine and Science in Sports and Exercise*, *40*(2), 193–199. http://doi.org/10.1249/mss.0b013e31815cb1fc

Macmull, S., Skinner, J. A., Bentley, G., Carrington, R. W. J., & Briggs, T. W. R. (2010). Treating articular cartilage injuries of the knee in young people. *BMJ*, *340*(mar05 1), c998–c998. http://doi.org/10.1136/bmj.c998

Ma, L. D. (1999). Magnetic resonance imaging of musculoskeletal tumors: skeletal and soft tissue masses. *Current Problems in Diagnostic Radiology*, *28*(2), 29–62.

Mankin, H. J., & Thrasher, A. Z. (1975). Water content and binding in normal and osteoarthritic human cartilage. *J Bone Joint Surg Am*, *57*(1), 76–80.

Mansour, J. M. (2003). Biomechanics of cartilage. *Kinesiology: The Mechanics and Pathomechanics of Human Movement*, 66–79.

Maquet, D. P. G. J. (1976). Biomechanical Treatment of Osteoarthritis of the Knee. In *Biomechanics of the Knee* (pp. 129–210). Springer Berlin Heidelberg. Retrieved from http://link.springer.com/chapter/10.1007/978-3-642-96360-5_7

Masani, K., Popovic, M. R., Nakazawa, K., Kouzaki, M., & Nozaki, D. (2003). Importance of Body Sway Velocity Information in Controlling Ankle Extensor Activities During Quiet Stance. *Journal of Neurophysiology*, *90*(6), 3774–3782. http://doi.org/10.1152/jn.00730.2002

Matzat, S. J., Kogan, F., Fong, G. W., & Gold, G. E. (2014). Imaging Strategies for Assessing Cartilage Composition in Osteoarthritis. *Current Rheumatology Reports*, *16*(11), 462. http://doi.org/10.1007/s11926-014-0462-3

Matzat, S. J., van Tiel, J., Gold, G. E., & Oei, E. H. G. (2013). Quantitative MRI techniques of cartilage composition. *Quantitative Imaging in Medicine and Surgery*, *3*(3), 162–174. http://doi.org/10.3978/j.issn.2223-4292.2013.06.04

McGinty, J. B., & Burkhart, S. S. (2003). *Operative Arthroscopy*. Lippincott Williams & Wilkins.

Meyer, E. G., Baumer, T. G., & Haut, R. C. (2011). Pure passive hyperextension of the human cadaver knee generates simultaneous bicruciate ligament rupture. *Journal of Biomechanical Engineering*, *133*(1), 011012. http://doi.org/10.1115/1.4003135

Miller, M. D., Thompson, S. R., & Hart, J. (2012). *Review of Orthopaedics*. Elsevier Health Sciences.

Moglo, K. E., & Shirazi-Adl, A. (2005). Cruciate coupling and screw-home mechanism in passive knee joint during extension--flexion. *Journal of Biomechanics*, *38*(5), 1075–1083. http://doi.org/10.1016/j.jbiomech.2004.05.033

Mow, V. C., Holmes, M. H., & Lai, W. M. (1984). Fluid transport and mechanical properties of articular cartilage: a review. *Journal of Biomechanics*, *17*(5), 377–394.

Mow, V. C., & Huiskes, R. (2005). *Basic Orthopaedic Biomechanics & Mechano-biology*. Lippincott Williams & Wilkins.

Mow, V. C., Kuei, S. C., Lai, W. M., & Armstrong, C. G. (1980). Biphasic Creep and Stress Relaxation of Articular Cartilage in Compression: Theory and Experiments. *Journal of Biomechanical Engineering*, *102*(1), 73–84. http://doi.org/10.1115/1.3138202

Mow, V. C., & Lai, and W. M. (1979). Mechanics of Animal Joints. *Annual Review of Fluid Mechanics*, *11*(1), 247–288. http://doi.org/10.1146/annurev.fl.11.010179.001335

Nagura, T., Dyrby, C. O., Alexander, E. J., & Andriacchi, T. P. (2002). Mechanical loads at the knee joint during deep flexion. *Journal of Orthopaedic Research: Official Publication of*

the Orthopaedic Research Society, *20*(4), 881–886. http://doi.org/10.1016/S0736-0266(01)00178-4

Nap, R. J., & Szleifer, I. (2008). Structure and Interactions of Aggrecans: Statistical Thermodynamic Approach. *Biophysical Journal*, *95*(10), 4570–4583. http://doi.org/10.1529/biophysj.108.133801

Netti, P. A., & Ambrosio, L. (2002). Articular Cartilage. In R. Barbucci (Ed.), *Integrated Biomaterials Science* (pp. 381–402). Springer US. Retrieved from http://link.springer.com/chapter/10.1007/0-306-47583-9_12

Nissi, M. J., Töyräs, J., Laasanen, M. S., Rieppo, J., Saarakkala, S., Lappalainen, R., … Nieminen, M. T. (2004). Proteoglycan and collagen sensitive MRI evaluation of normal and degenerated articular cartilage. *Journal of Orthopaedic Research*, *22*(3), 557–564. http://doi.org/10.1016/j.orthres.2003.09.008

Nordin, M., & Frankel, V. H. (2001). *Basic Biomechanics of the Musculoskeletal System*. Lippincott Williams & Wilkins.

Oatis, C. A. (2009). *Kinesiology: The Mechanics and Pathomechanics of Human Movement*. Lippincott Williams & Wilkins.

O'Connor, J. J. (1993). Can muscle co-contraction protect knee ligaments after injury or repair? *The Journal of Bone and Joint Surgery. British Volume*, *75*(1), 41–48.

O'Rahilly, R., & Müller, F. (1983). *Basic Human Anatomy: A Regional Study of Human Structure*. Saunders.

Otterness, I. G., & Eckstein, F. (2007). Women have thinner cartilage and smaller joint surfaces than men after adjustment for body height and weight. *Osteoarthritis and Cartilage / OARS, Osteoarthritis Research Society*, *15*(6), 666–672. http://doi.org/10.1016/j.joca.2006.12.003

Pal, S. (2014). *Design of Artificial Human Joints & Organs*. Boston, MA: Springer US. Retrieved from http://link.springer.com/10.1007/978-1-4614-6255-2

Pandy, M. G., & Shelburne, K. B. (1997). Dependence of cruciate-ligament loading on muscle forces and external load. *Journal of Biomechanics*, *30*(10), 1015–1024. http://doi.org/10.1016/S0021-9290(97)00070-5

Paolo A. Netti, L. A. (2007). Articular Cartilage, 381–402. http://doi.org/10.1007/0-306-47583-9_12

Paré, E. B., Stern, J. T., & Schwartz, J. M. (1981). Functional differentiation within the tensor fasciae latae. A telemetered electromyographic analysis of its locomotor roles. *The Journal of Bone and Joint Surgery. American Volume*, *63*(9), 1457–1471.

Peat, G., Croft, P., & Hay, E. (2001). Clinical assessment of the osteoarthritis patient. *Best Practice & Research Clinical Rheumatology*, *15*(4), 527–544. http://doi.org/10.1053/berh.2001.0171

Phillip, L. (1952). THE KNEE AND RELATED STRUCTURES. *California Medicine*, *77*(6), 431–432.

Poitout, D. G. (2013). *Biomechanics and Biomaterials in Orthopedics*. Springer Science & Business Media.

Préville, A.-M. (2011, December). *Électroarthrographie : mesure et analyse des potentiels électriques à la surface du genou pour l'évaluation de l'arthrose* (masters). École Polytechnique de Montréal. Retrieved from https://publications.polymtl.ca/733/

Préville, A.-M., Lavigne, P., Buschmann, M. D., Hardin, J., Han, Q., Djerroud, L., & Savard, P. (2013). Electroarthrography: a novel method to assess articular cartilage and diagnose osteoarthritis by non-invasive measurement of load-induced electrical potentials at the surface of the knee. *Osteoarthritis and Cartilage / OARS, Osteoarthritis Research Society*, *21*(11), 1731–1737. http://doi.org/10.1016/j.joca.2013.07.003

Primary Osteoarthritis Imaging: Overview, Radiography, Computed Tomography. (2015). Retrieved from http://emedicine.medscape.com/article/392096-overview

Robi, K., Jakob, N., Matevz, K., & Matjaz, V. (2013). The Physiology of Sports Injuries and Repair Processes. In M. Hamlin (Ed.), *Current Issues in Sports and Exercise Medicine*.

InTech. Retrieved from http://www.intechopen.com/books/current-issues-in-sports-and-exercise-medicine/the-physiology-of-sports-injuries-and-repair-processes

Ronald E. Hileman, J. R. F. (1998). Glycosaminoglycan-protein interactions: Definition of consensus sites in glycosaminoglycan binding proteins. *BioEssays : News and Reviews in Molecular, Cellular and Developmental Biology*, *20*(2), 156–67. http://doi.org/10.1002/(SICI)1521-1878(199802)20:2<156::AID-BIES8>3.0.CO;2-R

Ruhe, A., Fejer, R., & Walker, B. (2010). The test–retest reliability of centre of pressure measures in bipedal static task conditions – A systematic review of the literature. *Gait & Posture*, *32*(4), 436–445. http://doi.org/10.1016/j.gaitpost.2010.09.012

R U Kleemann, D. K. (2005). Altered cartilage mechanics and histology in knee osteoarthritis: Relation to clinical assessment (ICRS Grade). *Osteoarthritis and Cartilage / OARS, Osteoarthritis Research Society*, *13*(11), 958–63. http://doi.org/10.1016/j.joca.2005.06.008

Sakane, M., Fox, R. J., Woo, S. L., Livesay, G. A., Li, G., & Fu, F. H. (1997). In situ forces in the anterior cruciate ligament and its bundles in response to anterior tibial loads. *Journal of Orthopaedic Research: Official Publication of the Orthopaedic Research Society*, *15*(2), 285–293. http://doi.org/10.1002/jor.1100150219

Saladin, K. S. (2004). *Anatomy & Physiology: The Unity of Form and Function*. McGraw-Hill Higher Education.

Schmidler, C. (2015). Skeletal System | Skeleton Bones, Joints, Cartilage, Ligaments, Bursae. Retrieved from http://www.healthpages.org/anatomy-function/musculoskeletal-system-bones-joints-cartilage-ligaments/

Schmidt-Rohlfing, B., Schneider, U., Goost, H., & Silny, J. (2002). Mechanically induced electrical potentials of articular cartilage. *Journal of Biomechanics*, *35*(4), 475–482.

Scifers, J. R. (2008). *Special Tests for Neurologic Examination*. SLACK.

Screen, H. R. C. (2008). Investigating load relaxation mechanics in tendon. *Journal of the Mechanical Behavior of Biomedical Materials*, *1*(1), 51–58. http://doi.org/10.1016/j.jmbbm.2007.03.002

Sharma, L., & Berenbaum, F. (2007). *Osteoarthritis: A Companion to Rheumatology*. Elsevier Health Sciences.

Shelburne, K. B., & Pandy, M. G. (1997). A musculoskeletal model of the knee for evaluating ligament forces during isometric contractions. *Journal of Biomechanics*, *30*(2), 163–176. http://doi.org/10.1016/S0021-9290(96)00119-4

Shelburne, K. B., Torry, M. R., & Pandy, M. G. (2005). Muscle, ligament, and joint-contact forces at the knee during walking. *Medicine and Science in Sports and Exercise*, *37*(11), 1948–1956.

Sim, S., Chevrier, A., Garon, M., Quenneville, E., Yaroshinsky, A., Hoemann, C. D., & Buschmann, M. D. (2014). Non-destructive electromechanical assessment (Arthro-BST) of human articular cartilage correlates with histological scores and biomechanical properties. *Osteoarthritis and Cartilage*, *22*(11), 1926–1935. http://doi.org/10.1016/j.joca.2014.08.008

Sokoloff, L. (2014). *The Joints and Synovial Fluid*. Academic Press.

Soltz, M. A., & Ateshian, G. A. (1998). Experimental verification and theoretical prediction of cartilage interstitial fluid pressurization at an impermeable contact interface in confined compression. *Journal of Biomechanics*, *31*(10), 927–934.

Sophia Fox, A. J., Bedi, A., & Rodeo, S. A. (2009a). The Basic Science of Articular Cartilage. *Sports Health*, *1*(6), 461–468. http://doi.org/10.1177/1941738109350438

Sophia Fox, A. J., Bedi, A., & Rodeo, S. A. (2009b). The Basic Science of Articular Cartilage. *Sports Health*, *1*(6), 461–468. http://doi.org/10.1177/1941738109350438

Soulhat, J., Buschmann, M. D., & Shirazi-Adl, A. (1999). A fibril-network-reinforced biphasic model of cartilage in unconfined compression. *Journal of Biomechanical Engineering*, *121*(3), 340–347.

S Sim, A. C. (2013). Correlation of Non-destructive Electromechanical Probe (Arthro-BST) Assessment with Histological Scores and Mechanical Properties in Human Knee Joints. *Osteoarthritis and Cartilage*, *23*. http://doi.org/10.1016/j.joca.2015.02.440

Stolz, M., Gottardi, R., Raiteri, R., Miot, S., Martin, I., Imer, R., … Aebi, U. (2009). Early detection of aging cartilage and osteoarthritis in mice and patient samples using atomic force microscopy. *Nature Nanotechnology*, *4*(3), 186–192. http://doi.org/10.1038/nnano.2008.410

Tanaka, E., & van Eijden, T. (2003). Biomechanical behavior of the temporomandibular joint disc. *Critical Reviews in Oral Biology and Medicine: An Official Publication of the American Association of Oral Biologists*, *14*(2), 138–150.

Taylor, W. R., Heller, M. O., Bergmann, G., & Duda, G. N. (2004). Tibio-femoral loading during human gait and stair climbing. *Journal of Orthopaedic Research*, *22*(3), 625–632. http://doi.org/10.1016/j.orthres.2003.09.003

Thambyah, A. (2005, June 1). *Biomechanics of the tibiofemoral joint in relation to the mechanical factors associated with osteoarthritis of the knee* (Thesis). Retrieved from http://scholarbank.nus.edu.sg/handle/10635/14740

Tiderius, C. J., Olsson, L. E., Leander, P., Ekberg, O., & Dahlberg, L. (2003). Delayed gadolinium-enhanced MRI of cartilage (dGEMRIC) in early knee osteoarthritis. *Magnetic Resonance in Medicine*, *49*(3), 488–492. http://doi.org/10.1002/mrm.10389

Tobias, K. M., & Johnston, S. A. (2013). *Veterinary Surgery: Small Animal: 2-Volume Set*. Elsevier Health Sciences.

Trimmel, M., Streicher, F., Groll-Knapp, E., & Haider, M. (1989). The electromyographic DC potential as a correlate of muscular activity. *European Journal of Applied Physiology and Occupational Physiology*, *58*(5), 459–465. http://doi.org/10.1007/BF02330697

Vasara, A. I., Jurvelin, J. S., Peterson, L., & Kiviranta, I. (2005). Arthroscopic cartilage indentation and cartilage lesions of anterior cruciate ligament-deficient knees. *The American Journal of Sports Medicine*, *33*(3), 408–414.

Verzijl, N., DeGroot, J., Thorpe, S. R., Bank, R. A., Shaw, J. N., Lyons, T. J., … TeKoppele, J. M. (2000). Effect of Collagen Turnover on the Accumulation of Advanced Glycation End Products. *Journal of Biological Chemistry*, *275*(50), 39027–39031. http://doi.org/10.1074/jbc.M006700200

Whittle, M. W. (2014). *Gait Analysis: An Introduction*. Butterworth-Heinemann.

Wiegant, K., van Roermund, P. M., Intema, F., Cotofana, S., Eckstein, F., Mastbergen, S. C., & Lafeber, F. P. J. G. (2013). Sustained clinical and structural benefit after joint distraction in the treatment of severe knee osteoarthritis. *Osteoarthritis and Cartilage*, *21*(11), 1660–1667. http://doi.org/10.1016/j.joca.2013.08.006

Winby, C. R., Lloyd, D. G., Besier, T. F., & Kirk, T. B. (2009). Muscle and external load contribution to knee joint contact loads during normal gait. *Journal of Biomechanics*, *42*(14), 2294–2300. http://doi.org/10.1016/j.jbiomech.2009.06.019

Winter, D. (1995). Human balance and posture control during standing and walking. *Gait & Posture*, *3*(4), 193–214. http://doi.org/10.1016/0966-6362(96)82849-9

Winter, D. A. (1995). A.B.C. (anatomy, Biomechanics and Control) of Balance During Standing and Walking. Waterloo Biomechanics.

Winter, D. A., Prince, F., Frank, J. S., Powell, C., & Zabjek, K. F. (1996). Unified theory regarding A/P and M/L balance in quiet stance. Journal of neurophysiology, 75(6), 2334-2343.

Winter, D. A., Patla, A. E., Prince, F., Ishac, M., & Gielo-Perczak, K. (1998). Stiffness control of balance in quiet standing. Journal of neurophysiology,80(3), 1211-1221

Winter, D. A. (2009). *Biomechanics and Motor Control of Human Movement, Fourth Edition*. Retrieved from doi: 10.1002/9780470549148

Wittenauer, R., Smith, L., & Aden, K. (2013). WHO | Priority diseases and reasons for inclusion. Retrieved from http://www.who.int/medicines/areas/priority_medicines/prior_med_ch6_12/en/

Woolf, A. D., & Pfleger, B. (2003). Burden of major musculoskeletal conditions. *Bulletin of the World Health Organization*, *81*(9), 646–656. http://doi.org/10.1590/S0042-96862003000900007

Woo, S. L., Debski, R. E., Zeminski, J., Abramowitch, S. D., Saw, S. S., & Fenwick, J. A. (2000). Injury and repair of ligaments and tendons. *Annual Review of Biomedical Engineering*, *2*, 83–118. http://doi.org/10.1146/annurev.bioeng.2.1.83

Xia, Y., Ramakrishnan, N., & Bidthanapally, A. (2007). The Depth-dependent Anisotropy of Articular Cartilage by Fourier-Transform Infrared Imaging (FTIRI). *Osteoarthritis and Cartilage / OARS, Osteoarthritis Research Society*, *15*(7), 780–788. http://doi.org/10.1016/j.joca.2007.01.007

Zavatsky, A. B., Beard, D. J., & O'Connor, J. J. (1994). Cruciate ligament loading during isometric muscle contractions. A theoretical basis for rehabilitation. *The American Journal of Sports Medicine*, *22*(3), 418–423.

Zhang, Y., & Jordan, J. M. (2010). Epidemiology of Osteoarthritis. *Clinics in Geriatric Medicine*, *26*(3), 355–369. http://doi.org/10.1016/j.cger.2010.03.001

Zhu, L., Buschmann, M. D., & Savard, P. (2016). Mechanical loading of knee articular cartilage induced by muscle contraction can be assessed by measuring electrical potentials at the surface of the knee. *Journal of Biomechanics*, *49*(3), 338–343. http://doi.org/10.1016/j.jbiomech.2015.12.033